universität wien

DIPLOMARBEIT

HCRP1 in ovarian cancer

Verfasserin

Bettina Savarese Brenner

angestrebter akademischer Grad

Magistra der Naturwissenschaften (Mag.rer.nat.)

Wien, Oktober 2011

Studienkennzahl lt. Studienblatt:	A 441
Studienrichtung lt. Studienblatt:	Diplomstudium Mikrobiologie und Genetik
Betreuerin / Betreuer:	Universitäts Professor Dr. Erwin Heberle - Bors

Danksagung

Ich möchte mich herzlich bei Prof. Dr. Michael Krainer bedanken, dass er mir die Möglichkeit gegeben hat diese Arbeit zu verfassen.

Außerdem möchte ich mich bei all meinen Labor Kollegen für ihre Unterstützung bedanken, sei es nun Diskussion, Versuche oder sonstiges.

Ein besonderer Dank gilt natürlich auch jenen Menschen, die mich im Laufe meines Studiums immer unterstützt haben, sei es nun finanziell, mit Aufmunterung, Ansporn, Freundschaft oder Rückhalt.

Der erste Dank geht natürlich an meine Eltern für wundervolle 24 Jahre „die Eltern“ sein und alles was sie mir ermöglicht haben.

Ein Dankeschön geht auch an meine restliche Familie, ins besondere an meine liebe Oma.

Danke meinen liebsten zwei Mädels Jenufa und Andrea.

Zu guter Letzt geht der größte Dank an meinen Mann Fabio, für Geduld bei Prüfungen, Zuhören, da sein und weil du einfach der Beste bist.

Zusammenfassung

Unter normalen Umständen wird Zell Homöostase sowie Zellzahl und folglich die Gewährleistung der Gewebsarchitektur - und Funktion in gesundem Gewebe durch exakte Regulierung, Produktion und Freilassung von Wachstums fördernden Signalen gewährleistet, die den Eintritt in den Zellwachstums und Zellteilungs Zyklus dirigieren. Deregulierung dieser Signale, die hauptsächlich durch Wachstumsfaktoren gesteuert werden, führt oft zu erhöhter Proliferation und Wachstum und folglich Tumor Entstehung. Erhöhte Menge des Epidermalen Wachstums Faktor Rezeptor (EGFR) wurden in vielen Krebsarten, inklusive Ovar Karzinomen, nachgewiesen was meist mit einer schlechteren Prognose für Patienten verbunden war. In meiner Arbeit versuchte ich herauszufinden welchen Einfluss die Deregulierung der EGFR Degradierung durch den ESCRT (Endosomal Sorting Complex required for Transport) auf Tumorformation hat. HCRP1, ein Mitglied des ESCRT I, ist essentiell für korrekte Rezeptor Degradation von ubiquitinierten Membranrezeptoren und folglich korrekte Zellfunktion. Die in dieser Arbeit präsentierten Ergebnisse charakterisieren HCRP1 als neuartiges „Tumor Supressor Gen“ mit einer essentiellen Rolle bei der Degradation von Rezeptor Tyrosin Kinasen und als potentieller Biomarker bei Ovar Karzinomen.

Abstract

Under normal conditions, homeostasis of cell number and hence the maintenance of tissue architecture and function in healthy tissue is ensured by the tight regulation, production and release of growth- promoting signals that direct the entry into the cell growth- and division cycle. Deregulation of these signals, which are mostly mediated by growth factors, often leads to enhanced proliferation and growth and consequently tumor formation. Elevated levels of the epidermal growth factor receptor (EGFR) were found in many kinds of cancer including ovarian cancer and are associated with a negative outcome for patients. In my work, I aimed at understanding the impact of deregulated EGFR degradation via ESCRT (Endosomal sorting complex required for transport) on tumor formation, focusing on HCRP1, a member of ESCRT I, which is crucial for proper receptor degradation of ubiquitinated membrane receptors. The results presented in this thesis, characterize HCRP1 as a novel tumor suppressor gene with an essential role in the degradation of receptor tyrosine kinases and as a potential biomarker in ovarian cancer and beyond.

Table of Contents

1. Introduction

Cancer is a complex, multistep disease which is classically regarded to arise due to six distinct molecular pathways which are required for the development of human tumors (as reviewed in Hallmarks of cancer: The next generation (Hanahan and Weinberg)). These six “hallmarks of cancer” are believed to constitute the origin of human cancer: Sustaining proliferative signals, evading growth suppressors, resisting cell death, enabling replicative immortality, inducing angiogenesis and activating invasion and metastasis.

The formation of cancer cells involves their ability to sustain chronic proliferation. Normally, homeostasis of cell number and hence maintenance of normal tissue architecture and function is ensured by tight regulation production and release of growth- promoting signals that direct the entry into the cell growth- and division cycle. Deregulation of these signals, which are mostly growth factors that bind cell surface receptors containing intracellular tyrosine kinase domains, leads to enhanced proliferation and growth and hence tumor formation (Hanahan and Weinberg). Cancer cells use various ways to amplify proliferative signaling: 1) the production of growth factor ligands, to which cells respond through expression of and signaling via cognate receptors 2) sending of signals to stimulate normal cells in the tumor-associated stroma, which consequently respond by supplying cancer cells with growth factors 3) enhanced levels of receptor proteins at the cancer cell surface which leads to hyper-responsitivity to ligands or structural alterations of receptor molecules which alleviates ligand-independent firing. Yet another way to increase proliferation is the alteration of signaling pathways operating downstream of these receptors (Bhowmick et al., 2004; Cheng et al., 2008).

Constitutive activation of proliferative signaling is usually established by activated growth factor receptors and is often linked to certain somatic mutations in the cancer cell genome. For an instance, it was shown that approximately 40% of human melanomas display an activating mutation which affects the structure of the B - Raf protein, resulting in constitutive signaling through the Raf to mitogen - activated protein (MAP) - kinase pathway (Davies and Samuels; Hanahan and Weinberg).

The EGFR/ErbB receptor proto–oncogene family, which comprises four structurally related transmembrane receptors, plays an important role in molecular pathogenesis of human cancer and is a promising target for personalized anti cancer treatment, as it was shown that elevated levels of ErbB signaling are associated with poor prognosis in cancer patients (Holbro et al., 2003; Hynes and Lane, 2005; Yarden, 2001).

In this thesis, I characterize HCRP1, a member of the Endosomal Sorting Complex Required for Transport I (ESCRT I), which is crucial for proper (EGFR) - receptor degradation and hence correct signaling, as a promising target and marker for anti cancer therapy.

1.1. Growth factors- Introduction

Growth factor receptors play a crucial role in cellular proliferation, survival, migration and differentiation. To control their cell surface expression and hence the transduction of signals delivered in response to growth factors, proper down-regulation of mitogenic receptors is crucial. It was shown that overstimulation or hyperactivation through mutation of the EGFR was found to be associated with enhanced tumor development leading to a more aggressive disease and hence an unfavorable clinical outcome (Holbro et al., 2003; Hynes and Lane, 2005; Yarden, 2001). Due to these facts, signaling pathways and their associated downstream signaling cascades represent promising targets for cancer therapy. To ensure proper EGFR signaling, internalization via endocytosis is crucial for receptor down-regulation (Maxfield and McGraw, 2004). This step can lead to recycling of the receptor back to the cell surface, entry into the trans-Golgi network or transport into intraluminal vesicles and the formation of mutivesicular bodies (MVBs), which are then degraded by fusion with the lysosome (Katzmann et al., 2002; Raiborg et al., 2003). The Endosomal sorting complex required for transport ESCRT comprises four members (ESCRT 0-III) (Hurley and Hanson) and is discussed in detail later.

1.2. The EGFR pathway

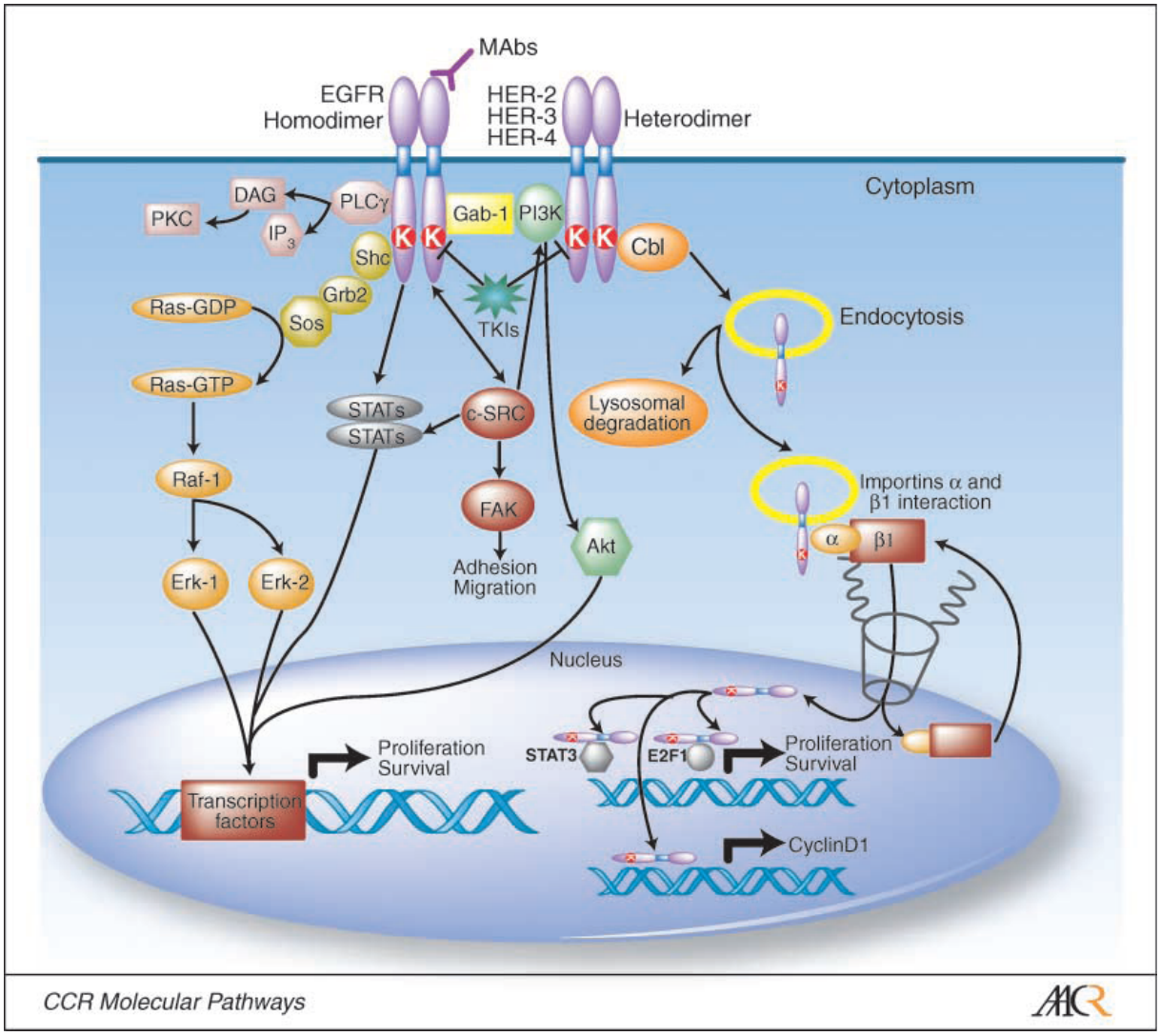

Figure 1: The EGFR signaling pathways and its inhibitors. Activation of EGFR leads to homo/heterodimerization and cytosolic tyrosine residue phosphorylation. STAT transcription factors and Phosphlipase C□ can bind directly to the EGFR receptor, compared to the Ras/Raf/MAPK – and PI3K pathway which need adaptor molecules (yellow) for activation. PI3K can also bind directly to the ErbB unit of a heterodimer formed with EGFR. The activated receptor can be internalized via endocytosis and can be either lysosomaly degraded or translocated into the nucleus leading to the activation of genes involved in proliferation, survival, invasion and metastasis. EGFR inhibition can be established by two main mechanisms: mAb which compete for ligand binding and small molecule TKI which block ATP binding to the kinase domain of the receptor. DAG, 1, 2-diacylglycerol; IP3, inositol 1,3,5-triphosphate; PLCg, phospholipase Cg; Erk-1, extracellular signal-regulated kinase-1; Erk-2, extracellular signal-regulated kinase-2; FAK, focal adhesion kinase; PKC, protein kinase C.
(figure taken from (Scaltriti and Baselga, 2006))

Signal transduction initiated by binding of extracellular ligands to transmembrane receptors and hence activation or repression of distinct target gene is essential for cellular response to environmental stimuli. The EGFR- family consists of four members: EGFR (ErbB1/Her-1), ErbB2/Neu/HER-2, ErbB3/HER-3 and ErbB4/HER-4 (Schlessinger, 2002; Sibilia et al., 2007) and is a class of receptor tyrosine kinases (RTKs) (SIMON 2000). Upon ligand binding, EGFR is activated which leads to receptor dimerization and autophosphorylation of cytoplasmatic tyrosine residues. Subsequently, the phosphor tyrosine residues serve as a docking platform for several adaptor molecules which induce the activation of a number of pathways including the RAS-RAF-MEK-ERK pathway, the STAT3 and STAT5, the PLC-gamma PKC and the PI3K-Akt-mTOR pathway. MAPK and STAT signaling mostly mediate differentiation and proliferation, whereas Akt – signaling leads to the activation of pro-survival and anti- apoptotic pathways (Schlessinger, 2002; Simon, 2000; Yarden, 2001). Ligand binding can induce the formation of hetero - or homodimers, which is the basis for the complexity of tissue specific ErbB signaling. This complexity is further amplified by the diversity of ligands which can bind to the ErbB receptors: in humans alone, more than 30 ligands have been identified that bind to the EGFR family, including the EGF-like ligands, transforming growth factor α (TGFα) and heregulins (HRGs also known as neuregulins) (Siwak et al.). This cell-type specific expression of ErbB receptors and the presence of the various ligands in the cellular environment result in the specificity of ErbB signaling for the individual cell types (Sibilia et al., 2007).

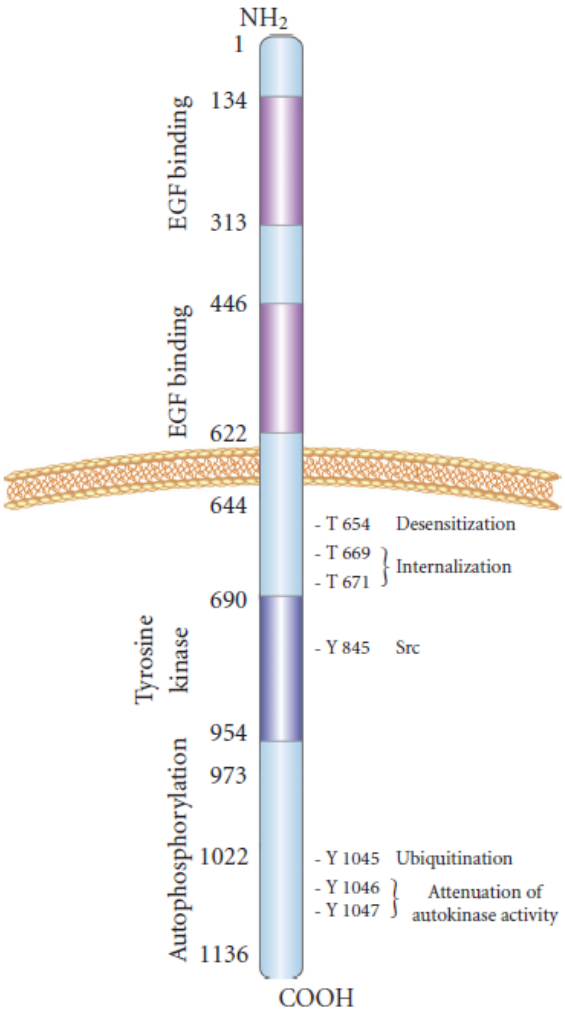

Figure 2: Structure of the Epidermal Growth Factor Receptor (EGFR). The EGFR is subdivided into three domains 1) extracellular (consisting of 4 subdomains, two ligand binding and two receptor dimerization domains), 2) transmembrane and 3) intracellular domains. The cytoplasmatic tail containing the tyrosine kinase domain is highly conserved among the EGFR family members. Phosphorylated tyrosine residues serve as docking sites for proteins with phosphotyrosine binding domains and SRC homology 2 binding domains.

(figure taken from (Siwak et al.))

The EGFR receptor comprises three domains 1) an extracellular domain (ECD) 2) a transmembrane domain (TMD) and 3) an intracellular domain (ICD). The ECD is highly glycosylated and can be divided into four subdomains (I – IV) of which I and III confer ligand binding specificity and the cysteine rich subdomains II and IV, which is characteristic for the type I receptor tyrosine kinases. The TMD which is built of

mainly hydrophobic amino acid residues is crucial for anchoring the receptor in the cell membrane, for signal transduction from the ECD to the ICD after ligand binding and for the stabilization of receptor dimerization. The ICD comprises three subdomains, a juxtamembrane (JD) domain, a tyrosine kinase domain (TKD) and a carboxy-terminal regulatory domain (RD). The JD reduces ligand affinity by reducing the tyrosine kinase activity and additionally increases receptor internalization after ligand binding, which leads to down regulated ErbB receptor signaling. The TKD is highly conserved between the ErbB/EGFR receptor tyrosine kinases and is needed for autophosphorylation upon ligand binding. The RD functions as a regulator of kinase activity and recruits exogenous substrates that have SH2 (Src homology 2) or PTB (protein tyrosine binding motifs) (Schlessinger, 2002).

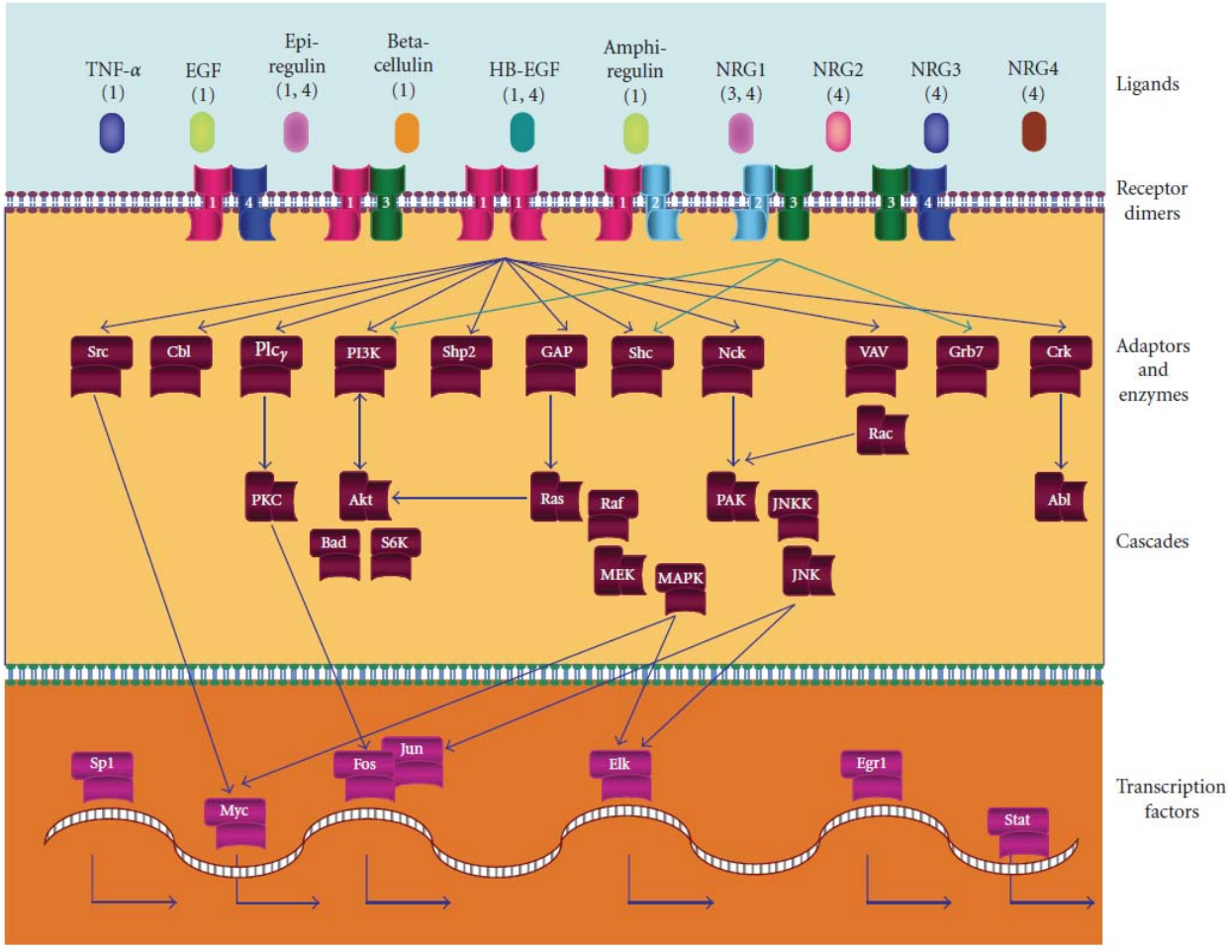

Figure 3 Representation of the signaling networks of the 4 EGFR family members EGFR, HER2, HER3 and HER4 (numbers 1-4). Multiple ligands are known to bind to the EGFR family including EGF-and EGF-like ligands, transforming growth factor (TGF)-*α* and heregulins (HRGs, also known as neuregulins, NRGs). Numbers

underneath the ligands indicate to which EGFR family member ligands preferably bind to. There is no known ligand binding to HER2, while it is the preferred binding partner for all EGFR family members. Signal transduction is established by intracellular adaptor proteins, activating cascades such as the Ras/Raf/MAPK and PI3K/Akt. Proteins downstream of these cascades can be translocated into the nucleus where they can activate transcription factors (TF) such as MYC, ELK and FOS/JUN. The activated TFs mainly control the expression of genes involved in cellular responses such as proliferation, differentiation, cell mobility, survival and tumorgenesis. PLC*γ*: Phospholipase C*γ*; SHP2: SRC homology phosphatase 2; GAP: GTPase activating protein; SHC: SRC homology 2 domain and collagen-containing protein; PKC: Protein kinase C; MEK: MAPK/ERK kinase; PAK: P21-activated kinase; JNKK: JNK kinase; JNK: JUN N-terminal kinase; EGR1: Early growth response protein 1; STAT: Signal transducer and activator of transcription
(figure taken from (Siwak et al.))

1.3. EGFR and hepatocellular carcinoma formation

Human hepatocellular carcinoma HCC is one of the most lethal cancers being one of the most common cancer-related causes of death worldwide (Huether et al., 2005). HCCs are complex heterogenous neoplasms and are the second most lethal cancer, with an 8,9 % 5-year survival rate, following pancreatic ductual adenocarcinoma. Studies show (Breuhahn et al., 2006) that growth factor pathways, including the EGFR pathway are often deregulated in HCC, often combined with EGFR-ligand over-expression (Breuhahn et al., 2006). This leads to altered signaling of various pathways, such as the RAS-RAF-MEK-ERK, the PI3K-AKT and the PLC-gamma-Pathway (Sibilia et al., 2007).

In general EGFR plays an important role in liver function, as mature liver cells express high levels of EGFR when compared with other adult cells. EGFR - ligands like EGF, TGF- α, AR and HB-EGFR were shown to be potent mitogens for cultured hepatocytes and seem to display hepatoprotective and regenerative potential. Additionally they are required for liver regeneration, which was demonstrated by partial hepatectomy in the corresponding knock-out mice. In HCC, EGFR or other growth factors are often deregulated, EGRF being up-regulated in 68%, ERbB2 in 21%, ErbB3 I 84% and ErbB4 in 61% of HCC (Sibilia et al., 2007). Especially over-expression of ERbB1 and ErbB3 contribute to more aggressive tumors and poorly differentiated HCCs additionally ErbB1 is associated with Metastasis and poor survival rate. Both genetic and pharmacological studies emphasize the importance of

EGFR signaling in HCC development. Studies with transgenic mice display that treatment with hepatocarcinogenes led to the development of well differentiated multifocal HCCs in mice expressing TGF – α, an important EGFR ligand, from the metallothionein- 1 (MT) promoter, whereas in TGF – α deficient mice this treatment led only to formation of small tumors (Jhappan et al., 1990). Treatment of HCC cells with the anti - EGFR antibody Cetuximab resulted in inhibited proliferation (Huether et al., 2005) and induced apoptosis (Breuhahn et al., 2006). Similar results were shown by treating HCC cells with Gefitinib, an EGFR-tyrosine kinase inhibitor, leading to growth inhibition and cell cycle arrest (Breuhahn et al., 2006; Sibilia et al., 2007).

1.4. EGFR in ovarian cancer

Aberrant signaling of the EGFR - receptor tyrosine kinase family and their downstream targets is associated with various kinds of cancer including epithelial ovarian cancer (Lafky et al., 2008; Salomon et al., 1995). Epithelial ovarian cancer accounts for 90% of ovarian cancer and it was shown that EGFR is over expressed in about 60% of ovarian cancers (Dimova et al., 2006; Lin et al., 2009). Treatment of human ovarian cancer cell lines with EGF resulted in significantly increased expression of proteins involved in invasion (Henic et al., 2006) and altered signaling of pathways associated with angiogenesis. EGF treatment of the ovarian adenocarcinoma cell line OVCAR – 3 led to elevated levels of H2O2 which triggers the activation of the AKT –P70S6K pathway and increases vascular endothelial growth factor transcription through hypoxia – inducible factor 1α expression (Liu et al., 2006).

1.5. The EGFR Degradation Pathway

As mentioned above, the phosphotyrosine residues in the cytoplasmic domain of EGFR serve as a docking platform of several adaptor molecules, some of which are crucial for proper degradation of ligand activated EGFR (Kirisits et al., 2007; Sweeney and Carraway, 2004). Proteins from the Cbl family play a key role in regulating RTK signaling including EGFR, platelet derived growth factor receptor (PDGFR), colony stimulation factor (CSF-1) and Her2 (Thien and Langdon, 2001). Ubiquitination is one of the major steps in EGFR degradation and was considered to

be responsible for proteasomal delivery of its substrates. As EGFR is degraded in lysosomes an alternative mechanism of ubiquitination is required. Normally, proteins destined for degradation by the proteasome get polyubiquitinated, whereas EGFR is monoubiquitinated at multiple sites as a signal to enter the endosomal pathway. C-Clb is an E3 ligase which is involved in EGFR degradation by being recruited to the plasma membrane upon ligand binding which in turn leads to tyrosine phosphorylation by EGFR and hence mediates ubiquitination and intracellular receptor handling (Kirisits et al., 2007). After attachment to the EGFR phosphorylated tyrosine residue 1045 (pTyr 1045), c-Clb attaches ubiquitin to the bound receptor. The actual internalization of the receptor is established by clathrin coated pits (CCPs) which requires guidance of the receptor to CCPs by the interaction of Epidermal Growth Factor pathway substrate 15 (Esp15) with the clathrin adaptor complex (AP-2) and the ubiquitinated receptor or EGFR associated c-Clb (de Melker et al., 2004). Cbl-interacting protein of 85 kDa (CIN85) also guides EGFR - c-Clb complexes to CCPs by interacting with Endophilin, which is a CCP regulatory element. The growth factor receptor binding protein 2 (Grb2) is another player involved in the internalization of EGFR by facilitating the interaction between EGFR and c-Clb (Huang and Sorkin, 2005). Vesicle fission from the plasma membrane is mediated by Dynamin, a GTPase (McNiven et al., 2000). This is followed by clathrin shedding which leads to the fusion of the EGFR containing vesicle with cytoplasmatic vesicular structures which is carried out by Ras associated protein 5 (Rab5) another GTPase (Kirisits et al., 2007; Zerial and McBride, 2001).

The Endosomal Sorting Complexes Required for transport (ESCRTs) comprises four members ESCR 0-III and is crucial for EGFR degradation and its sorting into lysosomes. ESCRT0 is responsible for clustering of ubiquitylated cargo, ESCRT I and ESCRT II are directly involved in membrane budding and ESCRTIII is responsible for membrane scission.

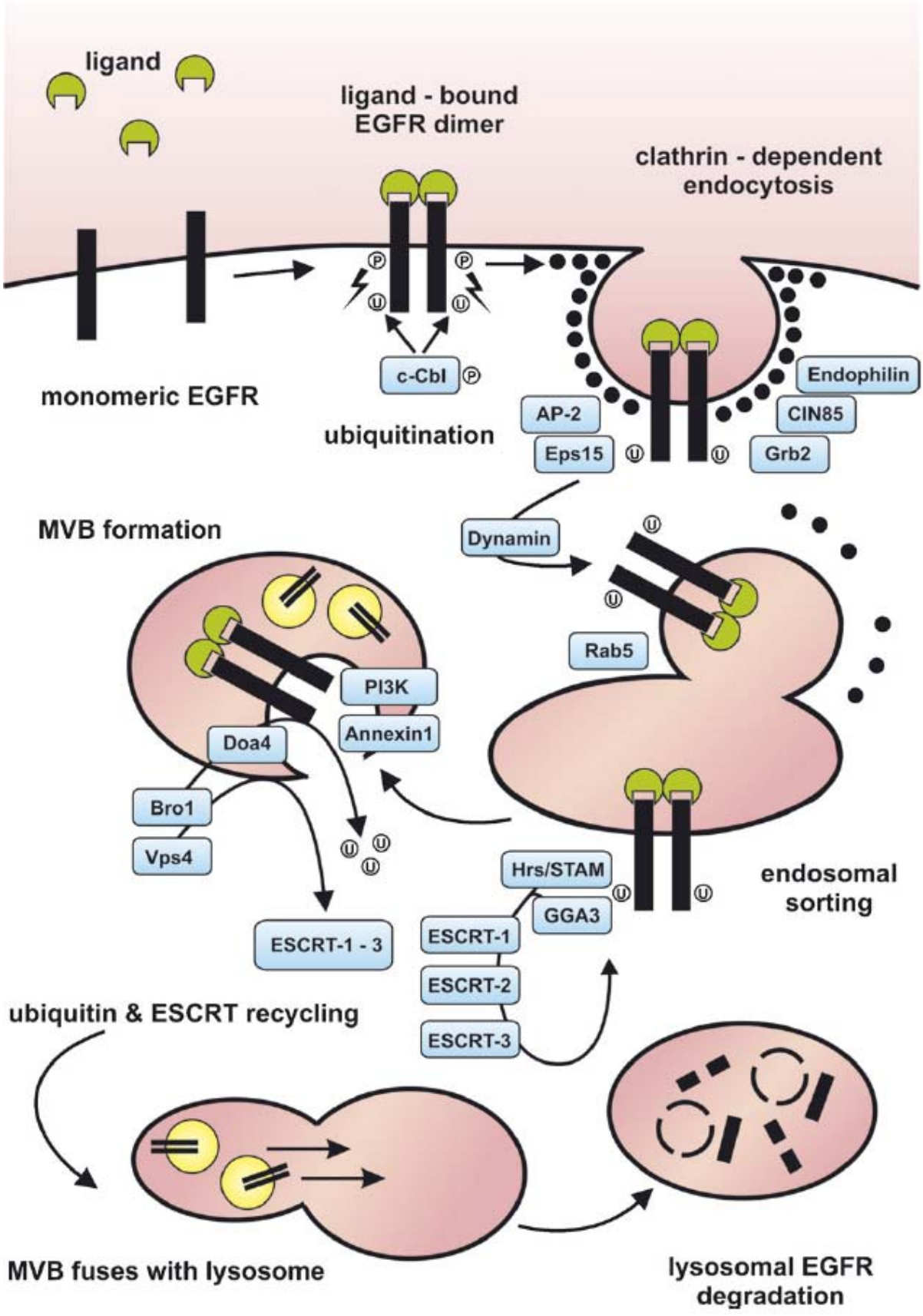

Figure 4 The EGFR degradation pathway. Upon ligand binding EGFR forms hetero- or homodimers followed by autophosphorylation. c – Cbl gets phosphorylated and is

recruited to the receptor where it induces EGFR monoubiquitination. This causes EGFR to accumulate in clathrin coated pits which are interalised. Clathrin is shed and the intenalised vesicle fuses with the early endosome. MVB formation is triggered by the ESCRT complexes (0-III), (described in detail in text). In the end MVB fuses with the lysosome and the inner vesicles containing EGFR are proteolytic degraded in the lysosomal interior.

(figure taken from(Kirisits et al., 2007))

1.6. The ESCRT complexes

EGFR is degraded by being sorted to the lysosome (Sorkin and von Zastrow, 2009). This endosomal sorting is established by bud formation of portions of the endosome's limiting membrane into the lumen of the endosome (Hurley and Hanson). Intralumenal vesicles (ILV) are formed by scission of these membrane buds, late endosomes filled with ILV are called multi vesicular bodies (MVB) (Gruenberg and Stenmark, 2004; Piper and Katzmann, 2007; Russell et al., 2006). In the end of the trafficking process, the MVB fuses with the lysosome where the contents are degraded at the hydrolytic lysosomal interior (Kirisits et al., 2007).

Initially, the factors involved in proper MVB formation have been identified in *saccharomyces cerevisiae*. In yeast, the so called vacuolar protein sorting (VPS) genes (also known as class E genes), regulate correct MVB biogenesis, as the vacuole is the equivalent to the mammalian lysosome (Hurley and Hanson; Raymond et al., 1992). Loss of function of the VPS genes in yeast was shown to lead to altered trafficking of transmembrane proteins, which then accumulate in the yeast-specific class E compartment, because MVB formation is abolished (Babst, 2005). As analogous observations were made regarding the mammalian VPS homologues, it is assumable that their function in protein sorting is an evolutionarily conserved feature in eukaryotes (Babst, 2005). A list of yeast and mammalian homologues of the four ESCRT complex components and related VPS genes is given in table 1. The VPS genes mainly compose the core subunits of the four ESCRT complexes, or like the AAA + ATPase Vps4 provide the only energy input and the multifunctional ESCRT-associated Protein Bro1 domain- containing protein (Bro1) which displays regulatory functions by modulating ESCRT assembly.

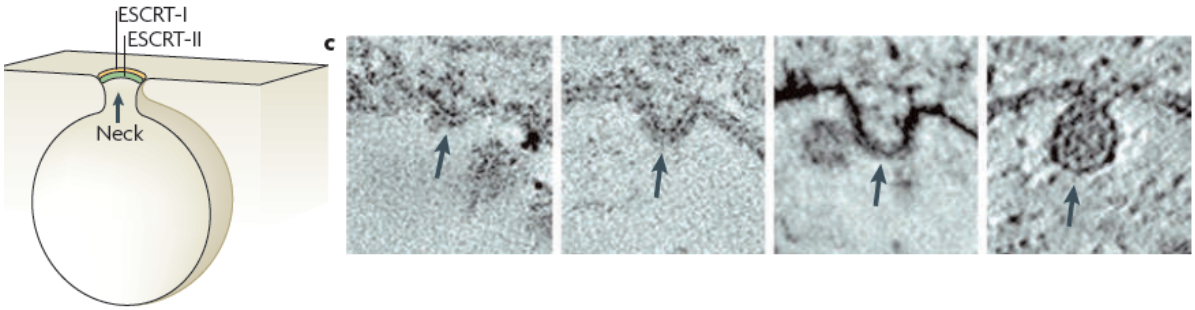

Figure 5: Bud formation is established by ESCRT I and ESCRT II, which are located at the neck of the bud, in order to stabilize bud formation. On the right side bud formation *in vivo* is shown by a series of images of fixed and negatively stained cells, which are arranged into a time series.
(figure taken from (Hurley and Hanson))

ESCRT activity	Yeast protein*	Metazoan protein*	Motifs and domains	Biochemical role*	Biological role
ESCRT-0					
Clustering of ubiquitylated cargo	Vps27	HRS (HGS)	VHS, FYVE, UIM (yeast), DUIM (metazoan), PTAP, GAT, coiled-coil core, clathrin-binding	Binds phosphatidylinositol-3-phosphate-containing membranes, ESCRT-I, ubiquitin and clathrin	MVB biogenesis, autophagy
	Hse1	STAM1, STAM2	VHS, UIM, SH3, GAT, coiled-coil core	Binds ubiquitin and DUBs	MVB biogenesis, autophagy
ESCRT-I					
Membrane budding (with ESCRT-II)	Vps23	VPS23 (TSG101)	UEV, Pro-rich linker, stalk, headpiece	Binds ubiquitin and ESCRT-0 in the MVB pathway and PTAP motifs in viral Gag proteins; adaptor for CEP55	MVB biogenesis, autophagy, viral budding, cytokinesis
	Vps28	VPS28	Headpiece, Vps28 C-terminal	Binds ESCRT-II	MVB biogenesis, autophagy, viral budding, cytokinesis
	Vps37	VPS37A, VPS37B, VPS37C, VPS37D	Basic helix, stalk, headpiece	Binds membranes (mammalian VPS37 binds ESCRT-III protein IST1)	MVB biogenesis, autophagy, viral budding, cytokinesis
	Mvb12	MVB12A, MVBB	Stalk, ubiquitin-binding C terminus	Stabilizes ESCRT-I oligomers by contacting each subunit; C terminus binds ubiquitin	MVB biogenesis, autophagy, viral budding, cytokinesis
ESCRT-II					
Membrane budding (with ESCRT-I)	Vps22	VPS22 (EAP30)	Basic helix, WH2	Binds membranes	MVB biogenesis, autophagy
	Vps25	VPS25 (EAP20)	WH2	Binds Vps20 of ESCRT-III to recruit ESCRT-III to the bud neck and activate it	MVB biogenesis, autophagy
	Vps36	VPS36 (EAP45)	GLUE, NZF1 (yeast), NZF2 (yeast), WH2	Binds phosphoinositide-containing membranes, ubiquitin and ESCRT-I	MVB biogenesis, autophagy
ESCRT-III					
Membrane scission	Vps20	VPS20 (CHMP6)	Myristoylated; MIM2	Initiates ESCRT-III assembly in MVB biogenesis by binding Snf7; initiates membrane scission; MIM2 binds Vps4 for subsequent disassembly	MVB biogenesis, autophagy
	Snf7 (Vps32)	SNF7A (CHMP4A), SNFB (CHMP4B), SNFC (CHMP4C)	MIM2	Main driver of membrane scission; recruits DUBs (in yeast); binds Bro1 domain-containing proteins, including ALIX	MVB biogenesis, autophagy, viral budding, cytokinesis
	Vps24	VPS24 (CHMP3)	MIM1	Completes membrane scission; recruits the DUB AMSH (in mammals)	MVB biogenesis, autophagy, viral budding, cytokinesis
	Vps2	VPS2A (CHMP2A), VPS2B (CHMP2B)	MIM1	Recruits Vps4; initiates ESCRT-III disassembly	MVB biogenesis, autophagy, viral budding, cytokinesis

ESCRT activity	Yeast protein*	Metazoan protein*	Motifs and domains	Biochemical role*	Biological role
ESCRT-III related					
Regulation of membrane scission and ESCRT-III disassembly	Did2 (Vps46)	DID2A (CHMP1A), DID2B (CHMP1B)	MIM1	Recruits Vps4 and the microtubule-severing enzyme spastin (mammalian DID2B)	MVB biogenesis, viral budding, cytokinesis
	Vps60	CHMP5	Not determined	Binds Vta1 with high affinity	MVB biogenesis, cytokinesis
	Ist1	IST1	MIM1, MIM2	Binds Vps4, Vta1, Did2 and ESCRT-I	MVB biogenesis, cytokinesis
	None	CHMP7	MIM1, MIM2	The tandem ESCRT-III domains bind SNF7B and the DUB UBPY (USP8)	MVB biogenesis, viral budding
Vps4 and Vta1					
ESCRT-III disassembly	Vps4	VPS4A, VPS4B (SKD1)	MIT, AAA	AAA + ATPase that acts as an assembled oligomer on ESCRT-III	MVB biogenesis, autophagy, viral budding, cytokinesis
	Vta1	VTA1 (LIP5)	MIT, VSL	Binds MIMs; binds Vps4 to promote oligomer assembly and ESCRT-III recycling	MVB biogenesis, autophagy, viral budding, cytokinesis
Other					
Multiple modulatory and targeting functions	Bro1 (Vps31)	ALIX (AIP1)	Bro1, V, Pro-rich	Recruits Snf7 for scission; recruits DUBs; adaptor for CEP55 and viral YPXL motifs; interacts with apoptosis factors and the cytoskeleton with unclear significance for the ESCRT pathway	MVB biogenesis, viral budding and cytokinesis

Table 1: The Endosomal sorting complex required for transport ESCRT – members and function Abbreviations: AMSH, associated molecule with the SH3 domain of STAM; Bro1, Bro1 domain- containing protein 1; CHMP, charged multivesicular body protein; DID, DOA4-independent degradation protein; DUB, deubiquitylating enzyme; DUIM, double -sided ubiquitin -interacting motif; ESCRT, endosomal sorting complex required for transport; GAT, GGA and TOM; GLUE, GRAM-like ubiquitin-binding in EAP45; HRS, hepatocyte growth factor- regulated Tyr kinase substrate; Ist1, increased sodium tolerance protein 1; MIM, MIT- interacting motif; MIT, microtubule-interacting and transport; MVB, multivesicular body; NZF, Npl4-type zinc finger; SH3, SRC homology 3; UBPY, ubiquitin isopeptidase Y; UEV, ubiquitin E2 variant; UIM, ubiquitin- interacting motif; VHS, Vps27, HRS and STAM; Vps, vacuolar protein sorting; VSL, VTA1, SBP1 and LIP5; WH2, winged helix 2

(table taken from (Hurley and Hanson))

The heterodimer ESCRT 0 consists of hepatocyte growth factor regulated tyrosine kinase substrate (Hrs), which is the human homologue of Vps27, and the signal transducing adaptor molecules 1 and 2 (STAM 1, STAM 2). Together with the Golgi -localised, □-ear containing, Arf – binding protein 3 (GGA3), ESCRT 0 binds ubiquitinated cargo upstream of ESCRT I and guide ESCRT I, by binding to TSG101, to the late endosome (Katzmann et al., 2003; Kirisits et al., 2007; Puertollano and Bonifacino, 2004). It was shown that mutations yielding perturbed Hrs/TSG101 interaction resulted in insufficient transfer of EGFR from early to late endosome (Kirisits et al., 2007; Lu et al., 2003). Consequently, treatment of cells with si-RNAs targeting GGA3 led to inhibited EGFR degradation (Kirisits et al., 2007; Puertollano and Bonifacino, 2004). Additionally, similar results were obtained in Hrs (-/-) and STAM1 (-/-)/STAM2 (-/-) mice (Kanazawa et al., 2003; Kirisits et al., 2007), which emphasizes the importance of both Hrs/STAM and GGA3 for cargo recognition and cargo feeding into the MVB.

ESCRT I is a heterotetramer comprising one copy each of the subunits Vps23 (in mammalians Tumor susceptibility gene 101; Tsg101), Vps28 (hVps28), Vps37A (hepatocellular carcinoma related protein 1; HCRP1) and the multivesicular body sorting factor 12 (Mvb12) (Chu et al., 2006; Curtiss et al., 2007; Kirisits et al., 2007; Kostelansky et al., 2007; Oestreich et al., 2007). The heteotetramer complex is

centred around a 13 nm long stalk and a 5nm long headpiece (Hurley and Hanson). Vps23 (Tsg101) contains an ubiquitin E2 variant (UEV) domain which binds ubiquitinated cargo (Katzmann et al., 2001; Sundquist et al., 2004; Teo et al., 2004b) as well as ESCRT 0, whereas the amino terminal basic helix of ESCRT I contributes to membrane binding (Hurley and Hanson) .At the end of the stalk another short ubiquitin binding domain of Mvb12 is located (Shields et al., 2009), as well as the N-terminal helix of Vps37A (HCRP1), which is involved in electrostatic interactions with acidic membrane lipids (Kostelansky et al., 2007). A GPPXXY motif builds a linker between the UEV motif and the stalk. The C-terminal helical domain of Vps28 is itself responsible for binding the ESCRT II complex. Separate inhibition of any of the ESCRT I subunits by siRNA or antibodies results in stalled EGFR degradation (Bishop et al., 2002). Like ESCRT I , the ESCRT II complex is a heterotetramer which contains one protein of Vps22 and Vps36 and to molecules of Vps25, which builds a rigid Y- shaped core of about 15nm (Hierro et al., 2004; Im and Hurley, 2008; Teo et al., 2004a). Vps25 contains two winged helix motif, one at the N-terminus of which binds to structurally analogous pockets in the C-terminal motif of Vps22 and Vps36. The second, C-terminal winged helix motif binds recruits and activates the upstream ESCRT III subunit Vps20 (Im et al., 2009; Saksena et al., 2009; Teo et al., 2004a). Vps22 is essential for the membrane recruitment of ESCRT II (Im and Hurley, 2008). Remarkably, Vps36 is quite complex in yeast compared to the human analogue which has a much simpler architecture. Both Vps36 homologues contain a GRAM-like ubiquitin binding in EAP45 (GLUE) domain, which is important for binding 3-phosphoinositides (and ubiquitin in humans) (Alam et al., 2006; Hirano et al., 2006; Slagsvold et al., 2005; Teo et al., 2006).

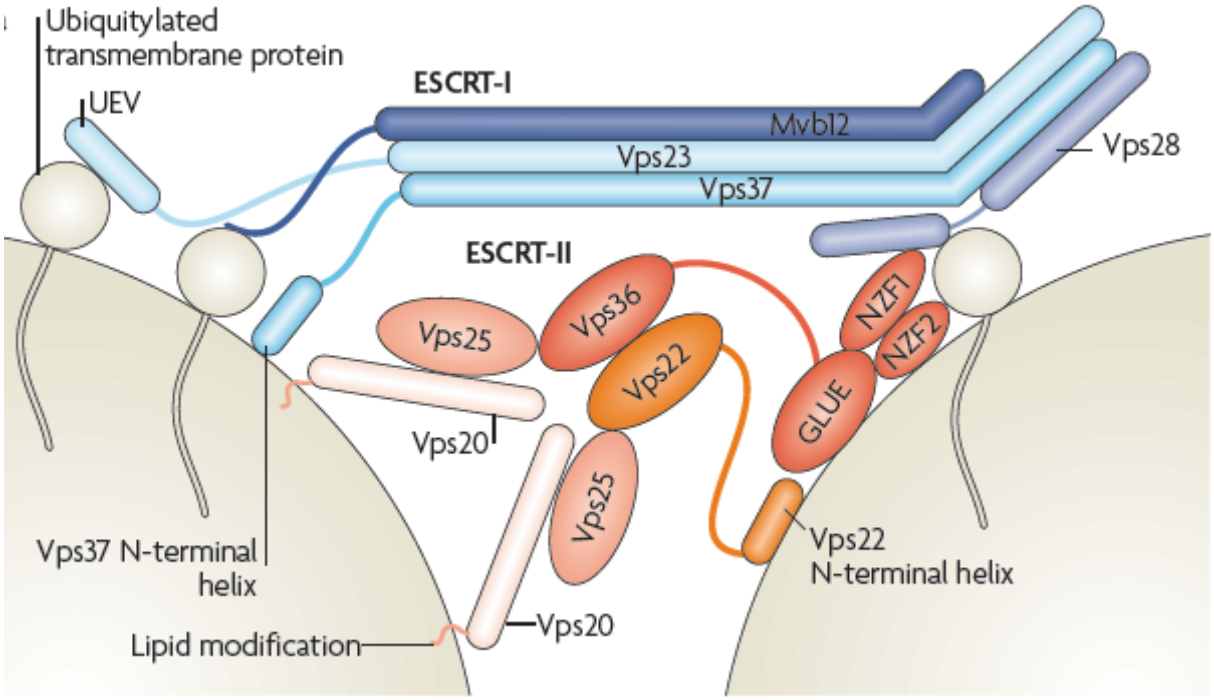

Figure 5: ESCRT complexes I and II; ESCRT I contains multivesicular body sorting factor 12 (Mvb12), vacuolar protein sorting 23 (Vps23), Vps28 and Vps37 and ESCRT-II consists of Vps20, Vps22, Vps25 and Vps36)
(figure taken from(Hurley and Hanson))

ESCRT III is a dynamic polymer that does not have a clearly defined composition of proteins. In yeast, ESCRT III contains four main subunits: Vps20, Sucrose non fermentor 7 (Snf7), Vps24 and Vps2 (which is also known as DOA4 independent degradation protein 4 (Did 4)) (Babst et al., 2002) and regulator subunits Did2, Vps60 and the increased sodium tolerance protein 1 (Ist 1). The human ESCRT III list contains twelve additional proteins, including three isoforms of SNF7 and two DID2 and two VPS2 proteins which can form alternative complexes. Interaction of ESCRT II with Vps20 initiates polymerization of the ESCRT III subunits (Babst et al., 2002; Kirisits et al., 2007) whereas the latter complex leads recycling proteins to the site of action, like Bro 1 which is required for the recruitment of Doa 4 a deubiquitinating enzyme and Vps4, which is the AAA- type ATPase which is responsible for ESCRT disassembly (Babst, 2005). The ESCRT III proteins share a common overall architecture (Hurley and Hanson) and the common behavior of cycling between a closed monomeric state in the cytosol and an open polymerized form on the endosomal membrane (Shim et al., 2007; Zamborlini et al., 2006). Intramolecular autoinhibition interactions prevent membrane binding and polymer assembly by

maintaining the closed cytosolic conformation of each ESCRT III protein. As ESCRT III assembles, which is an energetically favorable process, these autoinhibitory interactions are deallocated in their “open“ conformation and the subunits bind to each other and to the membrane (Hurley and Hanson).

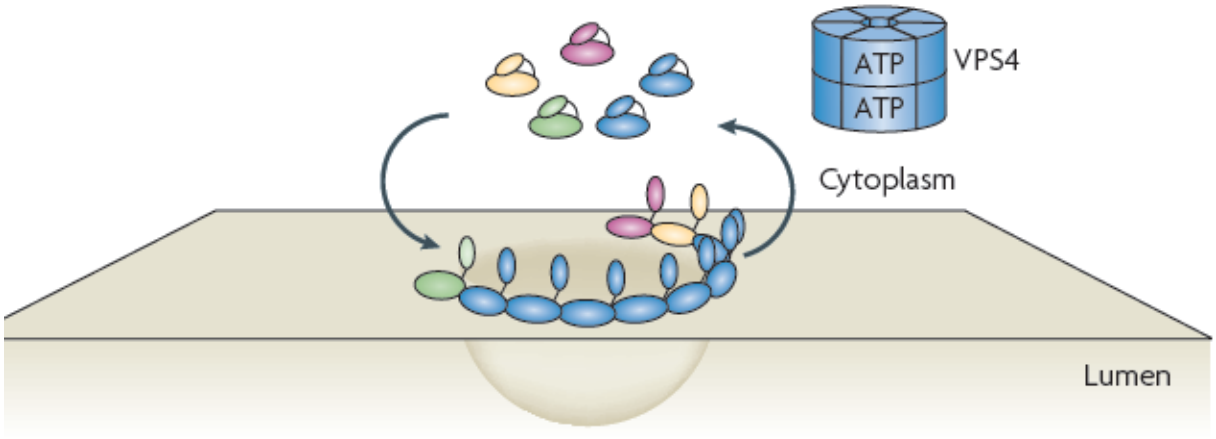

Figure 6: Schematic view of ESCRT III assembly and Vps4 mediated disassembly. In the cytosol ESCRT II proteins are in their monomeric “closed” conformation. In their “open” conformation ESCRT III subunits bind to each other and to the membrane as they assemble into functional ESCRT III polymers.

(figure taken from(Hurley and Hanson))

1.7. Membrane budding, scission and MVB formation

The deformation of the membrane into a bud (a vesicle that is still attached to the limiting membrane) is the first step in MVB formation, followed by scission of the vesicle. *In vitro* studies with purified proteins and GUVs showed that recrution of ESCRT I together with ESCRT II can lead to bud formation (Wollert and Hurley). ESCRT I and ESCRT II led to bud formation even at low concentrations (15 nM) compared to ESCRT III subunits Vps20 and Snf7 which can induce bud formation only at super-physiological concentrations (600nM for Snf7) (Babst et al., 2002), as ESCRT III is actually involved in membrane scission. Additionally, it was shown that the two ESCRT complexes I and II localize almost exclusively at the bud neck (Hurley and Hanson), as they are involved in the stabilization of the bud neck itself (Hurley and Hanson). After bud formation and stabilization by ESCRT I and II, ESCRT III is recruited to the membrane in order to additionally stabilize the neck and in succession it leads to cleaving of the membrane. ESCRT III subunits assemble at

the membrane neck, where Vps20 is required for coupling ESCRT III to ESCRT II (Im et al., 2009; Saksena et al., 2009; Teis et al.; Teo et al., 2004a). These strong intersubunit and subunit – membrane interactions, which occur as ESCRT III assembles at the membrane, provide energy for the scission reaction. Especially the strongly favorable electrostatic interactions with the acidic membrane seem to serve as parameters whether the energy barrier to scission and the followed release of the vesicle can be overcome (Hurley and Hanson). Finally after completion of the scission reaction, ESCRT III is disassembled by the AAA+ ATPase Vps4, which functions as a ring shaped dodecameric cylinder (Gonciarz et al., 2008; Hartmann et al., 2008; Inoue et al., 2008; Landsberg et al., 2009; Scott et al., 2005; Yu et al., 2008) with highly conserved amino acid residues in the central pore of Vps4 (Scott et al., 2005). ATP hydrolysis is the only step in the reaction where energy is put into the system, providing the only thermodynamic driving force for ESCRT mediated membrane budding and scission (Hurley and Hanson). It is suggested that polymeric ESCRT III subunits are pulled into or through the central pore in order to release them as monomeric subunits into the cytosol (Gonciarz et al., 2008; Scott et al., 2005; Yu et al., 2008). This interaction requires additional N-terminal microtubule – interacting and transport domains (MIT) with α – helical MIT interacting motifs (MIMs) at or close to the C- termini of the ESCRT III proteins (Kieffer et al., 2008; Obita et al., 2007; Stuchell-Brereton et al., 2007). MIMs are not only required for ESCRT III polymer assembly, but also to induce the normally inactive monomers or dimers in the cytosol to form a functional Vps4 AAA+ dodectamer. Additionally other proteins which bind to Vps4 regulate its oligomeric state and activity. Vta1 binds to Vps4 and is involved in its oligomerization, Did2 which functions as a positive and Ist1 which functions as a negative regulator and Vps60 which is also involved in Vps4 regulation (Hurley and Hanson).

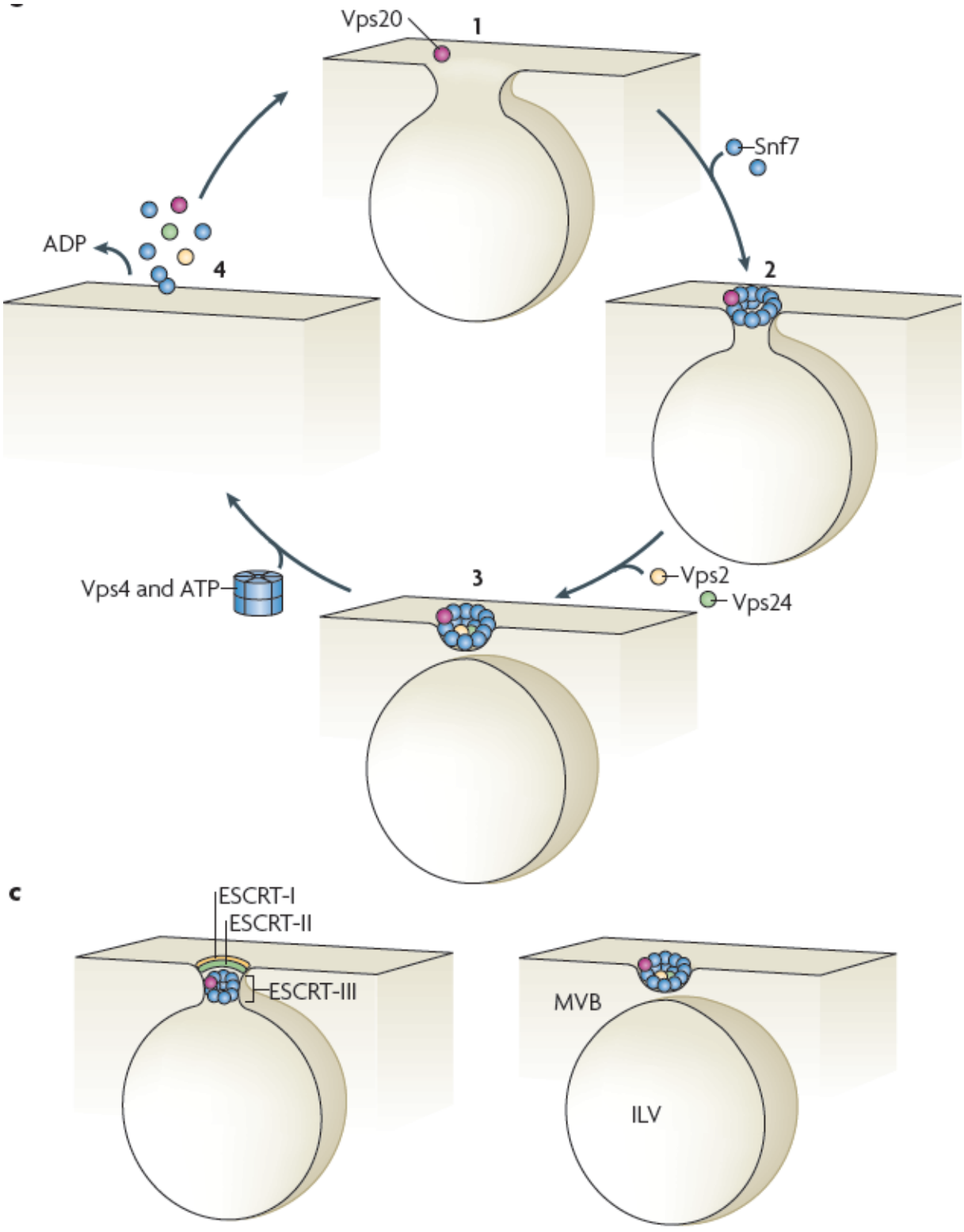

Figure 7: Membrane scission by ESCRT III. Vps20 initiates the assembly of ESCRT III (Hurley and Hanson); several Snf7 molecules form spiral structures by polymerizing downstream of Vps20 (Hanson et al., 2008; Saksena et al., 2009); Vps2 and Vps24 molecules close the formed spiral; The ESCRT III spiral assembles at the bud-proximal side of ESCRT II in order to carry out scission; Vps disrupts ESCRT III polymer formation under ATP hydrolysis. (figure taken from Hurley and Hanson)

1.8. HCRP1/ hVps37A – a member of ESCRT I

Originally, HCRP1 was described in yeast (where it is called Vps37A (vacuolar protein sorting 37 homolog A) as one of the three subunits of ESCRT I which actively drive the sorting away from nonubiquitinated cargo (Conibear, 2002; Katzmann et al., 2001). In yeast ESCRT I was reported as consisting of the three class E vps (vacuolar protein sorting) proteins Vps23, Vps28 and Vps37, which are responsible for sorting of ubiquitinated MVB (Bache et al., 2003; Katzmann et al., 2002). The human counterpart of Vps37A (hVps37A) was identified to interact with Tsg101 (human Vps38 homolog) and human Vps28 through its mod(r) domain(Bache et al., 2004). As the expression of the human homolog of Vps37 A (hVps37A) was shown to be undetectable or reduced in hepatocellular carcinoma (HCC) by a positional cloning approach (Xu et al., 2003), the name HCRP1 (hepatocellular cancer related protein) was suggested. HCRP1 overexpression in a HCC cell line led to reduced cell growth *in vitro*, whereas siRNA mediated reduction of HCRP1 levels resulted in inhibited EGFR down regulation and hence increased cellular proliferation (Xu et al., 2003).

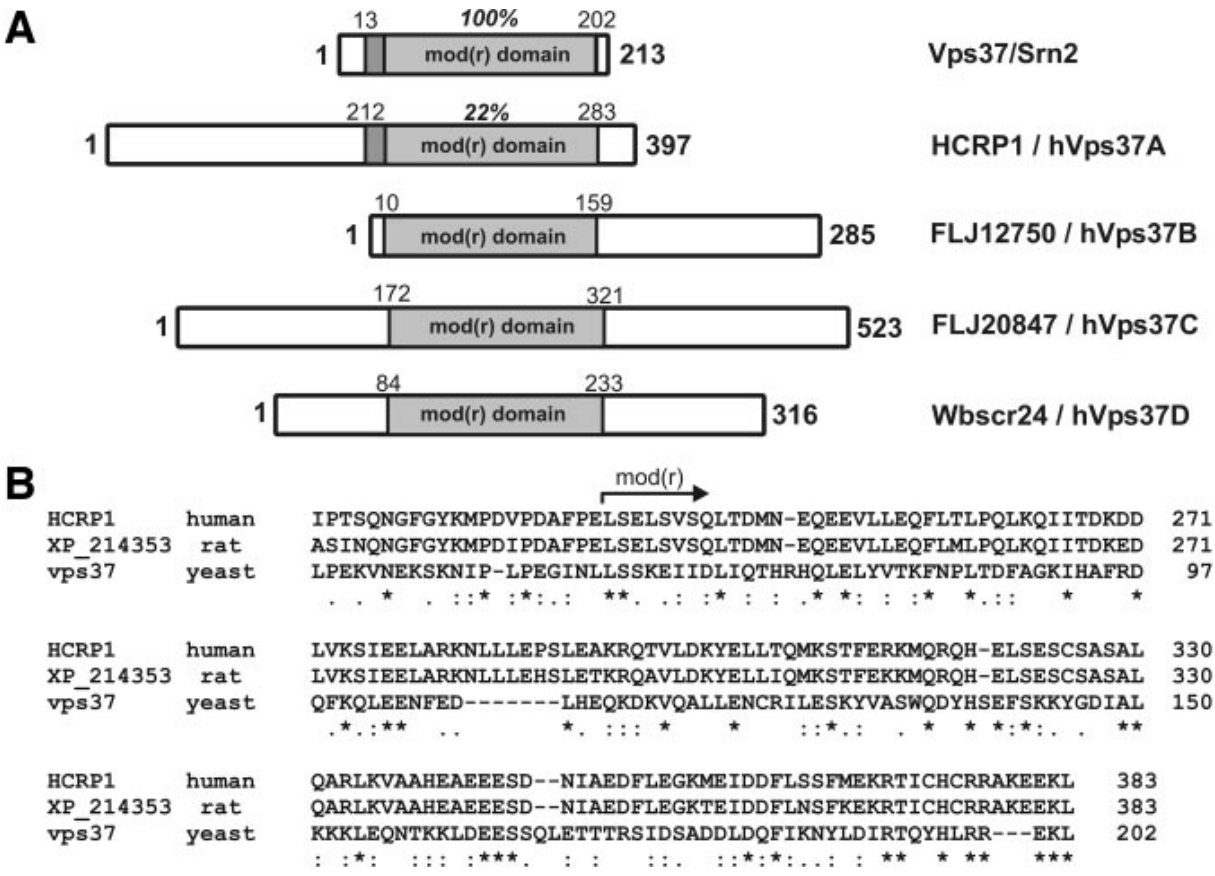

Figure 8: A) Domain structure of Vps37 and HCRP1. The most highly conserved regions between proteins are shown in gray, which contain a mod(r) domain (modifier of rudimentary). Three additional proteins contain this region: hVps37B, hVps37C and hVps37D. B) Alignment of the conserved region between Vps37, HCRP1 and the rat counterpart of Vps37 and HCRP1. The arrow indicates the start point of the mod(r) domain. HCRP1 shows 21% sequence identity (41% sequence similarity) with yeast Vps37A in the C-terminal part (Bache et al., 2004; Xu et al., 2003).

(figure taken from (Bache et al., 2004))

1.9. HCRP1 in ovarian cancer – therapeutic implications and prognostic influence

As there is a close connection between positive EGFR signaling and human cancer, two therapeutic implications have been developed in order to target the EGFR - pathway. One approach is ATP competitive inhibition of small molecule tyrosine kinase inhibitors or targeting the extracellular receptor domain with monoclonal antibodies, like Cetuximab, a chimeric monoclonal antibody (Wittinger et al 2011). Regarding the impact of altered EGFR signaling and of course its degradation in human cancer development, the EGFR degradation pathway and its members

display a promising target for future cancer therapy development and prognosis (Kirisits et al., 2007). Functional screens for tumor suppressor genes identified TSG 101 (tumor susceptibility gene 101), a member of ESCRT I, to be able to induce malignant development in NIH 3T3 cells (Kirisits et al., 2007; Li and Cohen, 1996), similar to HCRP1 which enhances cellular proliferation when knocked down (described before). Additionally HCRP1 was shown to be located at the short arm of chromosome 8, a region where loss of heterozygosity (LOH) occurs in a high percentage of human cancers including ovarian cancer (Pils et al., 2005) which makes HCRP1 an attractive target for cancer research and potentially a prognostic factor. Krainer and colleges (Wittinger et al 2011) showed that the prognostic value of EGFR and HER2 depends on the status of HCRP1 expression. (described in detail in Results) This was achieved via a Tissue Micro Array (TMA) of ovarian cancer patients, analyzing the co-expression of HCRP1 and EGFR and HER2. Overexpression of these two cancer markers was associated with a negative outcome for ovarian cancer patients, but this influence on overall survival was only observed in cases with low or absent HCRP1 expression (see in detail Results). In order to characterize the impact of HCRP1 expression in tumor development, an ovarian cancer (cell line) model was used to define its function *in vitro* and *in vivo*. The results of these experiments are presented in this thesis.

2. Results

The experiments I performed during my studies as a diploma student and which are presented in this thesis build on preliminary experiments performed in the laboratory of Professor Krainer. In a previous study, Krainer and colleagues (Kirisits et al., 2007) describe the importance of the ESCRT for proper receptor degradation and proposed HCRP1 as interesting candidate for further research due to its importance in endosomal sorting. As already mentioned, a tissue micro array (TMA) was performed in order to confirm a possible correlation of EGFR/HER2 and HCRP1 expression in ovarian cancer patients (described in detail below). To further characterize the consequences of deregulated HCRP1 expression, an inducible HCRP1 system was established. Krainer and colleges used this system to analyze the effect of HCRP1 knock down on EGFR signaling, anti EGFR antibody treatment (Cetuximab) as well

as the influence on proliferation and invasiveness. My work under this aspect was to further investigate the influence of depleted HCRP1 on tumor formation in a mouse xenograft model as well to further characterize the HCRP1 knock down *in vitro*. Additionally, I characterized a novel HCRP1 monoclonal antibody and repeated the previously performed TMA. Finally, I analyzed HCRP1 expression in cancers other than ovarian cancer, confirming the notion that loss of HCRP1 is associated with a negative clinical outcome.

2.1. Growth Factor Degradation – Influence on prognosis and clinical outcome - Correlating HCRP1 and EGFR/HER2 levels in ovarian cancer

As mentioned in the introduction, Krainer and colleagues proposed that HCRP1 influences the impact of EGFR/HER2 over-expression on the survival rate of ovary cancer patients (Pils et al., 2007). Since HCRP1 is involved in endosomal receptor degradation and hence influences receptor degradation, a Tissue micro array (TMA) of ovarian cancer patients was used to confirm this notion. The TMA was performed in order to analyze EGFR, HER2 and HCRP1 expression showing high protein expression for the two oncogenes EGFR and HER2, which was also associated with a negative outcome for cancer patients. Protein expression was graded according to staining intensity (see table 2 and 3; figure 31). Concerning HCRP1 expression, the patient cohort was divided into two groups according to their protein expression levels. A high percentage of the tumors displayed either low or absent HCRP1 expression.

Additionally, in order to confirm the loss of HCRP1 in ovarian cancer patients, an independent cohort of ovarian cancer patients was analyzed for HCRP1 expression on the mRNA level. It was shown that compared to normal (i.e. epithelial) ovarian tissue there is lower expression of HCRP1 in cancer patients. (see figure 29) For further confirmation of the prognostic value of HCRP1 the overall survival of the patients was stratified based on HCRP1 expression. As a result there was a high impact of HER2 as well as EGFR expression on overall survival only for cases with low or absent HCRP1 expression, whereas this prognostic aspect is lost in patients with regular or high HCRP1 expression. This aspect underlines the possible influence of endosomal receptor degradation on clinical relevance of growth factor expression.

Figures and tables are given below (see “HCRP1 in Ovarian cancer patients – Tissue Micro Array analysis”).

2.2. Molecular analysis of HCRP1 function by gene knock-down

2.2.1. A system for the inducible down - regulation of HCRP1

To mechanistically analyze the role of HCRP1 *in vitro* and *in vivo*, an inducible shRNA system (tet - Off) was established in Skov3 ovarian cancer cells (described in detail in Materials and Methods). Silencing effectiveness is given in figure 9 (Western Blot) and Figure 10 (qRT PCR).

2.2.2. Stable knock down of HCRP1 in MDAH-2774 cells

In addition to the inducible system, another ovarian carcinoma cell line, MDAH 2774, was stably transfected with a shRNA construct in order knock-down HCRP1. Silencing effectiveness is given in figure 26 (Western Blot) and figure 27 (IHC).

Figure 9: Skov3 tet cells were cultivated with Dox or PBS in order to gain HCRP1 knock down and were analyzed by SDS – PAGE. Silencing of HCRP1 leads to an increase in HER2 and EGFR phosphorylation.

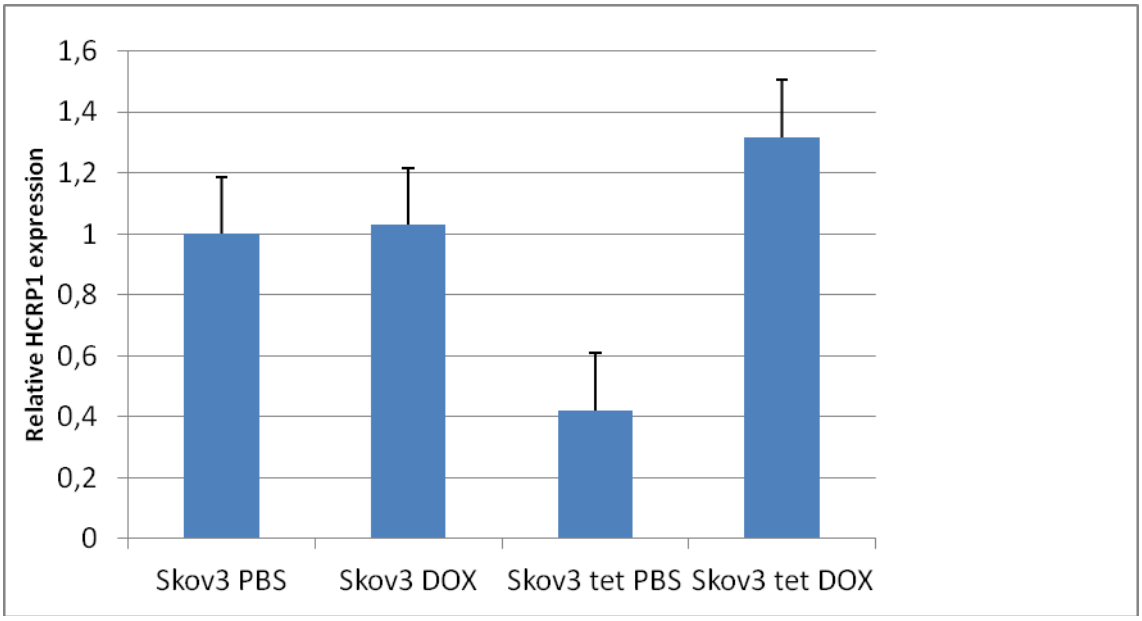

Figure 10: mRNA level of Skov3 cells and Skov3 tet cells treated with PBS/ DOX (1µ/µl). The figure shows shRNA mediated knock down of HCRP1 in Skov3 cells when DOX is removed from the media.

Analysis of the previously described cells lines revealed that both the transfected Skov3 and MDAH-2774 cells showed remaining HCRP1 expression of 30-40% (measured by qRT PCR; results shown in figure 10; data for MDAH cells not shown). In addition and consistent with the loss of HCRP1 activity, these cells displayed elevated levels of activated EGFR and HER2. Interestingly, juxtaposing HCRP1 expression with activated EGFR levels showed that only phosphorylated EGFR was elevated whereas normal EGFR levels stayed constant (see figure 9) and an increase of the pEGFR/EGFR ratio. This finding implicates that activated EGFR accumulates in cells with decreased HCRP1 expression due to disrupted EGFR degradation. Furthermore, immunofluorescence analyses were used in order to detect the localization of the retained pEGFR within the cells. These experiments demonstrated that whereas pEGFR was hardly detectable in control cells, in HCRP1 knock-down cells pEGFR was localized at high levels in the cytoplasm (see figure 11). Interestingly a frequent co -localisation with the early endosomal marker EEA1 was detectable, (see figure 11) which indicates that pEGFR accumulates mainly in sorting endosomes. This further underlines the effect of disrupted EGFR sorting in HCRP1 depleted cells.

Additionally an immunoblot analysis was done to quantify HCRP1, (p) EGFR and (p) HER2 in 15 ovarian and breast cancer cell lines. There was no significant correlation between HCRP1 and EGFR but a quite clear reciprocal correlation between HCRP1 and pEGFR. On the other hand, there was only a statistically weak correlation between HCRP1 and HER2 protein expression. This data additionally underscore that phosphorylated EGFR accumulates in ovarian cancer cells due to defect endosomal protein degradation. To study the dynamics of pEGFR degradation in wild type and HCRP1 knock down cells, the cell lines were incubated in serum free medium followed by stimulation with 100ng/ml EGF for 15min in order to trigger receptor activation, which was followed by re-incubation in serum free medium. Cells were harvested at defined time points and pEGFR protein expression measured by Western Blotting (see figure 12). Degradation of pEGFR was significantly impaired in HCRP1 deficient cells, whereas total receptor levels remained constant in both SKOV3 and MDAH-2774 cells, which suggests sustained EGFR signaling in these cell lines.

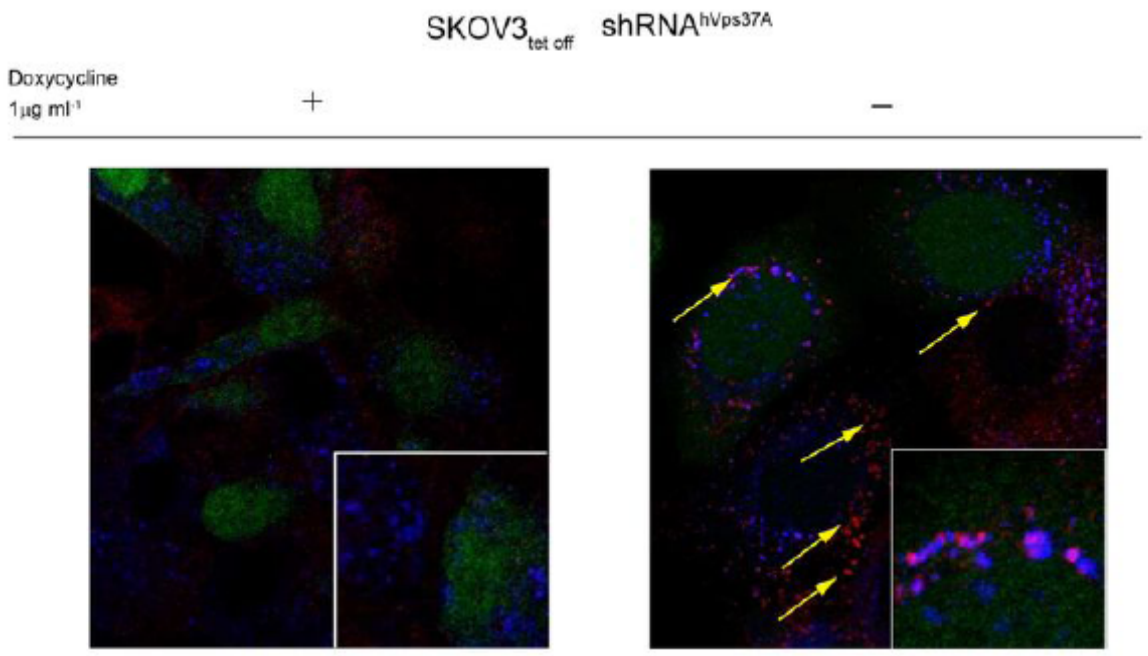

Figure 11: pEGFR (red) accumulates in HCRP1 silenced cells and is colocalized with early endosomal marker EEA1, (blue). SKOV3tet off cells were cultivated in presence or absence of doxycycline on chamber slides, probed against pEGFR and EEA1 and analyzed by confocal microscopy. Colocalization of the pEGFR (red) and EEA1

(blue) signal is indicated by arrows. Green fluorescence of the nuclei arises from the presence of an EGFP cassette in the Tet-Off vector.

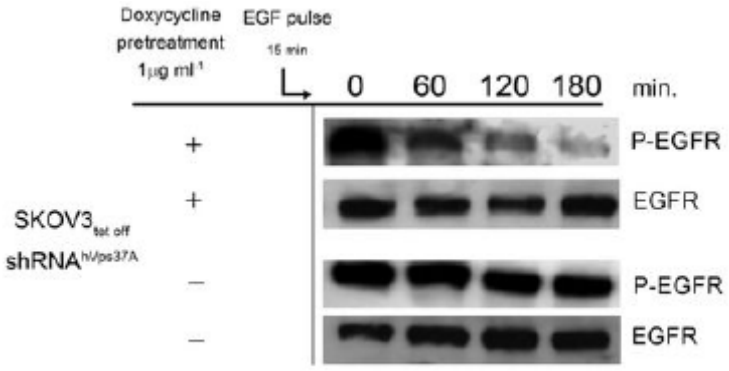

Figure 12: SDS – PAGE showing that time-pulsed activation of pEGFR is sustained in HCRP1 silenced cells. SKOV3tet off cells cultivated in presence or absence of doxycycline were starved by serum withdrawal, then pulsed with 100ng/ml EGF and cultivated for indicated time in serum-free medium.

2.3. HCRP1 – influences on EGFR signaling and anti EGFR antibody treatment

To test the effect of HCRP1 knock-down on downstream EGFR signaling HCRP1 the inducible HCRP1 knock down system was used. Knock-down of HCRP1 led to increased phosphorylation of Erk1/2, consistent with extensive receptor phosphorylation and downstream pathway activation. Akt phosphorylation at serine 473 was not changed in the two studied cell lines.

The next step was to test the effect of the anti-EGFR antibody Cetuximab and the EGFR/HER2 inhibitor Lapatinib on EGFR phosphorylation in HCRP1 knock-down cells. After Lapatinib treatment, EGFR signaling was inhibited in both wild type and HCRP1 knock down cells, shown by the dephosphorylation of Erk1/2 and Akt in both Skov3 and MDAH 2774 cell lines. In contrast, Cetuximab treatment of HCRP1 knock down cells caused Erk1/2 and Akt to stay phosphorylated, which suggests the importance of cytoplasmatic EGFR degradation for Cetuximab dependent inhibition of its downstream pathways. On the other hand, Lapatinib mediated EGFR inhibition seems to be mediated by its direct interaction with the tyrosine kinase domain, which is independent of endosomal processing and hence unaffected by HCRP1 status.

2.4. Defective activation of Erk-signaling leads to increased cellular proliferation, invasion and tumorgenesis in HCRP1 knock-down cells

The comparison of Skov3 control cells with HCRP1 knock-down cells regarding their doubling times (25,5 and 24,9 hours) revealed that there was only a very moderate impact of HCRP1 knock-down on cellular proliferation under unstressed *in vitro* conditions. However, after incubation with Cetuximab there was a significant decrease of the proliferative potential in cells expressing HCRP1 compared to HCRP1 knock-down cells, which remained unaffected. This emphasizes the notion that the presence of HCRP1 is crucial for proper degradation of the receptor - antibody – complex, which is further essential for proper cetuximab mediated anti–tumor activity (Wheeler et al., 2008). Treatment with Lapatinib reduced cell proliferation independent of HCRP1 expression levels.

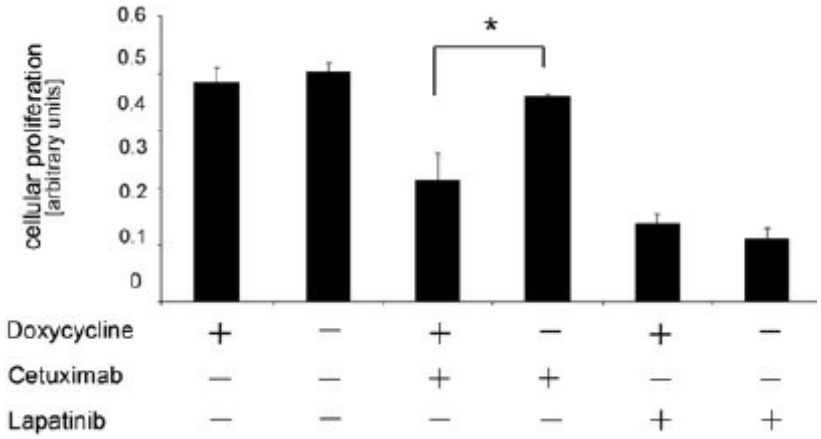

Figure 13: HCRP1 silenced cells are resistant to cetuximab. 2x105 SKOV3tet off cells were cultivated in presence or absence of doxycycline and exposed to 20µg/ml cetuximab, or 4µM lapatinib or remained untreated. Cell number was determined every 48 hours by a CASY cell counter over 8 days. Doubling time (dt) was calculated, normalized to untreated control and depicted as 1/dt. The columns indicate the mean of three independent experiments

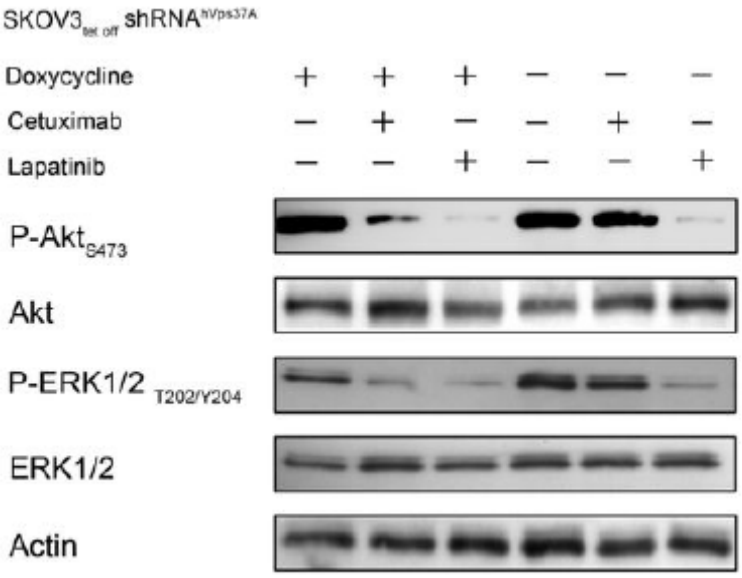

Figure 14: hVps37A silencing leads to resistance against cetuximab mediated EGFR inhibition. SKOV3tet off cells cultivated in presence or absence of doxycycline were incubated for 24 hours with either 20µg/ml cetuximab, or 4µM lapatinib or remained untreated. Protein levels of pAkt, Akt, pErk1/2, Erk1/2 and actin

2.5. HCRP1 knock down increases invasive potential of tumor cells

To mimic physiological tumor growth conditions, Skov3 cells were seeded into non adhesive 96 – well plates containing methylcellulose complemented media in order to generate tumor- like spheroids of several hundred cells. These spheroids were transferred to 3D culture - collagen gels and incubated for 72h. The overall growth rate was not affected by HCRP1 expression, however HCRP1 knock-down cells could invade the collagen matrix more efficiently (see figure 15), which underlines the impact of HCRP1 on the invasiveness of cancer cells rather than their proliferation. The invasive potential was calculated as percentage of outgrowing cells relative to the central area of the spheroid (73, 5 % compared to 30% for the control cells).

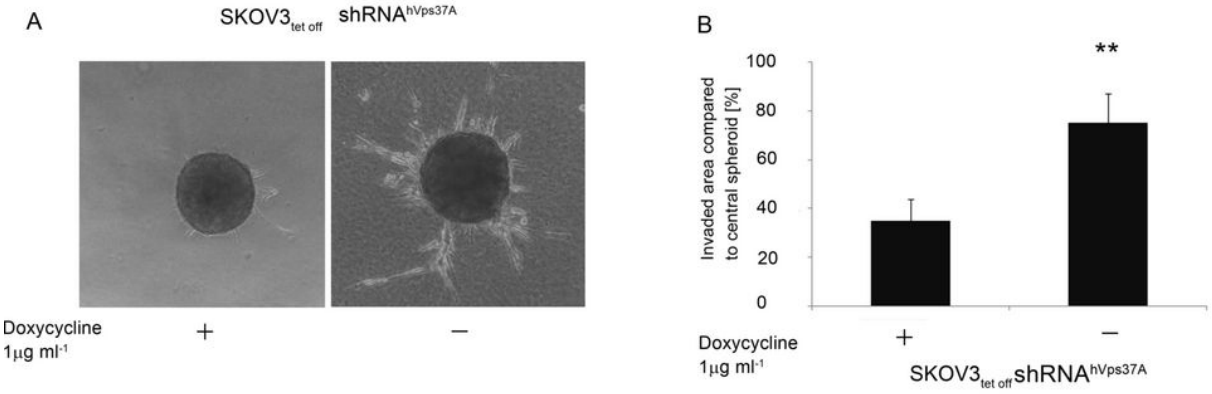

Figure 15: (A) shows Skov3 tet cells cultivated in presence or absence of doxycycline in a collagen matrix. Spheroids were analyzed by light microscopy. (B) shows the area of outgrowing cells depicted in percentage relative to central spheroid. Error bars indicate mean +/- SEM.

Additionally we performed a wound healing assay by simply cultivating Skov3 tet cells which were treated with PBS (induced HCRP1 knock down) or Dox and scratched them with a spatula. We could observe a clear difference between the two cell lines as HCRP1 knock down in Skov3 tet PBS treated cells led to enhanced proliferation and hence better “wound” healing ability.

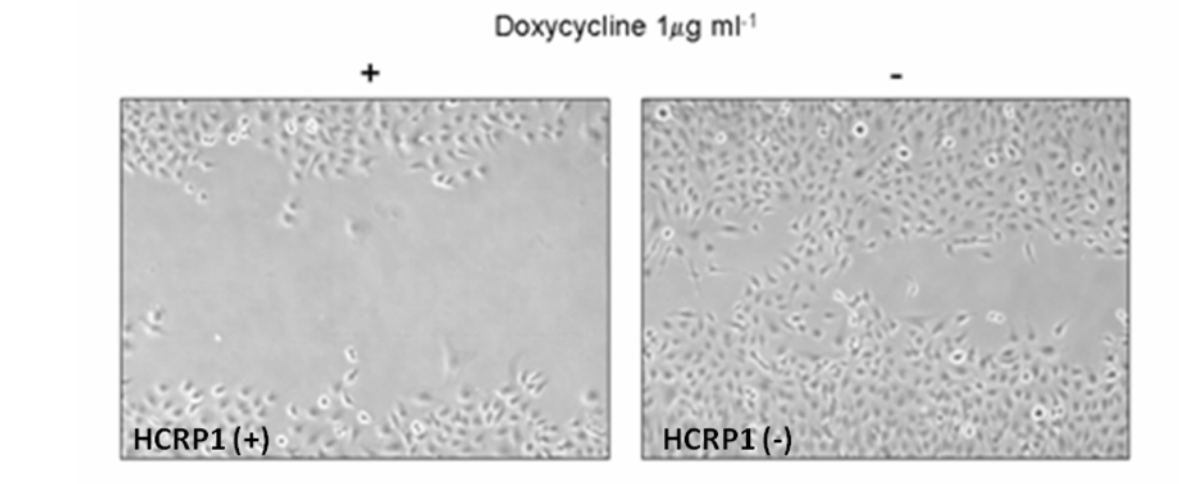

Figure 16: A wound healing assay with Skov3 tet cells was performed in order to see the effect of HCRP1 knock down on stress induced proliferation. Cells were plated on cell culture dishes and scratched with a spatula. The cells were treated with Dox (HCRP1 (+), left) or PBS (HCRP1 (-), right) and incubated for 24 hours. HCRP1 knock down led to significantly enhanced proliferation.

2.6. A mouse Xenograft model shows enhanced tumor growth in HCRP1 silenced tumors

A mouse Xenograft model was used to address the effect of HCRP1 down - regulation in tumor formation caused by hyperactivation of EGFR due to the lack of proper receptor degradation. Two cell lines were subcutaneously injected into nude mice: the Skov3 ovarian cancer cell line as a control and additionally the Skov3 cell line with the inducible shRNA tet-Off system in order to down - regulate HCRP1 when cells/mice are not treated with Doxycycline (DOX). Effectiveness of the inducible tet system is given in figure 10.

Before the Skov3 and Skov3 tet cells were injected into mice a PCR (Venor ® GeM; Minerva biolabs) was performed in order to detect mycoplasma in cells (see figure 17). We used cells from bottles number 3, 4 and 6 for further cultivation and injection. 5 x 10^6 cells were subcutaneously injected into four eight week old Foxn1nu mouse groups with 10 mice each. The groups were treated either with PBS or DOX which were injected into the flanks of mice. Tumor size was measured weekly. In line with the in vitro results, HCRP1 knock-down tumor growth was elevated resulting in mean tumor volumes of 1027mm^3 compared to 683mm^3 for the un-induced tumors. The

tumors started to grow after seven days whereas both Skov3 tet PBS and Dox treated tumors showed almost equal growth. After four weeks there was a significant difference in tumor growth observed between the two groups. In week six and seven tumors started getting necrotic hence mice had to be sacrificed. The mice were sacrificed according to the institutional ethics committee protocols, tumor samples were frozen in liquid Nitrogen and the rest was embedded in paraffin.

The successful knock-down of HCRP1 was confirmed via IHC staining of mouse tumor samples (see figure 20). Also, significantly decreased apoptosis rates for the HCRP1 knock down tumors were observed. This indicates that the tumor growth effect can be ascribed to sustained survival rather than elevated proliferation. Problems occurred during the detection of HCRP1 mRNA and protein levels from mouse tumors extracts (discussed in detail later).

Control groups with injected Skov3 cells were also treated with PBS and DOX. There was no difference in growth observed between the two mouse groups, indicating that DOX treatment does not influence tumor growth. Interestingly tumors originating from these cells grew much slower compared to tumors arising from Skov3 tet cells with the inducible HCRP1 knock down system. This might be caused by several reasons: 1) the cells could have been in bad shape at the time of injection, 2) the induction of the inducible system might cause the cells to gain enhanced proliferation ability and 3) the inducible tet system was leaky which led to reduced HCRP1 levels even in Skov3 tet cells treated with Dox. Though, immunhistochemical staining of Skov3 tet tumor samples showed a clear difference. The same was true for mRNA level detected with qRT PCR protein expression level and protein level, analyzed with Western blotting (data not shown) of the Skov3 (tet) cells before injection. These findings confirm that the inducible tet system was working properly before injection and in the mouse experiment.

Further analysis of the used cell lines is described and discussed below. Analysis of HCRP1 protein levels extracted from mouse tumor samples did not lead to satisfying results as there was no reasonable difference observed between the samples. HCRP1 bands were smeary and additional bands appeared when blotting protein samples from mouse tumors. (see figure 25) mRNA level measurement with qRT

PCR also did not lead to satisfying results (see figure 17). Although we could observe HCRP1 knock down in Skov3 tet cells, the HCRP1 mRNA level measured for Skov3 cell tumors was very low compared to Skov3 tet cells both with induced and un - induced HCRP1 knock down. Both problems with Western Blotting and qRT PCR presumably result from problems with protein and RNA extraction. For extraction of both RNA and protein I crushed the tumor samples (which were frozen in liquid nitrogen before) with a mortar for tissues and used the same protocol I used for protein and RNA extraction of cell line cells. As the protocol worked very well for extraction of cells from cell culture I assume that either the procedure of extracting was not sufficient due the tumor was not grounded sufficiently or, especially concerning RNA extraction, the sample was contaminated with extracellular protein. Currently I am aim to establish a proper RNA and protein isolation protocol.

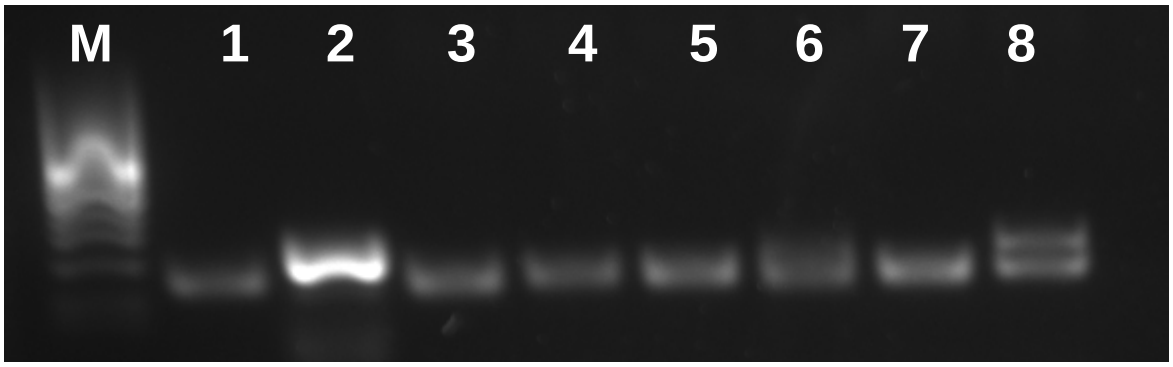

Figure 17: PCR for mycoplasma detection. Skov3 and Skov3tet cells were tested for mycoplasma. Cells from bottles number 3, 4 and 6 were used for further experiments. Numbers indicate cell culture bottle numbers; marker (M).

(A)

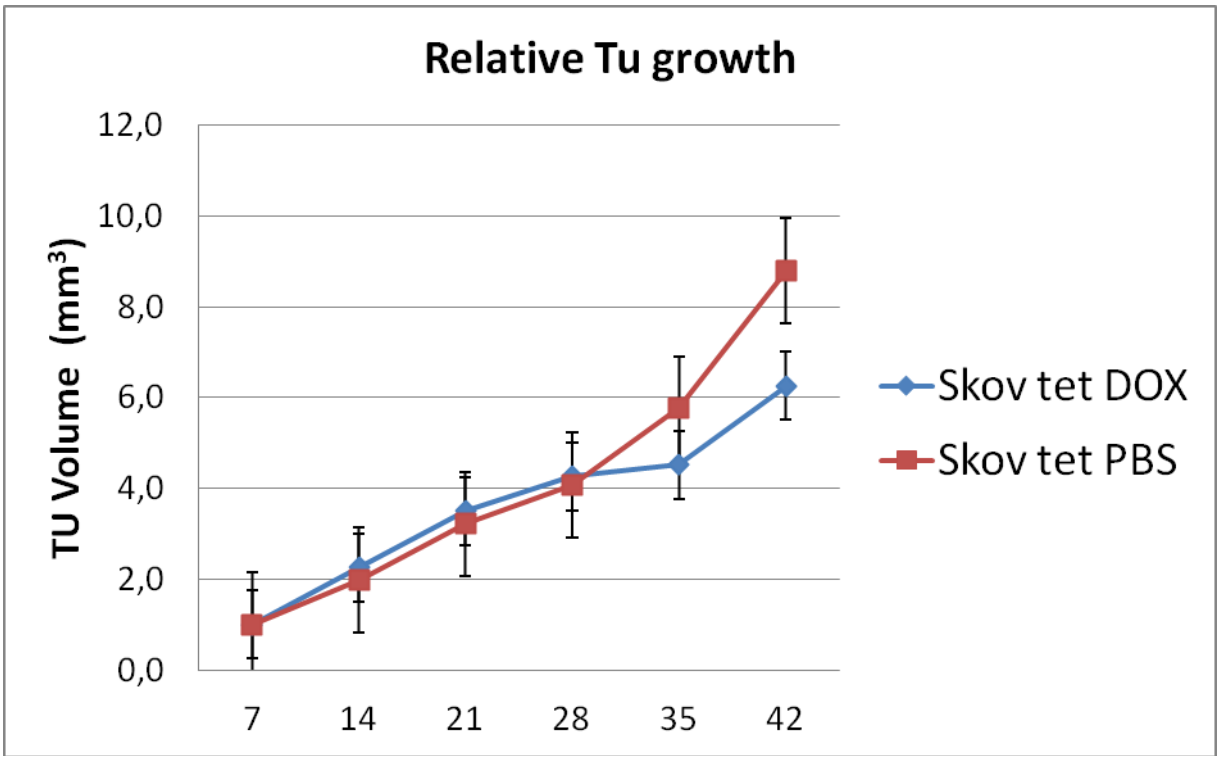

(B)

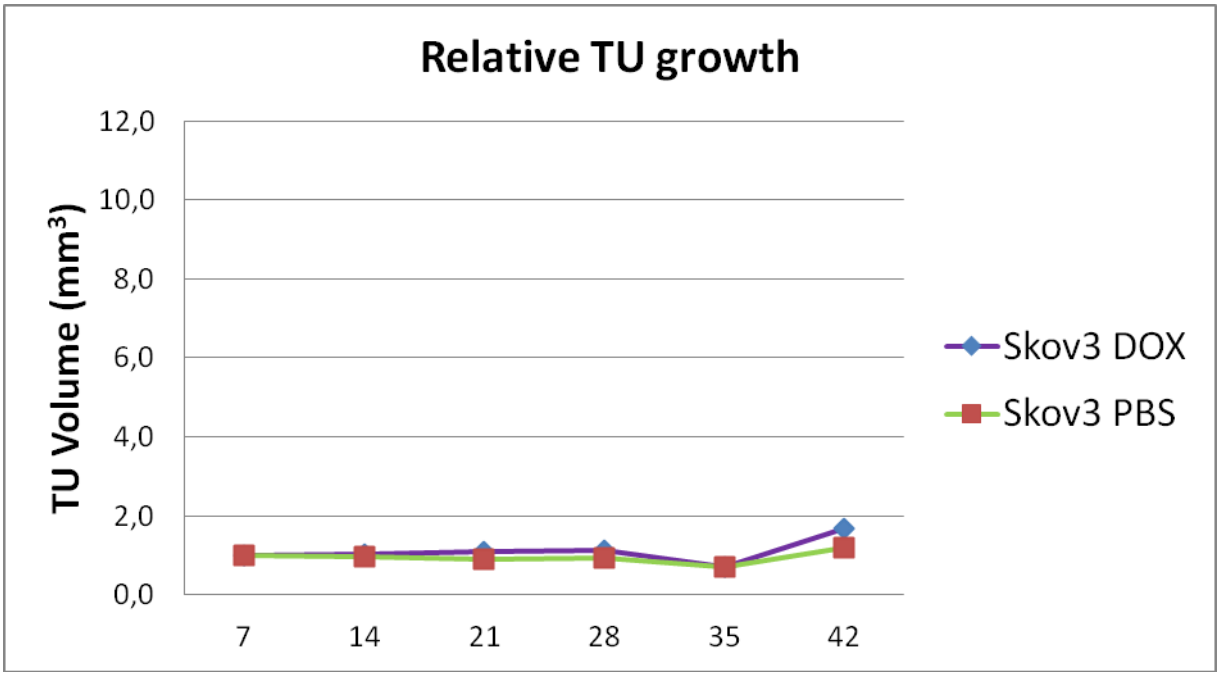

Figure 18: (A) *In vivo* growth of HCRP1 knock-down cells. Tumors arising from HCRP1 knock-down Skov3 cells showed elevated growth compared to un - induced Skov tet cells. Relative tumor growth (x-fold volume initially measured) is depicited

against time (days). Tumor growth was measured weekly. (B) Control mice with injected Skov3 cells treated with PBS/DOX did not show elevated growth.

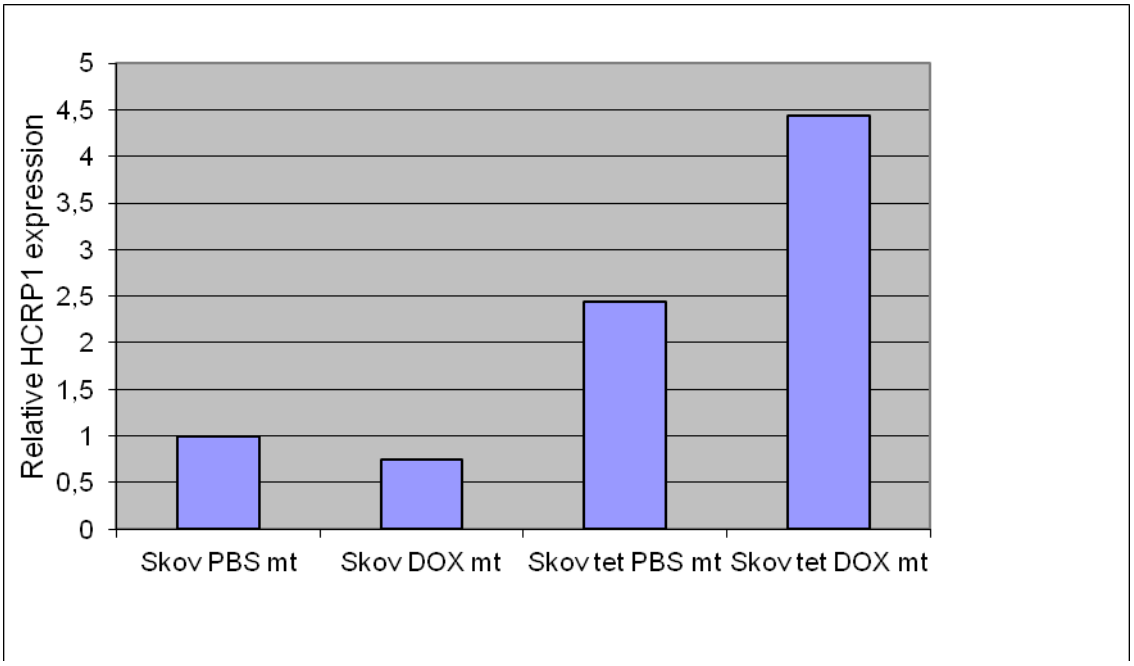

Figure 19: qPCR analysis of HCRP1 mRNA levels of mouse xenograft tumors resulting from injected Skov3 - and Skov3 tet cells treated with PBS/ DOX (1µ/µl) (Skov3 (tet) mt). PBS treatment of mice with injected Skov3 tet cells should induce HCRP1 knock down whereas HCRP1 levels of tumors originating from Skov3 (PBS and Dox treated) and Skov3 tet Dox treated cells should be about the same. This is true for Sko3 tet cells treated either with Dox or PBS, although the observed knock down was not as significant as it was shown in *in vitro* experiments with Skov3 and Skov3 tet cells before (see Figure 10). HCRP1 mRNA levels of Skov3 PBS and Dox treated cells were quite low which might result from problems with mRNA isolation.

(A)

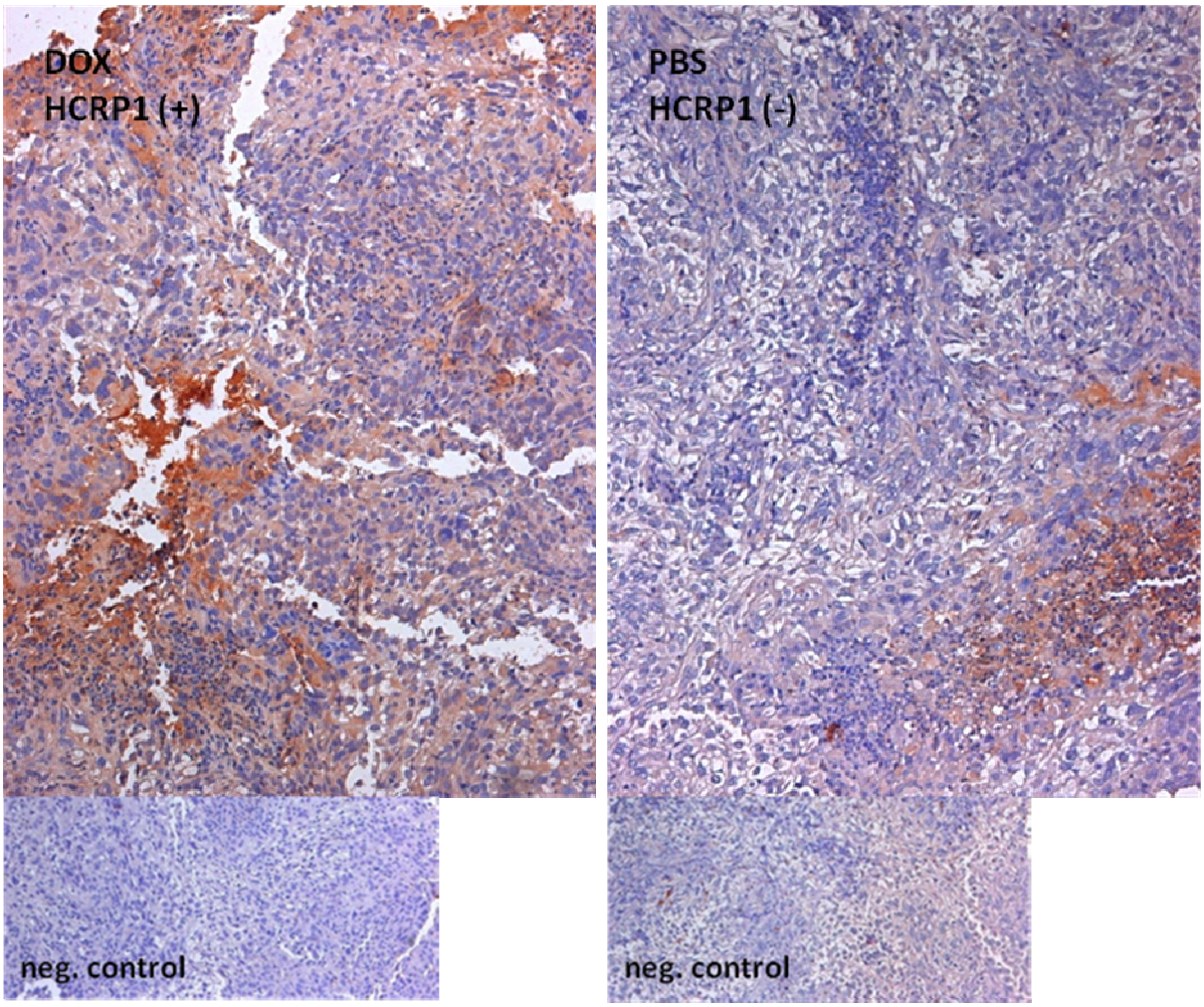

(B)

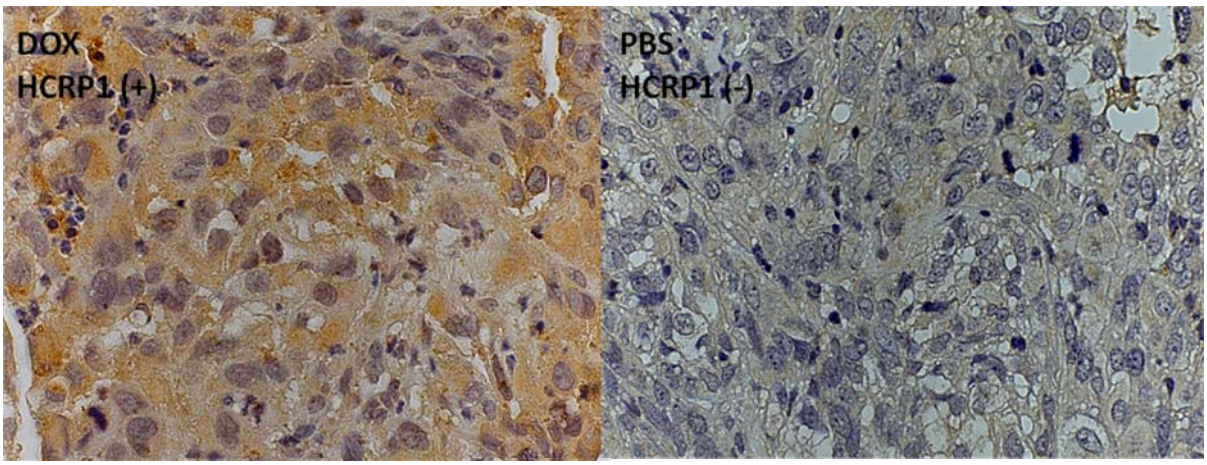

Figure 20: Formalin paraffin – embedded mouse tumor (subcutaneously injected Skov3tet cells, sections were immunostained with the HCRP1 specific monoclonal antibody. Tumors from mice treated with DOX (125µg/day) showed normal (HCRP1

(+)) HCRP1 levels whereas PBS treated mice should displayed reduced HCRP1 expression (HCRP1 (-)). (A) shows stainings from mice treated with DOX (left) and PBS (right) with corresponding control staining where no antibody was used. Magnification 10x (B) shows stainings from mice treated with DOX (left) and PBS (right). Magnification 40x

In the tumors arising from the xenografts, cellular proliferation was not significantly affected as determined by a Ki67 assay (see figure 21). However there were significantly decreased apoptosis rates for the HCRP1 knockdown tumors (see figure 22). Hence this suggests that enhanced tumor growth can be explained by sustained survival rather than by elevated proliferation.

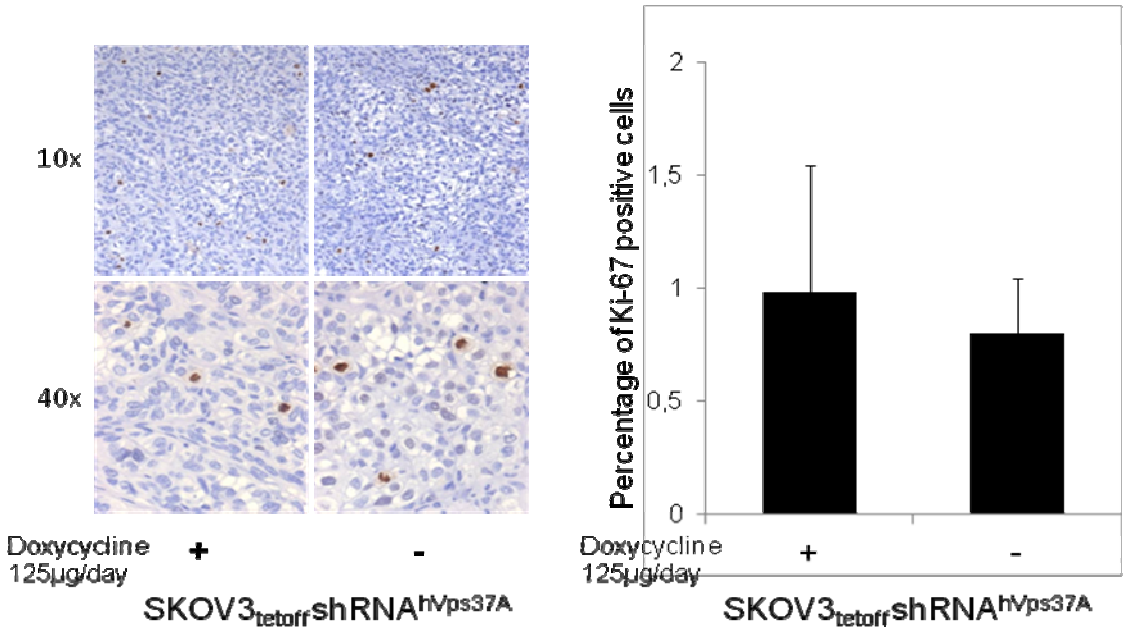

Figure 21: (A) Ki-67 stainings in the mouse xenograft model. The left panel shows representative Ki-67 stainings (magnification 10x and 40x). The right panel shows a quantitation (percentage) of Ki-67 cells. Error bars indicate +/- SEM.

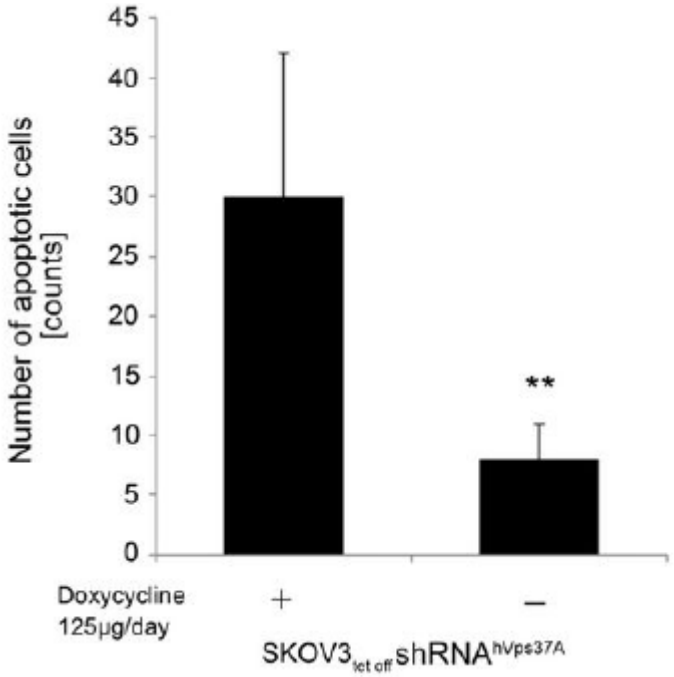

Figure 22: Average counts of apoptotic cells in tumors examined. Error bars indicate +/- SEM.

2.7. Challenging titration of a novel monoclonal HCRP1 antibody

Preliminary experiments were performed with a polyclonal HCRP1 antibody. After selecting the following peptide sequence MSPYASQGFPFLPPY a monoclonal antibody against this peptide was produced and affinity purified by Eurogentec (Seraing, Belgium). TMA stainings were repeated with the new antibody (described below). Mouse Xenograft tumors, Skov3 HCRP1 knock down cells and MDAH – 2774 cells were stained with the novel antibody. Multiple staining conditions have been tested in order to get an optimized and reproducible protocol. Figure 23 shows different staining protocols with either too high ((A) 1:500) or too low ((B) 1:2000) antibody concentration. Figure 29 shows results of the TMA stained with the finally established protocol.

.

(A)

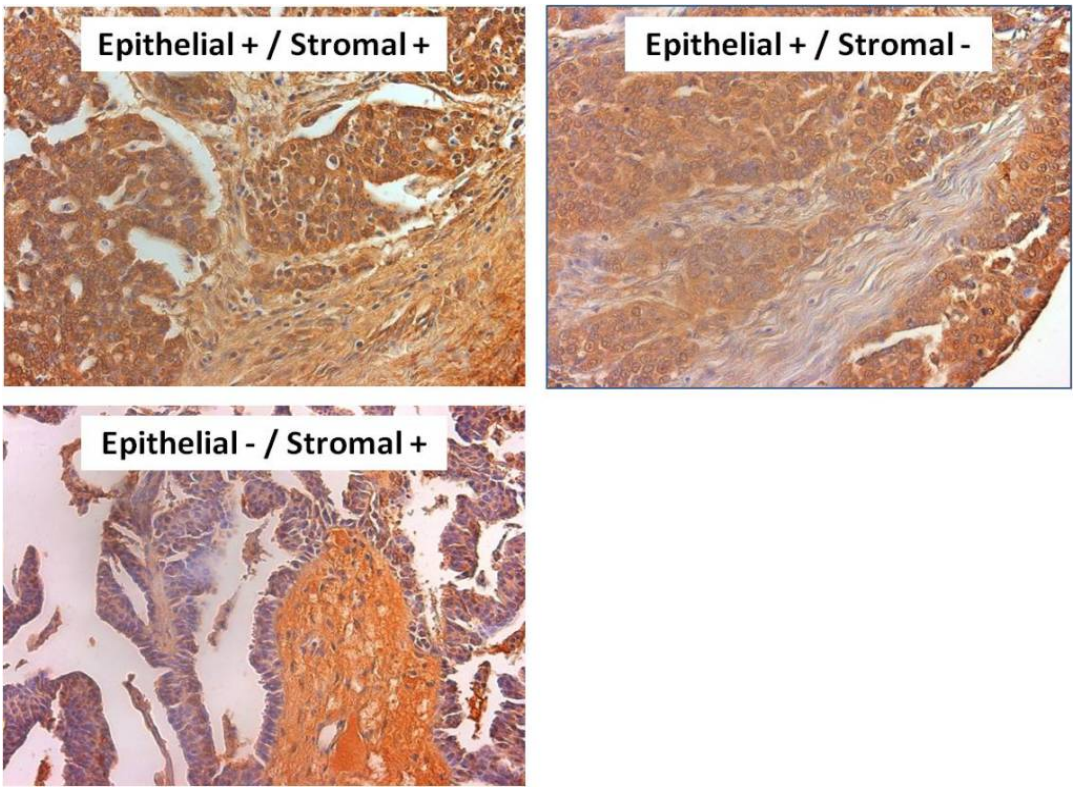
Epithelial + / Stromal +
Epithelial + / Stromal -
Epithelial - / Stromal +

(B)

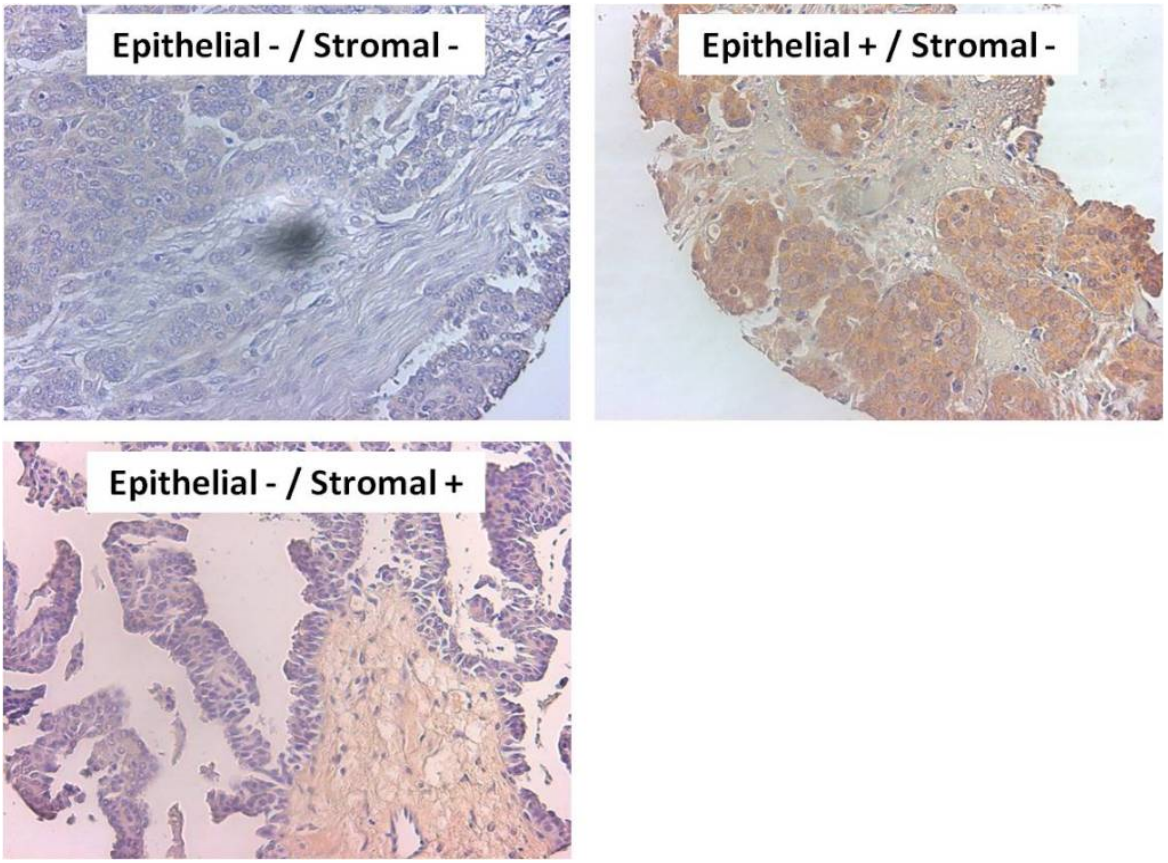
Epithelial - / Stromal -
Epithelial + / Stromal -
Epithelial - / Stromal +

Figure 23: (A) Titration of the monoclonal HCRP1 antibody. Pictures show examples of a TMA staining attempt which was over - stained (used antibody concentration: 1:500). Not a single slide showed negative staining and there was no negative control. (B) Pictures show examples of a TMA staining attempt which was stained to weak (used antibody concentration: 1:2000). There was not a single slide which showed strong epithelial staining. Some slides were absolutely negative.

Antibody titration for Western blotting was quite more challenging. Several antibody concentrations were tested in order to establish a reproducible protocol (data not shown). Also various and long washing steps especially between first and second antibody were crucial in order to avoid strong background signals (further details see Materials and Methods). Unfortunately although the antibody eventually gave clear and strong HCRP1 signals, there was no clear difference observed between the various Skov3 cells with the inducible HCRP1 knock down system (discussed in detail below). HCRP1 protein detection by Western Blotting from mouse xenograft tumors did not show reasonable results, as there was no coherent difference between the samples and bands were smeary (discussed in detail below; see Figure 25). On the other hand, MDAH – 2774 cells with stable HCRP1 knock down showed clear differences in HCRP1 protein level compared to MDAH – 2774 “wild type” cells (see Figure 25; 26; 27). This suggests that detection difficulties of HCRP1 knock down in Skov3 tet cells is not only caused by problems with the novel established protocol but due to problems with the inducible tet off – system. Further protocol establishment and inducible tet – system analysis is discussed below in “HCRP1 protein and mRNA detection in Skov3 cells with inducible HCRP1 knock down system – Challenges and trouble - shooting”.

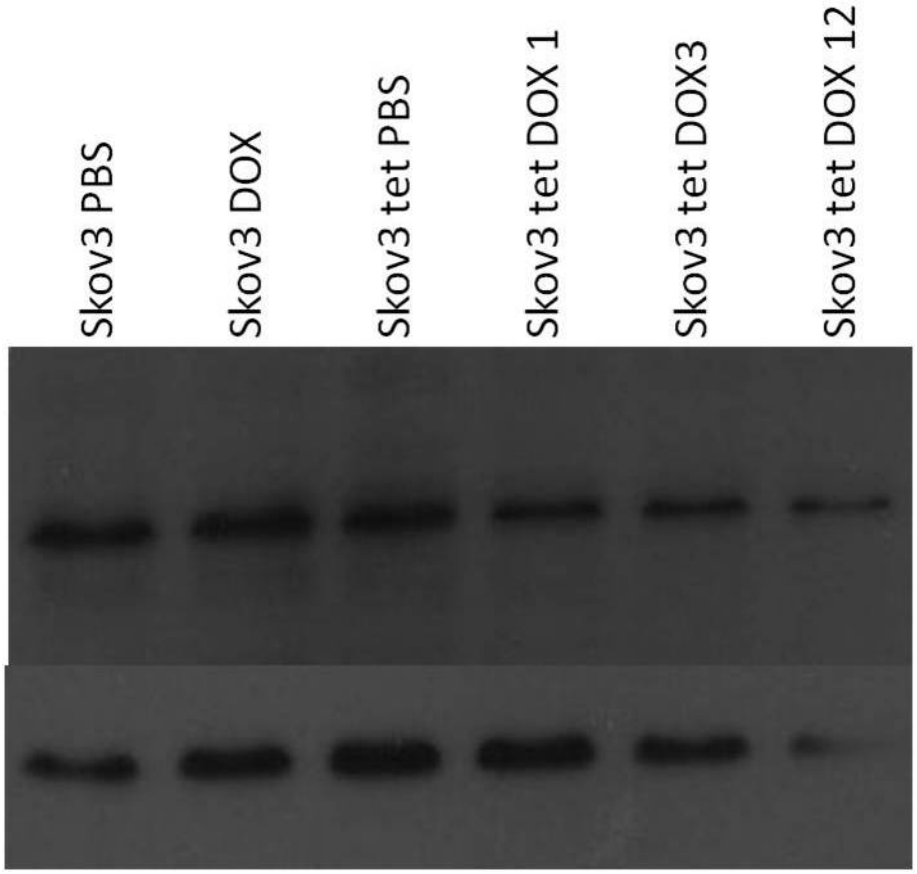

Figure 24: Western blot of Skov3 and Skov3 tet cells treated with PBS/DOX (numbers indicate used Dox concentration 1µ/µl etc.). For this WB the finally established protocol has been used. Upper line shows HCRP1 expression, bottom line corresponding actin detection. Although the established protocol resulted in a clear signal, there was no difference observed between the different samples.

(A)

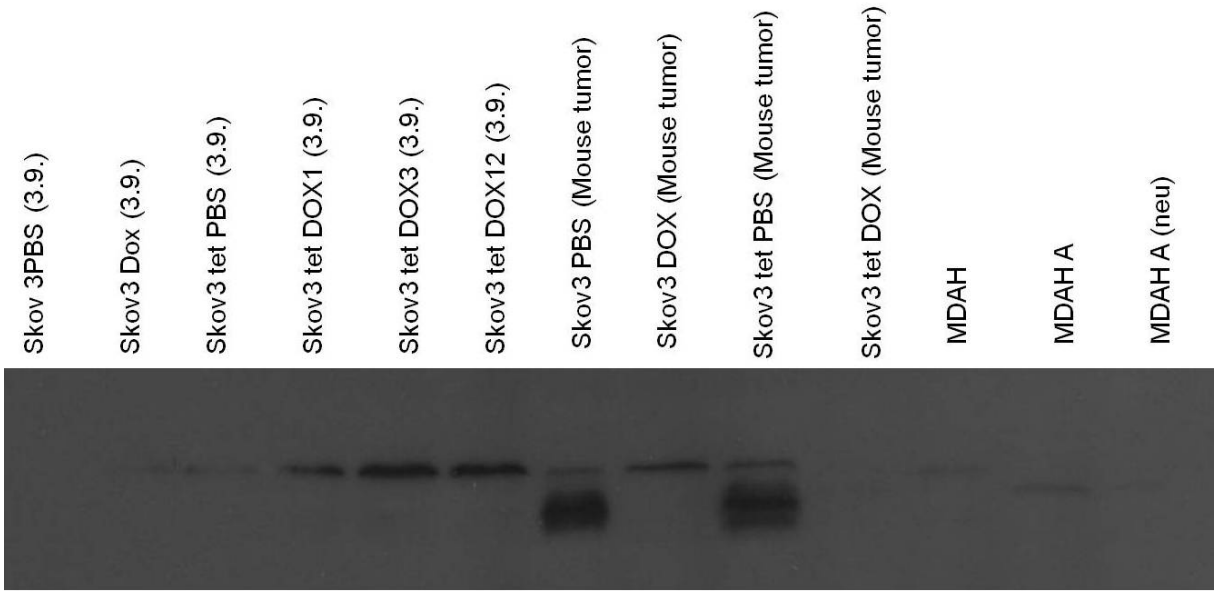

(B)

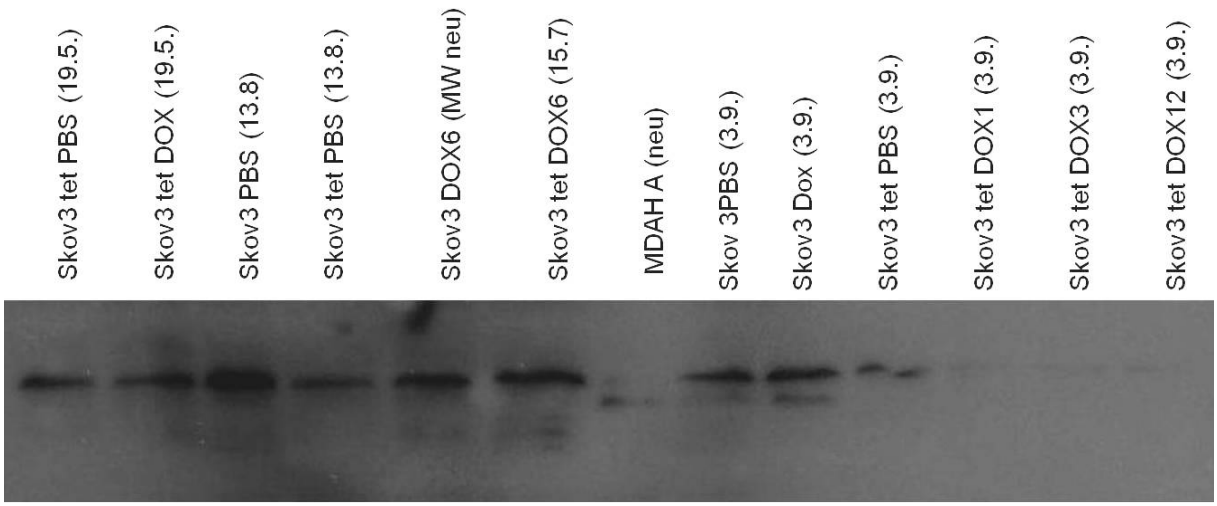

Figure 25: Western Blot with the monoclonal HCRP1 antibody showing no clear difference between Skov3 tet PBS and Dox cells due to problems with the inducible HCRP1 system. MDAH cells with stable knock down of HCRP1 show reduced protein expression. Mouse tumor tissue samples show smeary bands. This figure shows WB with Skov3 and Skov3 tet cells treated with PBS/DOX (numbers indicate used Dox concentrations 1µ/ml etc.), MDAH cells and Skov3/Skov3 tet cells from the mouse xenograft model (A) and (B).

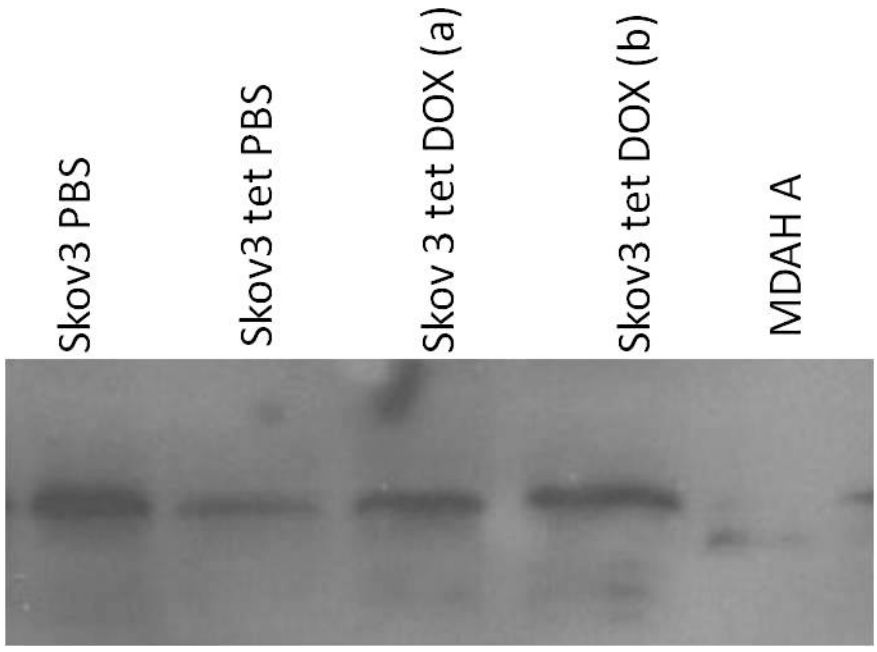

Figure 26: WB with HCRP1 antibody of Skov3, Skov3 tet (cell batches (a) and (b)) and MHAD- 2774 A cells with stable HCRP1 knock down. There is a clear difference between the Skov3 cells and MDAH knock down cells and a weaker but clear difference between Skov3 (PBS) cells, Skov3 tet PBS (with HCRP1 knock down) and Skov3 tet DOX cells, whereas the difference between Skov3 tet PBS and Skov3 tet Dox (b) is stronger than compared to batch (a).

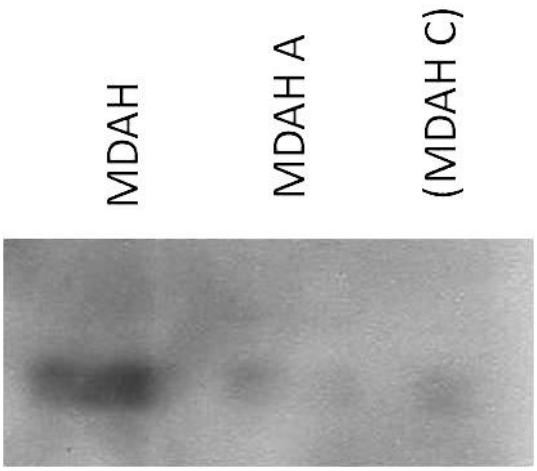

Figure 27: Western Blott with HCRP1 monoclonal antibody, showing prober knock down in stabely transfected MDAH cells (MDAH A and MDAH C, are both stabely transfected cells, but derive from different clones).

(A)

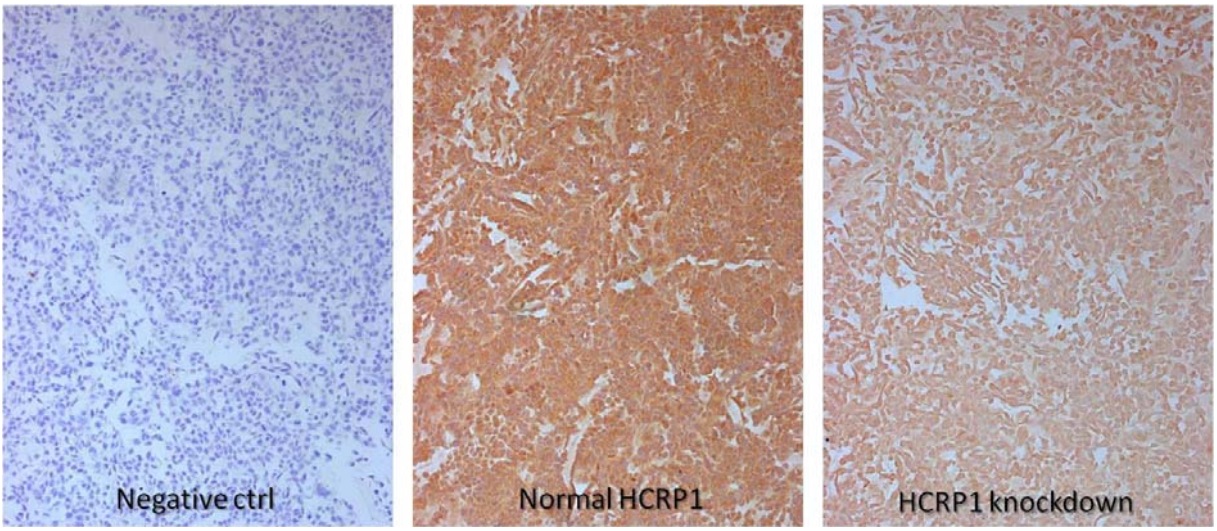

(B)

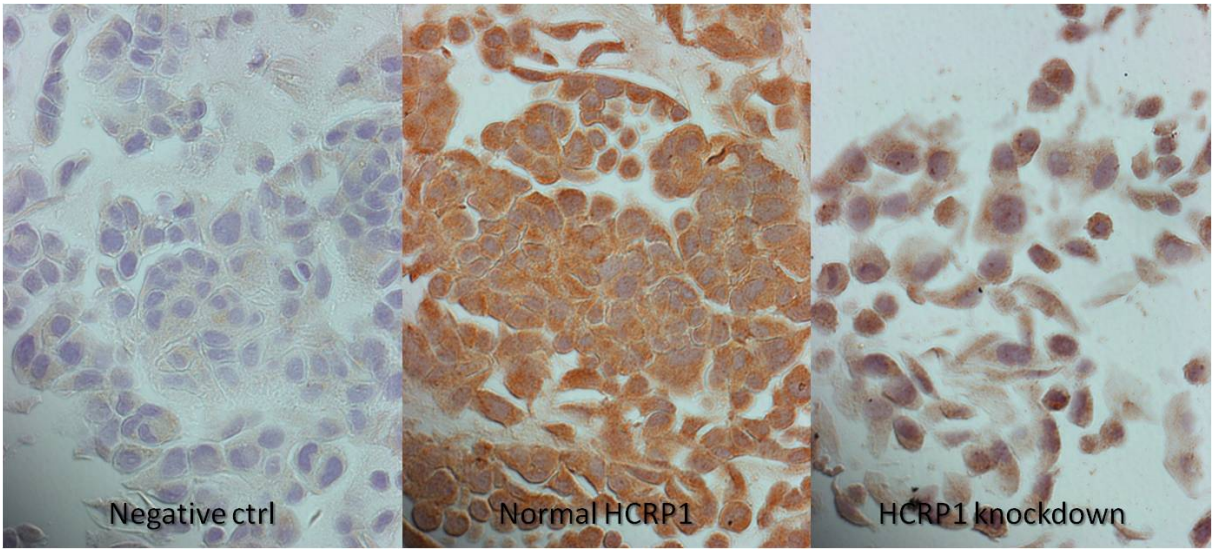

Figure 28: IHC of MDAH (normal HCRP1; middle picture) and MDAH (HCRP1 knock down; right picture) cells with stable HCRP1 knock down with HCRP1 monoclonal antibody; used dilution 1:5000, magnification 10x (A) and 40x (B), The left picture displays the negative control without antibody.

2.8. HCRP1 protein and mRNA detection in Skov3 cells with inducible HCRP1 knock down system – Challenges and trouble - shooting

As mentioned above, several problems occurred during titration of the novel monoclonal HCRP1 antibody. Figures 25 -28 show several WB with Skov3 (PBS and Dox treated), Skov3 tet (PBS and Dox treated) and MDAH – 2774 “wild type” and knock down cells. Skov3 cells were cultivated with Dox or PBS in order to see if Dox influences HCRP1 expression in general. It was shown that neither protein level, nor HCRP1 mRNA level were influenced by Dox treatment. MDAH – 2774 cells with stable HCRP1 knock down showed a clearly reduced HCRP1 protein level. This suggests that problems which occurred with the inducible HCRP1 system in Skov3 tet cells is not caused by technical problems. One possibility is the fact that the cells used for protein and RNA extraction were kept in culture for too long. Multiple cell passages and constant HCRP1 knock down caused by insufficient Dox treatment can lead to altered gene expression and hence potential compensatory mutations. I tested various Doxycycline concentrations of 0,5; 1; 2; 3; 6 and 12 µg/µl (data for concentrations 0,5; 2 and 6 µg/µl not shown) which did not cause different HCRP1 protein levels. As a result I thawed fresh aliquots of cells and repeated the

experiments. This time qRT PRC results for HCRP1 in Skov3 (tet) cells led to reasonable results, showing significant HCRP1 knock down (as previously shown in figure 10). This finding confirms proper HCRP1 knock down in Skov3 tet cells. HCRP1 detection by WB is still challenging, also regarding the fact that stripping of the membrane and following Actin antibody staining hardly led to satisfying results as there was always a high background signal (figures not shown). Currently I am further improving the Western blot protocol.

2.9. HCRP1 in Ovarian cancer patients – Tissue Micro Array analysis

As standards for our tissue micro array, ovarian tissues with normal epithelium were taken as positive controls and tissues stained without primary antibody were taken as negative control. It was observed that the normal ovarian epithelium showed specific positive HCRP1 expression while no staining was seen in the negative control (see figure 29).

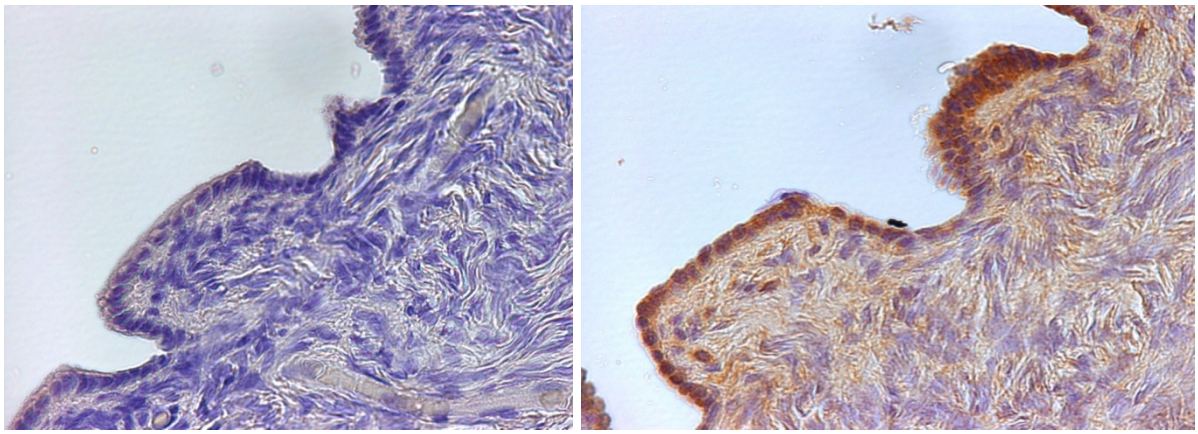

Figure 29: Immunhistochemical staining of ovarian tissue with the HCRP1 monoclonal antibody staining with the HCRP1 monoclonal antibody, left negative control, right brownish staining of epithelial structure (magnification 40X).

After titration of the novel HCRP1 antibody and establishment of a proper protocol TMAs were stained with the new antibody. The TMAs comprising 125primary tumor samples and 19 borderline tumors spotted in triplicates with corresponding normal tissue were previously stained with EGFR and HER2 as these two receptors represent well known markers in ovarian cancer. Representative stainings are given below.

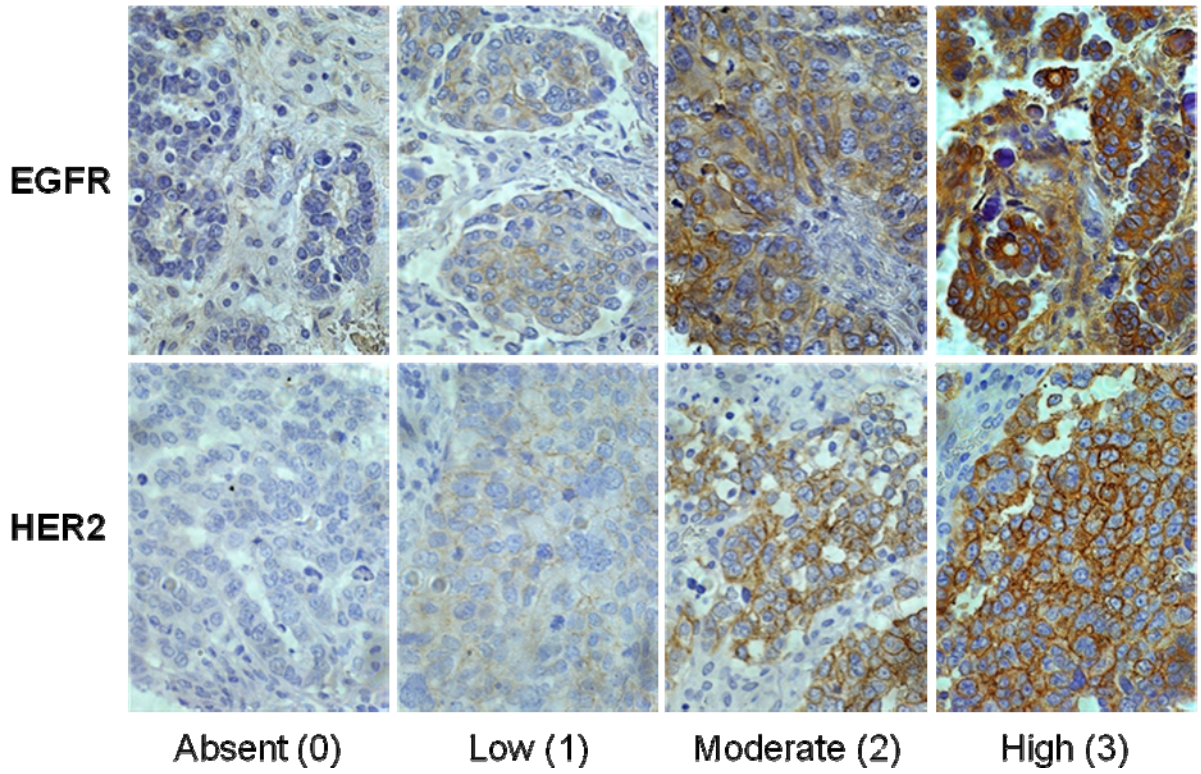

Figure 30: Tissue microarrays of 125 primary ovarian tumor samples and 19 borderline tumors, with corresponding normal tissue were stained for EGFR and HER2. Stainings were graded according to their intensity: 0 (absent); 1 (low), 2 (moderate) and 3 (strong).

As shown by others before (Pils et al., 2007) elevated expression of these oncogenes is associated with negative outcome for patients and their overall survival rate (data not shown). According to their HCRP1 expression patients were subdivided into two groups, whereas a quite high percentage of patients (62%) showed low or missing HCRP1 expression (see table 2 and 3). Representative HCRP1 stainings graded according to their intensity are given below.

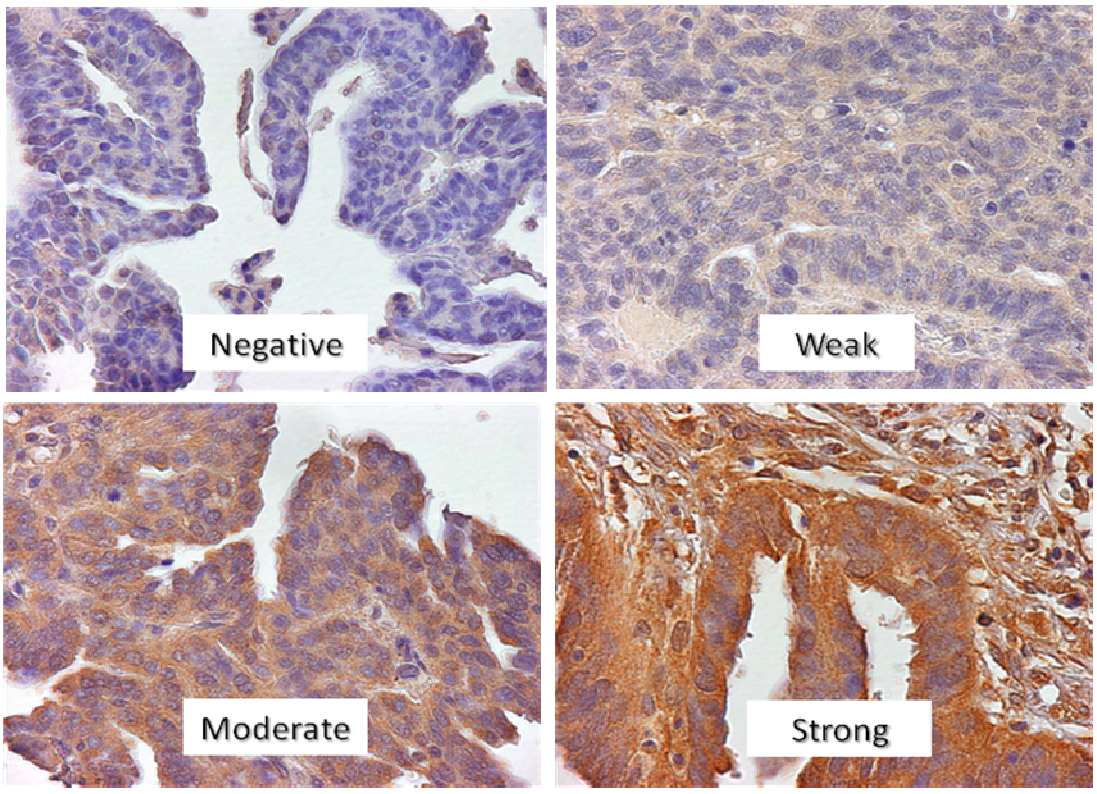

Figure 31: Tissue Micro array of 125 primary ovarian tumor samples and 19 borderline tumors, with corresponding normal tissue were stained with HCRP1 antibody. Staining intensity was determined on a scale of 0 to 3, with 0 for “negative”, 1 for “weak”, 2 for “moderate” and 3 for “strong” staining. (magnification40X)

Comparing HCRP1 mRNA levels of an “independent cohort” of 115 ovarian cancer patients (PT) and 20 age matching controls (N; normal) showed lower expression in ovarian cancer when compared normal ovarian tissue.

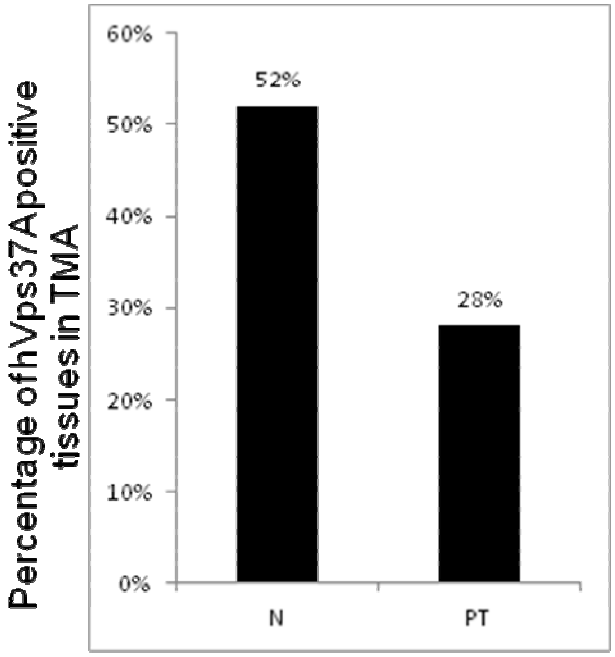

Figure 32: Quantification of HCRP1 expression in ovarian tissue micro arrays percentage of hVps37A positive cases in the benign (N) and ovarian cancer (PT) tissues

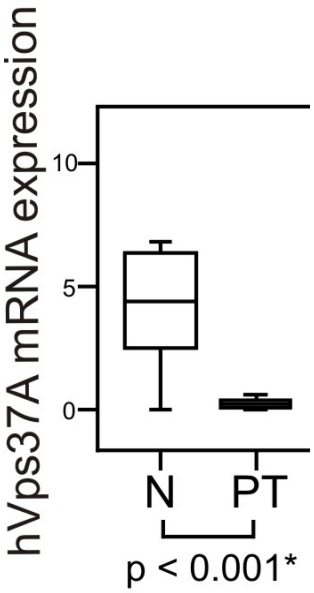

Figure 33: hVps37A mRNA expression in tumor tissue of 115 ovarian cancer patients (PT) and 20 age matched normal controls (N); a Student's t-test was used to compare mean mRNA expression levels of hVps37A.

Table 2	**Tissue Microarray**	**RNA**
Patients' characteristics	**N (percent)**	**N (percent)**
Type		
Normal ovaries		20
Primary tumors	125	115
Recurrent tumors		
Borderline tumors	19	
Grade	117 (8 missing)	114 (1 missing)
1	20 (17.1)	3 (2.6)
2	26 (22.2)	52 (45.6)
3	71 (60.7)	59 (51.8)
FIGO	125	113 (2 missing)
I	31 (24.8)	19 (16.8)
II	14 (11.2)	10 (8.9)
III	72 (57.6)	59 (52.2)
IV	8 (6.4)	25 (22.1)
Histology	125	115
Serous	70 (56.0)	70 (60.9)
Non-serous	55 (44.0)	45 (39.1)

Table 3 **Immunohistochemical staining**

hVps37A	No of Patients
high	55
low	89

	hVps37A	
	high	**low**
EGFR		
high	39	44
low	16	45
HER2		
high	14	25
low	41	64
Grade		
1	8	12
2	11	15
3	30	41
FIGO		
I	14	33
II	7	7
III	31	44
IV	3	5
Histology		
Serous	29	41
Non-serous	24	31

2.10. HCRP1 expression in pancreatic, lung and oral cavity cancer

As a next step I looked at HCRP1 expression in pancreatic (figures not shown), lung and oral cavity cancer in order to see if individual patients express different levels of HCRP1. I could observe varying HCRP1 expression levels in all three kinds of cancer. Figure 34 shows representative stainings of two lung cancer patients. Samples from patient number one display almost negative stromal staining, whereas

the tumor shows moderate HCRP1 expression. In contrast patient number two shows strong HCRP1 staining in tumor and stromal tissue.

(A)

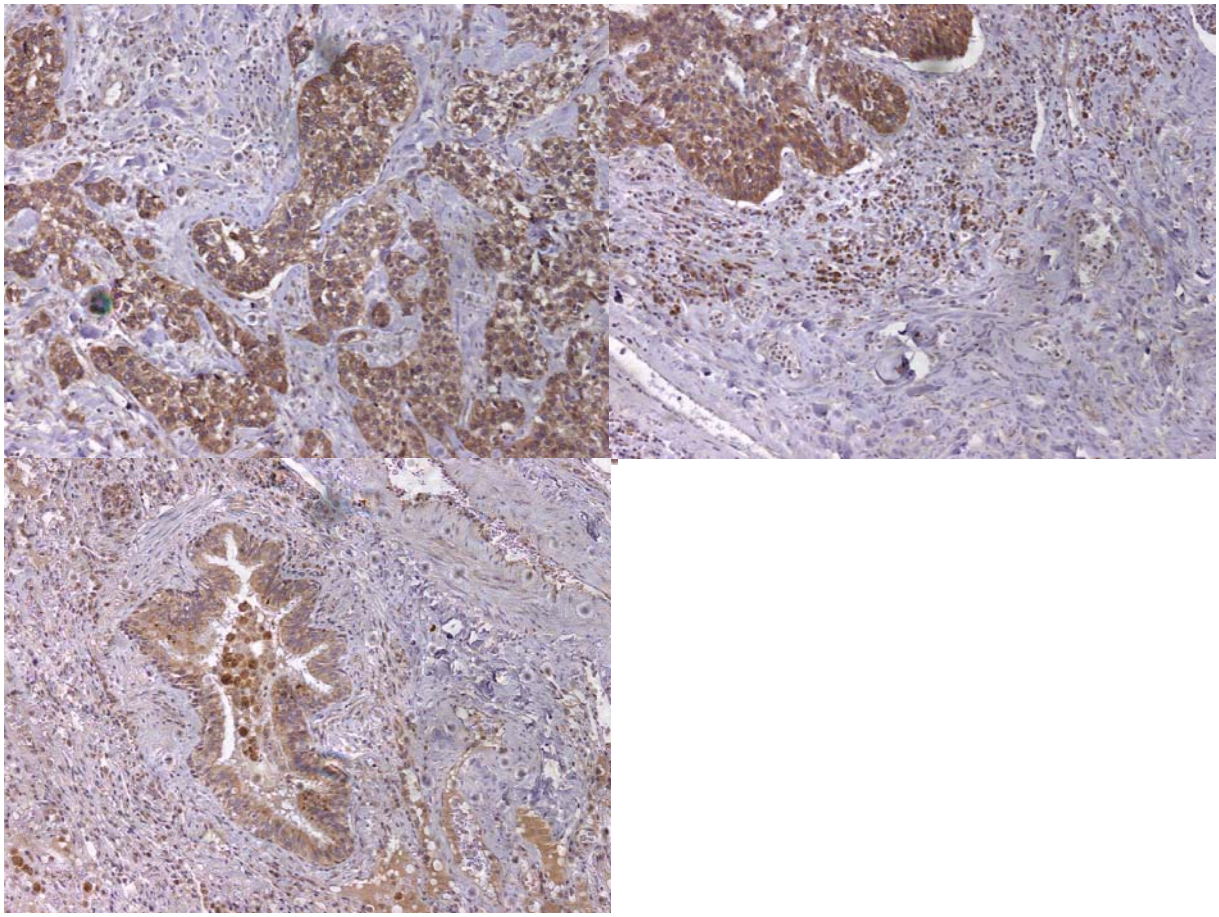

(B)

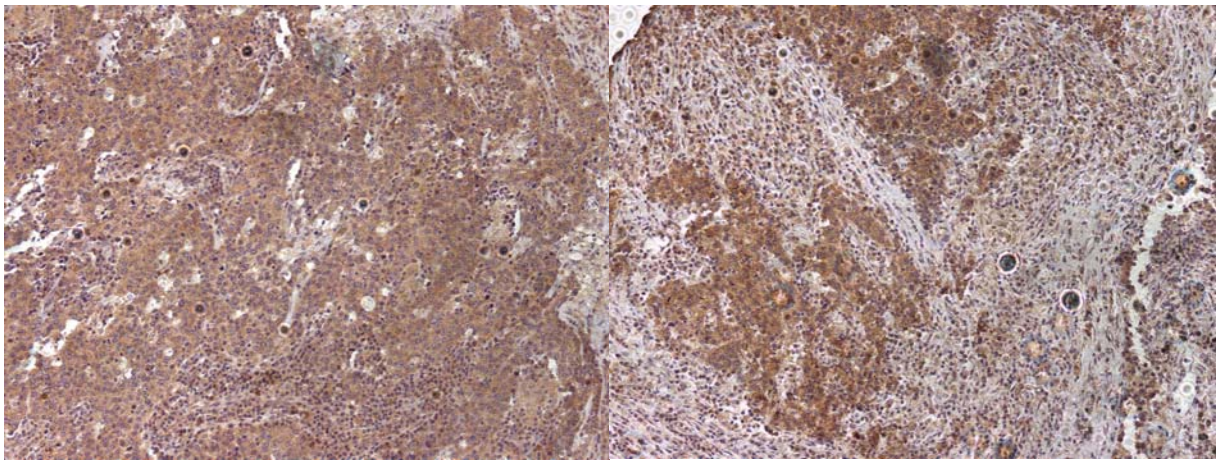

Figure 34: HCRP1 stainings of lung cancer patient tissue. (A) Patient number one shows moderate HCRP1 staining in the tumor and almost negative stromal staining. The lower picture shows stained epithelial structure. (B) Patient number two shows strong HCRP1 expression in both tumor and stroma.

A cohort of 111 oral cavity cancer patients was analyzed for their HCRP1 expression using Immunhistochemestry. Figure 35 shows representative stainings of samples with staining intensities weak (1), moderate (2) and strong (3). As a result 18% of the analyzed patients showed weak HCRP1 expression. Interestingly these patients displayed a more negative clinical outcome when compared to patients with normal or high HCRP1 expression (statistical data not shown) confirming previous findings that low HCRP1 expression is linked to a more negative course of disease.

(A)

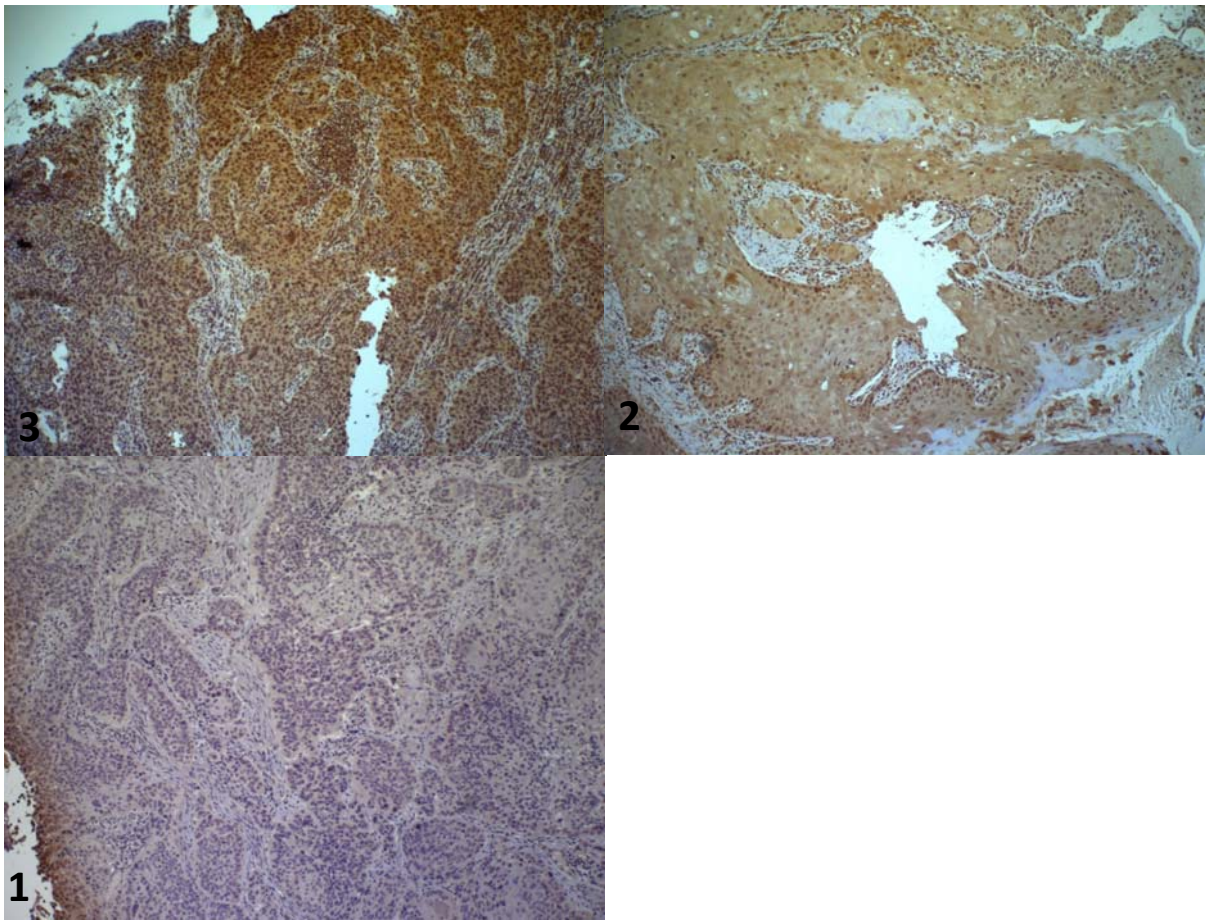

(B)

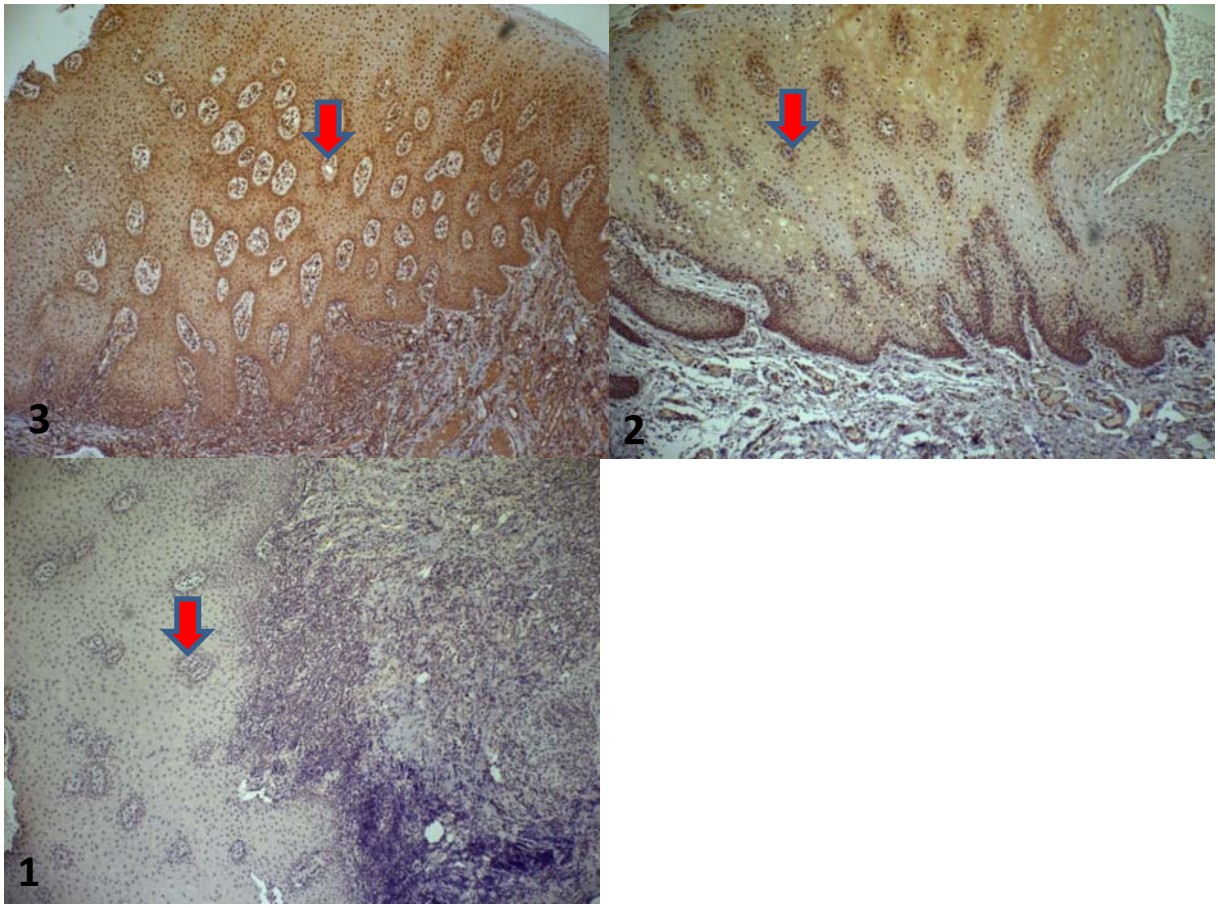

Figure 35: HCRP1 stainings of oral cavity cancer patient tissue. (A) shows representative stainings with weak (1), moderate (2) and strong (3) HCRP1 staining intensity in tumors. (B) shows weak (1), moderate (2) and strong (3) HCRP1 staining of epithelial structures. Arrows indicate ducts.

3. Discussion

Deregulated activation of ErbB family growth factor receptors is associated with tumor development due to enhanced cell proliferation and invasiveness. As this hyperactivation is often a result of dysfunctional receptor degradation, the ESCRT complex member HCRP1, which is crucial for proper receptor degradation via endosomal sorting, is a promising target for anti cancer therapy. Upon ligand binding RTKs are phosphorylated at distinct residues located in their cytosolic domains. Interestingly, receptors targeted for ESCRT mediated degradation are still capable to

continue signaling due to the cytosolic orientation of the phosphorylated tail structures. This effect is probably even further increased by the cytoplasmatic retention of pEGFR (Pennock and Wang, 2003). We observed elevated levels of ErK1/2 in HCRP1 knock down cells, whereas basal Akt phosphorylation remained unchanged. This may result from the fact that pEGFR located in the endosome is not able to activate PI3K signaling whereas other pathways stay unaffected (Haugh and Meyer, 2002).

The EGFR family is a key therapeutic target in many kinds of cancer, including ovarian cancer and holds great promise for personalized cancer treatment, as the main goal in personalized medicine is to target the individual underlying molecular and biological deficiencies of a patient. Two types of inhibitors are currently used in clinical trials treating ovarian cancer, monoclonal antibodies (mAb) and small molecule tyrosine kinase inhibitors (TKI) (Arteaga, 2002; Palayekar and Herzog, 2008; Siwak et al.). Due to their low efficiency in phase I and II trials (Kimball et al., 2008; Sheng and Liu), the application of several therapies targeting EGFR has been limited. As the loss of HCRP1 leads to enhanced selective advantages in tumor cells, these cells could be more sensitive to EGFR targeted therapy by the usage of mAb and small TKI. Cetuximab, an IgG1 monoclonal antibody targeting EGFR, has been extensively studied in ovarian cancer but was shown to be ineffective in several phase II trials (Konner et al., 2008; Schilder et al., 2009; Siwak et al.). Some other TKIs and MAbs (erlotinib, matuzumab, trastuzumab, pertuzumab, CI-10337) used in ovarian cancer studies have also yielded disappointing response rates of 0–7% (Konner et al., 2008). Cetuximab was shown to inhibit EGFR signaling by competing with endogenous ligands, resulting in stalled cellular growth and division as well as angiogenesis, invasiveness and metastasis (Fan et al., 1993; Konner et al., 2008; Petit et al., 1997; Prewett et al., 1998). Another mechanism to interfere with EGFR activity, is antibody dependent cellular cytotoxity (ADCC), which is an immune response against the Fc - region of antibodies (Peipp et al., 2008).

The inhibitory effect on EGFR signaling by Cetuximab is abolished by loss of HCRP1. Resistance to anti EGFR therapy can be caused by several mechanisms including autocrine EGR activation, mutation of downstream signaling effectors and cross activation of alternative RTKs. It was shown that cells resistant to cetuximab

expressed elevated levels of steady state EGFR secondary to alterations in trafficking and degradation as well as an elevated activation of HER2, HER3 and cMET. Additionally, enhanced EGFR expression led to increased dimerization with HER2 and HER3 followed by their transactivation, whereas blockage of EGFR and HER2 caused loss of HER3 and stalled PI(3)K/Akt activity (Wheeler et al., 2008). Studies in Cetuximab resistant cancer cell lines after long term exposure showed increased EGFR levels resulting from dysfunctional receptor degradation (Wheeler et al., 2008).

Our HCRP1 knock-down system, which showed Cetuximab resistance, confirmed this study and is hence a potential model for pre-existing Cetuximab resistance in advanced ovarian cancer. In HCRP1 knock-down cells treated with Cetuximab, the MAPK – and Akt- pathway remained active, compared to cells treated with Lapatinib where the MAPK – and PI3K/Akt pathways are inhibited. This indicates that the EGFR- Cetuximab complex is still actively signaling, resulting in resistance to Cetuximab, whereas Lapatinib directly blocks EGFR activation by targeting the ATP – binding domain, leading to abolished EGFR signaling independent from ESCRT mediated receptor down regulation (Xia et al., 2002) and hence HCRP1 expression.

An important step was the generation and characterization of the novel and improved monoclonal HCRP1 antibody in order to establish reproducible protocols for further research. During this process I unfortunately observed that although I could detect clear HCRP1 signals in immunoblotting experiments, there was no strong difference between cells with or without HCRP1 knock-down. In line with the protein data, HCRP1 mRNA levels quantified with qRT PCR equally led to such results. Possible explanations for this could be that either the inducible system got leaky or that the cells had been in culture for too long leading to a change in gene expression. I also tested different Doxycycline (Dox) concentrations in order to observe the influence of various levels of Dox treatment on the inducible tet system - still I could not detect a clear HCRP1 knock-down. Interestingly, immunhistochemical staining showed reasonable results, displaying clear differences between xenograft tumor samples (tumors from injected Sov3 (tet) cells) and MDAH – 2774 “wild type” and knock-down cells. This indicates that the monoclonal HCRP1 antibody is working properly for stainings, suggesting that problems with RNA and protein sample preparation might

have caused detection problems. In line with this, freshly thawed cells showed reasonable and significant HCRP1 knock-down measured on mRNA level by qRT PCR, confirming that the inducible system is working properly. Though there have still been problems with HCRP1 detection with Western Blotting and this discrepancy between mRNA and protein levels on the one hand, and differences in protein detection between IHC stainings and western blotting using the same antibody will be addressed in future experiments. The results presented in this thesis demonstrate that loss of HCRP1 leads to enhanced invasive potential of cells *in vitro* and increased tumor growth *in vivo*.

I used the Inducible HCRP1 system in order to observe the impact of HCRP1 knock down on tumor formation in a mouse xenograft model. Mouse groups with injected Skov3 tet cells displayed a significant difference in tumor growth. This certifies our thesis that HCRP1 knock down enhances tumor growth *in vivo.* Two mouse groups with injected Skov3 cells (treated with PBS or DOX) served as control groups to see a possible effect of Dox treatment on tumor growth in general. Both control groups showed equal growth suggesting that there is no effect on tumor growth in general. As a next step additional mouse experiments including groups treated with Cetuximab and TKI would be required to strengthen our finding that the inhibitory effect on EGFR signaling by Cetuximab is abolished by HCRP1 knock down. As determined by a Ki67 assay cellular proliferation of tumors was not significantly affected, however tumors with HCRP1 knock down displayed significantly decreased apoptosis rates. These findings assume that enhanced tumor growth is caused by sustained survival rather than elevated proliferation.

Additionally, we could also observe that HCRP1 protein expression levels are often reduced in primary ovarian tumors. Overall, EGFR is overexpressed in 60% of ovarian cancers (Dimova et al., 2006; Lin et al., 2009) and this is associated with poor clinical outcome for ovarian cancer patients (Sheng and Liu; Siwak et al.). Furthermore it was shown that stimulation of human ovarian cancer cell lines with EGF resulted in significantly increased expression of proteins involved in invasion and altered signaling of pathways associated with angiogenesis (Henic et al., 2006; Liu et al., 2006). We found that HCRP1 has a strong impact on the prognostic value of EGFR and HER2; while both of these oncogenes can be highly accurate

prognostic markers this is actual only the case when HCRP1 is highly expressed. In contrast under conditions of low HCRP1 expression this prognostic value is lost. Therefore, further analysis of HCRP1's role as a novel player in EGFR and HER2 mediated ovarian cancer holds great promise for personalized cancer treatment and prognosis.

As already mentioned, hyperactivation of EGFR and dysfunctional receptor degradation is found in many kinds of cancer (Holbro et al., 2003; Hynes and Lane, 2005; Sibilia et al., 2007; Yarden, 2001). Stained Tissue micro arrays for HCRP1 expression show that HCRP1 levels are elevated compared to normal ovarian tissue. We further observed that there is a strong impact of the two cancer markers EGFR and HER2 on the overall survival of ovarian cancer patients but only in cases with normal (high) HCRP1 expression. This prognostic value is lost in patients with low HCRP1 knock down. As a step beyond ovarian cancer, we looked at HCRP1 expression and addressed possible correlations between protein expression level and clinical outcome and prognosis in different kinds of cancer. Therefore we tested HCRP1 expression among several patients with pancreatic, lung and oral cavity cancer. We found a significant difference in HCRP1 expression levels between patients in all three kinds of cancer. To verify the previous findings, biopsies of a cohort of 101 oral cavity patients were analyzed concerning their HCRP1 expression by immunhistochemestry. As a result 18, 9 % of the patients showed low or reduced HCRP1 expression. Interestingly these patients showed a much more negative course of disease compared to patients with regular or high HCRP1 expression. These findings fortify our thesis that HCRP1 expression level is correlated with the clinical outcome for cancer patients not only in ovarian but also in other kinds of cancer.

4. Materials and Methods

4.1. Western Blotting

4.1.1. Sample Preparation

Remove media and wash two times with ice cold PBS, add 180µl RIPA+ to a 100mm dish. Leave on ice for 5 minutes. Scrape the cells with a cell scraper and transfer the lysate to an Eppendorfer tube. Vortex several times (10 seconds each) and leave on ice for 5 minutes. Afterwards spin 30 minutes at 12500 rpm at 4°C, save the supernatant and discard the pellet. The samples can be stored in RIPA+ up to 6 month at – 80°C.

4.1.2. RIPA+ buffer

Reagent	MW	Stock	Store	Vol	Final
NaCl	58,44	5M	RT	3ml	150mM
Tris pH 7,4	121,14	1M	RT	5ml	50mM
DOC (Na-deoxycholate)	414,6	10%	RT (keep dark)	5ml	0,5%
EGTA	380,4	50mM	RT	4ml	2mM
EDTA pH 7.4	372,2	50mM	RT	10ml	5mM
NaF	41,99	500mM	RT	6ml	30mM
b-Glycerophosphate pH 7,2	216	400mM	4°C	10ml	40mM
Tetrasodium Pyrophosphate	446,06	100mM	RT	10ml	10mM
Benzamidine	156,6	30mM	4°C	10ml	3mM
Nonindet P-40		Pure	RT	1ml	1%

Set to pH 7,4 and fill with ddH2O to a volume of 95ml. Nonidet P-40 is interchangeable with Triton-X-100

4.1.3. Complete Stock Solution and 2ml RIPA +

Dissolve one tablette of Complete (stored at 4°C ind the cell culture) in 2ml ddH2O.

Take 1,90 ml RIPA, add 20 µl 200mM Na-Orthovanadate and 80 µl 25x Complete stock solution.

4.1.4. Determination of protein concentration (Protein assay)

In order to determine the concentration o the protein, a Bradford assay was done.

4.1.5. Gels and Buffers

According to the size of the protein (41kD) a 12% acrylamide gel was done.

Acrylamide Concentration (%)	Linear Range of Separation (kD)
12	12 – 60

Separating Gel (for 2 gels)

H_2O	6,6 ml
30% acrylamide	8 ml
1,5 M TRIS (pH=8,8)	8ml
10% SDS	5ml
10% APS	200 µl
TEMED	200 µl

Stacking gel (for 2 gels)

H_2O	5,4 ml
30% acrylamide	1,34 ml
1 M TRIS (pH=6,8)	1 ml

10% SDS	80 µl
10% APS	80 µl
TEMED	8 µl

After pouring the separating gel, add 200-500 µl of Isobutanol to obtain a sharp edge at the top of the gel. When the gel is polymerized, discard the Isobutanol and fill in the stacking gel and add an appropriate comb.

4.1.6. Sample preparation

Add DTT to a final concentration of 0,2M to the loading buffer. Dilute the protein samples 1:1 with loading buffer and denaturate the samples for 5minutes at 95°C. Run the gel at 30V for 15 minutes, then at 160V for approximately 60 minutes.

4.1.7. Blotting

Cut the membrane and the filter paper to the dimensions of the gel. Soak the filter paper and fibre pads in transfer buffer. Activate the PVDF membrane with methanol for 10 seconds. Afterwards wash the membrane with ddH_2O for 5 min

Equilibrate the membrane in transfer buffer for 10 min, while shaking it. In the meantime prepare the gel-sandwich and blotting apparatus: Place the cassette with the grey side down on a clean surface, put one pre-wetted fibre pad on the grey side of the cassette. Two sheets of filter paper are put on the fibre pad, the gel placed on the filter paper and the pre-wetted membrane on the gel. Add two more pieces of filter papers and finally the last fibre pad. Remove all air bubbles that may have been formed. The cassette is placed into the ice cooled module. Run the blot at 300mA for one hour.

4.1.8. Blocking, incubation with antibodies and visualization

The membrane was placed into 100% methanol twice for 10 seconds and washed with H_2O for 5 minutes. The blocking solution was prepared by diluting western blocking reagent 1:10 in PBS/Tween (0,1%). 5 ml of blocking reagent were added to the membrane (proteins facing the inner side) in a 50 ml falcon tube and agitated for 1 hour at RT. Dilute primary antibody in PBS/Tween complemented with 5% Western Blocking Solution. Incubate membrane with primary antibody for 1 hour or at 4°C overnight. Wash membrane 3x 5 min in PBS/Tween. Incubate with 2^{nd} antibody diluted in PBS/Tween complemented with 5% Western Blocking Solution. Wash membrane 3x 5 min in PBS/Tween. Place membrane on a Clingfilm. Mix ECL detection reagents 1:1 and apply 3ml for each membrane. Incubate the membrane for 1-5 minutes. Transfer membrane onto a new Clingfilm.

4.2. Used Antibody

Antibody production - Polyclonal and monoclonal peptide antibodies against hVps37A were used for immunohistochemistry experiments and western blotting. Tissue microarrays were analyzed using (at that time available) polyclonal antibody, whereas immunohistochemistry of mouse tumors and western blotting were performed using the monoclonal antibody. The following peptide sequence was selected: MSPYASQGFPFLPPY. Rabbit antiserum raised against this peptide sequence was prepared and affinity purified by Eurogentec (Seraing, Belgium). Rabbit monoclonal antibody was also prepared by Eurogentec.

4.3. Immunostaining

The slides were placed into Xylene for 10 minutes. For rehydration of the samples the slides were put into a series of solutions containing a decreasing amount of alcohol (100%; 85%; 70%). Afterwards they were put into AquaDest which was changed twice. The slides were put into pH6 Citrate buffer or Epitope Retrieval Solution Dako pH9 into a pre warmed water bath for 20 minutes. After cooling, the slides were rinsed twice with AD and 5 min with PBS. In order to block the endogenous Peroxidase, 3% H_2O_2 (in PBS) was put on the slides for 10 minutes and washed with PBS two times for each 5 minutes. For blocking the samples 10% serum

was put on the slides for 10 minutes at room temperature. The first antibody was incubated over night at 4°C. Next day 30 min at RT, washing 2-3 times for 5 min and incubated with the second antibody. The next day the samples were rinsed twice for 5 minutes with PBS. In order to amplify the signal an ABC complex was used (1ml PBS + 10 µl A + 10 µl B) which was incubated for 45 minutes at RT. The slides were rinsed twice for 5 minutes. For signal detection we employed the DAB system which through peroxidase activity gives a brownish precipitate. After rinsing again with AD a Hematoxylin staining was done on all slides. Thereafter the slides were washed with water and dehydrated again with a series of solutions containing an increasing amount of alcohol (up to absolute alcohol). Finally the slides were put into n-Butylacetate. This technique was used for staining of Skov3 and MDAH – 2774 cells, as well as staining of the mouse tumour slides. For mouse tumours the slides were pre - treated with according to the M.O.M. kit for detecting mouse primary antibody on mouse tissue (from Vector laboratories).

4.4. Immunhistochemistry of the Tissue Micro Array (TMA)

An arrayed panel of ovarian cancer tissues was prepared. A tissue array was assembled by taking core needle “biopsies” from specific locations in the pre-existing paraffin-embedded tissue blocks and re-embedding them in an arrayed “master” block, using techniques and an apparatus developed by Beecher Instruments, Micro-Array Technology. To achieve good representation of the tumor, three biopsies of tumor material were selected from each patient sample. The ovarian tissue microarray was cut into 3 µm thick slices using a microtome. The sections were deparaffinized by heating at 60C and rehydrated in descending alcohol grades followed by Depp-9 epitope retrieval treatment (EB-depp9-250, eubio, Vienna, Austria). Endogenous peroxidase activity was quenched using 0.2% H_2O_2 in PBS (pH 7.4) for 10 minutes. After blocking with 10% secondary antibody host serum (goat) for 45 minutes, the sections were incubated in primary HCRP1 antibody [monoclonal EGT290 (1:1000)] for 1 hr at room temperature. Primary antibody dilution was made in 10% goat serum. The sections, after 2 PBS washes, were incubated in biotinylated secondary antibody [Biotinylated anti-mouse IgG (BA-9200), raised in goat; Vector Laboratories, Inc. Burlingame, CA] diluted 1:200 in 10% goat serum for 30 minutes at room temperature followed by 45 minute incubation in

StreptABComplex/HRP (K0377 Dako, Denmark). The sections were again washed twice with PBS and incubated in Dako Liquid DAB+ Substrate Chromogen System (K3468 Dako, CA, USA) until the development of brown colour. This was followed by counterstaining with Meyer's hematoxylin, dehydration and mounting using Eukitt medium. Staining analysis was performed on Olympus BX50F microscope (Olympus Optical Co. Ltd., Japan) using 'Cell Imaging Software for Life Science Microscopy' (Soft Imaging Solutions GmbH, Münster, Germany). The cells were counted and grouped according to percentage of positive cells as <10%, 10-30% and >30% positively stained cells. The intensity of staining was determined on a scale of 0 to 3, with 0 for absent, 1 for weak, 2 for moderate and 3 for strong staining. The staining analysis was performed by three independent investigators.

4.5. Patient material

Samples of formaldehyde fixed-paraffin embedded (FFPE) ovarian tumors for establishing the tissue microarray (TMA) were obtained from archival material of 144 patients who underwent radical cytoreductive surgery or between the years 1987 and 2002 at the Medical University of Vienna, Vienna, Austria. Written and oral informed consent was obtained from all patients according to the Ethics Committee of the Medical University of Vienna for further processing and analysis of the clinical data. The clinical characteristics of patients from the cohort used for the tissue microarray are described in Table 1. Microarrays were composed by taking core needle "biopsies" from specific locations in the pre-existing paraffin-embedded tissue blocks and re-embedding them in an array master block, using techniques and an apparatus developed by Beecher Instruments Inc., Micro-Array Technology (Sun Prairie, WI, USA). To achieve good representation of the tumor, three biopsies of tumor material were selected from each patient. None of the patients with borderline tumors died during the follow-up time and were excluded from the survival analysis. No data on chemotherapy treatment was available in this cohort, although most patients received platinum and taxane based adjuvant regimen according to the institutional standard operating procedures. Samples of ovarian tumors for mRNA expression analysis were obtained from a second cohort of 115 patients who underwent radical surgery the Charité University Hospital, Berlin, Germany between years 2000 and 2004. Epithelial-enriched normal ovarian and benign cyst samples came from patients

diagnosed without malignant disease at the Medical University of Vienna. In total, 20 benign ovarian samples and 115 primary tumour samples were assessed. Informed consent to sample and data collection by all patients was given according to the institutional review board of the Charité University Hospital Berlin and the Medical University of Vienna, as stated above. 85 (78.0%) of the patients with ovarian cancer in the second cohort underwent chemotherapy with a platinum and taxane based regimen.

4.6. Used Antibody

Antibody production - Polyclonal and monoclonal peptide antibodies against HCRP1 were used for immunohistochemistry experiments and western blotting. Tissue microarrays were analyzed using (at that time available) polyclonal antibody, whereas immunohistochemistry of mouse tumors and western blotting were performed using the monoclonal antibody. The following peptide sequence was selected: MSPYASQGFPFLPPY. Rabbit antiserum raised against this peptide sequence was prepared and affinity purified by Eurogentec (Seraing, Belgium). Rabbit monoclonal antibody was also prepared by Eurogentec.

4.7. Used cell lines

For this thesis two ovarian cancer cell lines have been used which have been transfected in order to gain stable (MDAH- 2774) and inducible (Skov3) knock down of hVps37A protein.

4.8. shRNA silencing of hVps37A

The human ovarian carcinoma SK-OV-3 cell line was cultured in McCoy´s medium enriched with 10% fetal bovine serum (FBS) and cultured in humidified incubator (37°C / 5% CO2). For applying the Tet-Off inducible system, founder cell lines were generated by transfecting SK-OV-3 cells with the pTet-Off vector (neor) encoding a tetracyclin repressible transactivator (tTA). Resistant colonies were selected with 200 µg/ml G418 and characterized by transient transfection with the

luciferase reporter plasmid (pTRE-Luc) containing luciferase under the control of tTA. Cell lines with highest response were used to establish cells inducible for hVps37Aspecific shRNA (Open Biosystems; #V2HS_21202, #V2HS_21203), which were subcloned into the SIN-TREmiR30-PIG vector (purr) downstream of the tetracycline inducible promoter. Presence of tetracycline (doxycycline) in the culture medium then suppresses shRNA expression, while its withdrawal would induce the knockdown of hVps37A. Puromycin-resistant colonies were isolated in the presence of doxycycline, and screened for silencing efficiency of hVps37A by qRT-PCR and Western blotting. The human ovarian carcinoma cell line MDAH-2774 was cultured in RPMI medium with 10% FCS (fetal calf serum), 50 units/ml penicillin G, and 50 µg/ml streptomycin sulfate at 37 °C in a humidified atmosphere of 95% air with 5% CO2. Three different shRNA constructs complementary exclusively to the *hVps37A* mRNA, in addition to 1 nonsense construct serving as a control, were cloned into the vector pSilencer 4.1-CMV neo. Transfection was performed with Lipofectamine 2000 according to the manufacturers' protocol (Invitrogen, Carlsbad, CA, USA). Stable clones were selected with 700 µg/ml G418, picked, and sub-cultured with 350 µg/ml G418. Silencing efficiency was quantified by qRT-PCR and western blot.

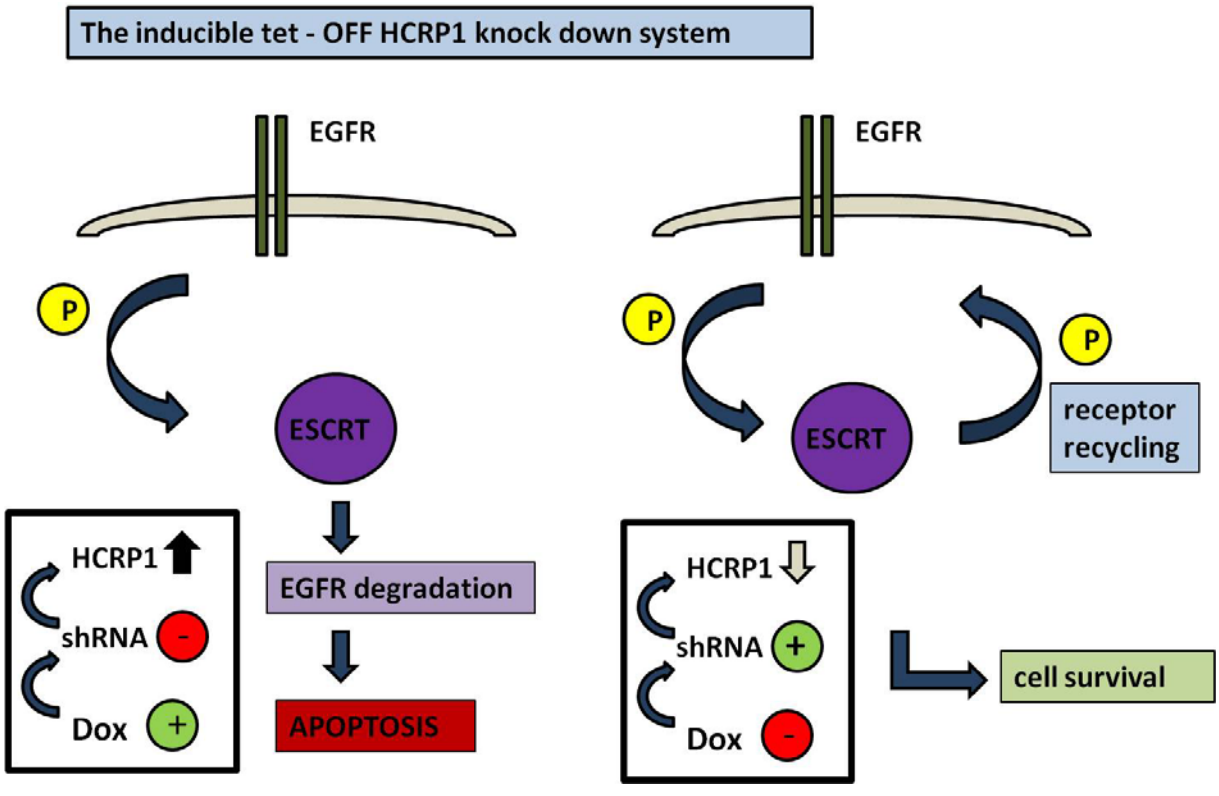

Figure 34: Inducible tet - Off HCRP1 knock down system. This system was established in Skov3 ovarian cancer cells. These cells were used for the mouse xenograft experiment. Upon Dox removal (Dox (-)), shRNA is expressed leading to HCRP1 knock down. This leads to abolished EGFR receptor degradation followed by receptor recycling and hence cell survival. These tumors showed enhanced growth. Dox treatment (Dox (+)) abolishes shRNA expression and HCRP1 knock down. Sufficient HCRP1 expression allows EGFR receptor degradation by the ESCRT complexes followed by induced apoptosis in tumor cells. These tumors showed reduced tumor growth compared to non – Dox treated tumors (PBS treated).

4.9. The Tet- Off System (reviewed in (Nishijima et al., 2009) and Clontech protocol)

In biological research the precise regulation of transgene expression is an important tool. The tetracycline- regulated gene depletion system (Tet- Off) system is used in cultured eucaryotic cells including Drosophila, mice, rats and yeast as well as in plants, to control gene activity. The Tet- Off system uses the fact that in E.coli the Tet repressor protein (TetR) negatively regulates the genes of the tetracycline resistance operon on the Tn 10 transposon. The TetR protein blocks the transcription of these genes by binding to the tet operator sequence (tetO) in the absence of Tetracycline (Tc). In order to obtain a functional Tet – Off system in a stable cell line, two different expression units are needed. The first component is a regulatory protein which is based on TetR, which in the Tet – Off system comprises of the fusion of TetR protein and the C-terminal activation domain of the Herpes simplex virus VP16. This hybrid protein which is called tetracycline controlled transactivator (tTA) in which TetR functions as a transcriptional activator. Additionally the plasmid encoding the tTA (the pTet – Off regulator plasmid) contains a neomycin resistance gene for selection of stably transfected cells. The second component is a Response plasmid which expresses a gene of interest (Gene X) which is under control of a tetracycline response element (TRE). The TRE is a minimal RNA polymerase II promoter sequence (minimal CMV promoter; CMV - Constitutive mammalian promotor) which is fused downstream from the multiple Tet resistance operator (TetO) consists of the tetO and CMV. Hence in a double stable Tet – Off system cell line Gene expression is turnerd on, when Doxicycline (a member of the tetracycline antibiotics group) is removed from the media. In our case the controlled Gene of interest (gene X) was a HCRP1 specific shRNA in order to obtain an inducible knockdown in transfected

Skov3 cells. When Dox was removed from the cell culture media, or in case of the xenograft no Dox was injected, HCRP1 specific shRNA was produced which led to Gene knock down.

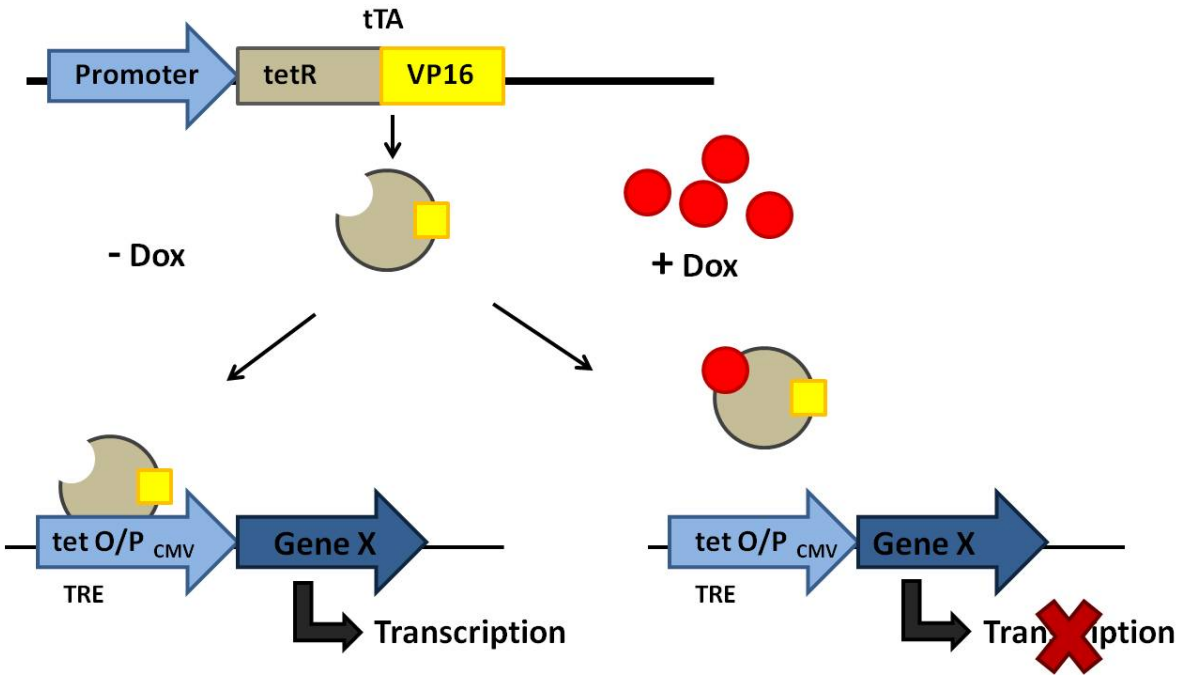

Figure 34: The tet Off system comprises a fusion of the TetR- protein and the activator domain of Herpes simplex virus VP16. Both combined are called tTA (tetracycline controlled transactivator). The tTa is encoded by the p Tet Off regulator plasmid. The response plasmid expresses a gene of interest (Gene X) under control of the tetracycline response element (TRE) which consists of the tetO and CMV (Constitutive mammalian promoter). Gene expression is turned on, when Dox (Tetracycline derivate) is removed from the media.

4.10. Mice xenograft experiment

10 eight week old athymic *Foxn1nu* mice were maintained under specific Pathogen - free conditions. Mice were subcutaneously inoculated with SK-OV-3 ovarian cancer cells bearing a Dox inducible shRNA construct specific against hVps37A (described above). Dox (125µg/day) was intraperitoneal injected in 50% of the mice in order to suppress hVps37A knockdown. The remaining mice were treated with PBS under the same conditions. Tumor size was measured every third day by calliper. Further, the relative tumor growth was calculated as x-fold volume relative to

the first measurement. Animal experiments were performed according to protocols approved by the Austrian Federal Ministry for Education, Science and Art.

4.11. RNA isolation, cDNA synthesis and quantitative RT-PCR

Total RNA from cell lines was prepared with the RNeasy Mini Kit (Qiagen, Hilden, Germany). All steps were accomplished according to the manufacturers' protocols. cDNA was synthesized from 1µg total RNA using the DuraScript RT-PCR Kit (Sigma-Aldrich, Saint Louis, MO, USA) in a volume of 20µl. The following Assay-on-Demand™ probes were selected for TaqMan real-time PCR: *FLJ32642*, Hs00329751_m1 and *beta 2-microglobulin (B2M)*, Hs99999907_m1, HPRT1 and GAPDH (Applied Biosystems, Foster City, CA, USA). The real-time PCR reaction mix was composed of 10µl TaqMan® Universal PCR Master Mix (Applied Biosystems) supplemented with 2µl of the obtained cDNA, 1µl of the probe and 8µl of ddH2O to a total volume of 20µl. The reaction was performed on the 5700 Sequence Detection System (Applied Biosystems, Foster City, CA, USA) with default cycle conditions. Expression was relatively quantified as described elsewhere 35. Briefly, PCR efficiencies were calculated from calibration curves for individual probes and expression rates were compared with control cells (calibrator). All PCR reactions were performed from three independent experiments, and reverse transcriptase-negative and template-negative controls were included.

4.12. Data analysis and statistics

In the tissue microarray analysis, staining intensities were evaluated by two independent investigators and classified as 0 (missing expression), 1 (low expression), 2 (moderate expression), and 3 (high expression). The tissues were graded positive (high or moderate expression) only when more than 10% cells were positive for the respective stainings. Patients were dichotomized into two groups at the median of hVps37A expression. For EGFR and HER2, results of triplicates and both interpretations were averaged and re-scaled (0-3). Staining for HER2, according to standard procedures for breast cancer, was divided into two groups with low (0, 1) or high (2, 3) expression (Table 2). Since 40% of the tumor samples stained negatively or very weakly positively for EGFR, we also dichotomized the samples into two groups of low and high EGFR expression (Table 2). Kaplan-Meier plots and overall survival analysis were calculated with a median follow-up of 40.0 months (range 0.4–168.7 months) and event rate of 30.4%. Groups were compared using the log-rank test. Only patients with available staining for EGFR, HER2 and hVps37A

were included in the survival analysis. Logistic regression (ROC curves) was used to calculate specificity and sensitivity for the 5-year survival prognosis of EGFR and HER2. Nonparametric correlations between expression levels and categorical clinical variables were calculated using Spearman's rho test.

In the mRNA expression analysis we used relative normalized expression values for hVps37A expression of the normal (N) and ovarian patient (PT) cohort as measured by qRT-PCR. Group means were compared using Student's t-test. All statistical analyses were performed using the SPSS statistical software (Chicago, IL, USA).

4.13. Fluorescence microscopy and TUNEL assay

Cells were seeded on chamber slides, grown for 48 hours, fixed with 4% paraformaldehyde for 15 minutes, and permeabilized with 0.1% Triton X-100. The subsequent staining procedure was performed as described for immuno-histochemistry. The cells were incubated with the primary antibodies directed against pEGFR or EEA1 (1:100) for 1 hour. Alexa 610/350 secondary antibodies (1:100) were applied for 45 minutes. Afterwards the cells were analyzed on a confocal microscope. The "In Situ Cell Death Detection Kit, Fluorescin" (TUNNEL Assay) was obtained from Roche (Mannheim, Germany) and conducted according to the manufacturers protocol. DNaseI-treated samples served as positive controls.

4.14. Proliferation assays

2x105 SK-OV-3 (with and without doxycyclin) and MDAH (hVps37A silenced, nonsense control and wildtype) cells were seeded in 6-well plates in media complemented with 10% FCS and treated with 20 µg/ml cetuximab (Merck, Whitehouse Station, NJ, USA), 4 µM lapatinib (GlaxoSmithKline plc. London, UK), or were mock-treated. To maintain the logarithmic phase, cells were split at intervals of 48 hours, along with the determination of the cell number by a CASY cell counter (Innovatis AG, Bielefeld, Germany). This procedure was performed in triplicate over a

time-span of 6 days and confirmed by a replication of the whole experiment. From the obtained data, doubling times (dt) were calculated and depicted as dt-1.

4.15. 3D cell culture experiments

SK-OV-3 ovarian cancer cells bearing a Dox inducible shRNA construct specific against hVps37A (described above) were induced to form multicellular spheroids in non-adhesive 96-well plates in the presence (control) or absence (knockdown) of Dox and grown for 72 hours. The spheroids were transferred to collagen gels (rat Collagen 1, Becton Dickinson, 1.75mg/ml Collagen) and incubated in FGM supplemented with 2.5% serum (+/- Dox) and grown for further 72 hours. Spheroids were photographed and the areas of invasive structures were determined with the Axiovision software (Zeiss).

5. References

Alam, S.L., Langelier, C., Whitby, F.G., Koirala, S., Robinson, H., Hill, C.P., and Sundquist, W.I. (2006). Structural basis for ubiquitin recognition by the human ESCRT-II EAP45 GLUE domain. Nat Struct Mol Biol *13*, 1029-1030.

Arteaga, C.L. (2002). Overview of epidermal growth factor receptor biology and its role as a therapeutic target in human neoplasia. Semin Oncol *29*, 3-9.

Babst, M. (2005). A protein's final ESCRT. Traffic *6*, 2-9.

Babst, M., Katzmann, D.J., Estepa-Sabal, E.J., Meerloo, T., and Emr, S.D. (2002). Escrt-III: an endosome-associated heterooligomeric protein complex required for mvb sorting. Dev Cell *3*, 271-282.

Bache, K.G., Brech, A., Mehlum, A., and Stenmark, H. (2003). Hrs regulates multivesicular body formation via ESCRT recruitment to endosomes. J Cell Biol *162*, 435-442.

Bache, K.G., Slagsvold, T., Cabezas, A., Rosendal, K.R., Raiborg, C., and Stenmark, H. (2004). The growth-regulatory protein HCRP1/hVps37A is a subunit of mammalian ESCRT-I and mediates receptor down-regulation. Mol Biol Cell *15*, 4337-4346.

Bhowmick, N.A., Neilson, E.G., and Moses, H.L. (2004). Stromal fibroblasts in cancer initiation and progression. Nature *432*, 332-337.

Bishop, N., Horman, A., and Woodman, P. (2002). Mammalian class E vps proteins recognize ubiquitin and act in the removal of endosomal protein-ubiquitin conjugates. J Cell Biol *157*, 91-101.

Breuhahn, K., Longerich, T., and Schirmacher, P. (2006). Dysregulation of growth factor signaling in human hepatocellular carcinoma. Oncogene *25*, 3787-3800.

Cheng, N., Chytil, A., Shyr, Y., Joly, A., and Moses, H.L. (2008). Transforming growth factor-beta signaling-deficient fibroblasts enhance hepatocyte growth factor signaling in mammary carcinoma cells to promote scattering and invasion. Mol Cancer Res *6*, 1521-1533.

Chu, T., Sun, J., Saksena, S., and Emr, S.D. (2006). New component of ESCRT-I regulates endosomal sorting complex assembly. J Cell Biol *175*, 815-823.

Conibear, E. (2002). An ESCRT into the endosome. Mol Cell *10*, 215-216.

Curtiss, M., Jones, C., and Babst, M. (2007). Efficient cargo sorting by ESCRT-I and the subsequent release of ESCRT-I from multivesicular bodies requires the subunit Mvb12. Mol Biol Cell *18*, 636-645.
Davies, M.A., and Samuels, Y. Analysis of the genome to personalize therapy for melanoma. Oncogene *29*, 5545-5555.
de Melker, A.A., van der Horst, G., and Borst, J. (2004). Ubiquitin ligase activity of c-Cbl guides the epidermal growth factor receptor into clathrin-coated pits by two distinct modes of Eps15 recruitment. J Biol Chem *279*, 55465-55473.
Dimova, I., Zaharieva, B., Raitcheva, S., Dimitrov, R., Doganov, N., and Toncheva, D. (2006). Tissue microarray analysis of EGFR and erbB2 copy number changes in ovarian tumors. Int J Gynecol Cancer *16*, 145-151.
Fan, Z., Masui, H., Altas, I., and Mendelsohn, J. (1993). Blockade of epidermal growth factor receptor function by bivalent and monovalent fragments of 225 anti-epidermal growth factor receptor monoclonal antibodies. Cancer Res *53*, 4322-4328.
Gonciarz, M.D., Whitby, F.G., Eckert, D.M., Kieffer, C., Heroux, A., Sundquist, W.I., and Hill, C.P. (2008). Biochemical and structural studies of yeast Vps4 oligomerization. J Mol Biol *384*, 878-895.
Gruenberg, J., and Stenmark, H. (2004). The biogenesis of multivesicular endosomes. Nat Rev Mol Cell Biol *5*, 317-323.
Hanahan, D., and Weinberg, R.A. Hallmarks of cancer: the next generation. Cell *144*, 646-674.
Hanson, P.I., Roth, R., Lin, Y., and Heuser, J.E. (2008). Plasma membrane deformation by circular arrays of ESCRT-III protein filaments. J Cell Biol *180*, 389-402.
Hartmann, C., Chami, M., Zachariae, U., de Groot, B.L., Engel, A., and Grutter, M.G. (2008). Vacuolar protein sorting: two different functional states of the AAA-ATPase Vps4p. J Mol Biol *377*, 352-363.
Haugh, J.M., and Meyer, T. (2002). Active EGF receptors have limited access to PtdIns(4,5)P(2) in endosomes: implications for phospholipase C and PI 3-kinase signaling. J Cell Sci *115*, 303-310.
Henic, E., Sixt, M., Hansson, S., Hoyer-Hansen, G., and Casslen, B. (2006). EGF-stimulated migration in ovarian cancer cells is associated with decreased internalization, increased surface expression, and increased shedding of the urokinase plasminogen activator receptor. Gynecol Oncol *101*, 28-39.
Hierro, A., Sun, J., Rusnak, A.S., Kim, J., Prag, G., Emr, S.D., and Hurley, J.H. (2004). Structure of the ESCRT-II endosomal trafficking complex. Nature *431*, 221-225.
Hirano, S., Suzuki, N., Slagsvold, T., Kawasaki, M., Trambaiolo, D., Kato, R., Stenmark, H., and Wakatsuki, S. (2006). Structural basis of ubiquitin recognition by mammalian Eap45 GLUE domain. Nat Struct Mol Biol *13*, 1031-1032.
Holbro, T., Civenni, G., and Hynes, N.E. (2003). The ErbB receptors and their role in cancer progression. Exp Cell Res *284*, 99-110.
Huang, F., and Sorkin, A. (2005). Growth factor receptor binding protein 2-mediated recruitment of the RING domain of Cbl to the epidermal growth factor receptor is essential and sufficient to support receptor endocytosis. Mol Biol Cell *16*, 1268-1281.
Huether, A., Hopfner, M., Baradari, V., Schuppan, D., and Scherubl, H. (2005). EGFR blockade by cetuximab alone or as combination therapy for growth control of hepatocellular cancer. Biochem Pharmacol *70*, 1568-1578.
Hurley, J.H., and Hanson, P.I. Membrane budding and scission by the ESCRT machinery: it's all in the neck. Nat Rev Mol Cell Biol *11*, 556-566.
Hynes, N.E., and Lane, H.A. (2005). ERBB receptors and cancer: the complexity of targeted inhibitors. Nat Rev Cancer *5*, 341-354.
Im, Y.J., and Hurley, J.H. (2008). Integrated structural model and membrane targeting mechanism of the human ESCRT-II complex. Dev Cell *14*, 902-913.
Im, Y.J., Wollert, T., Boura, E., and Hurley, J.H. (2009). Structure and function of the ESCRT-II-III interface in multivesicular body biogenesis. Dev Cell *17*, 234-243.
Inoue, M., Kamikubo, H., Kataoka, M., Kato, R., Yoshimori, T., Wakatsuki, S., and Kawasaki, M. (2008). Nucleotide-dependent conformational changes and assembly of the AAA ATPase SKD1/VPS4B. Traffic *9*, 2180-2189.

Jhappan, C., Stahle, C., Harkins, R.N., Fausto, N., Smith, G.H., and Merlino, G.T. (1990). TGF alpha overexpression in transgenic mice induces liver neoplasia and abnormal development of the mammary gland and pancreas. Cell *61*, 1137-1146.
Kanazawa, C., Morita, E., Yamada, M., Ishii, N., Miura, S., Asao, H., Yoshimori, T., and Sugamura, K. (2003). Effects of deficiencies of STAMs and Hrs, mammalian class E Vps proteins, on receptor downregulation. Biochem Biophys Res Commun *309*, 848-856.
Katzmann, D.J., Babst, M., and Emr, S.D. (2001). Ubiquitin-dependent sorting into the multivesicular body pathway requires the function of a conserved endosomal protein sorting complex, ESCRT-I. Cell *106*, 145-155.
Katzmann, D.J., Odorizzi, G., and Emr, S.D. (2002). Receptor downregulation and multivesicular-body sorting. Nat Rev Mol Cell Biol *3*, 893-905.
Katzmann, D.J., Stefan, C.J., Babst, M., and Emr, S.D. (2003). Vps27 recruits ESCRT machinery to endosomes during MVB sorting. J Cell Biol *162*, 413-423.
Kieffer, C., Skalicky, J.J., Morita, E., De Domenico, I., Ward, D.M., Kaplan, J., and Sundquist, W.I. (2008). Two distinct modes of ESCRT-III recognition are required for VPS4 functions in lysosomal protein targeting and HIV-1 budding. Dev Cell *15*, 62-73.
Kimball, K.J., Numnum, T.M., Kirby, T.O., Zamboni, W.C., Estes, J.M., Barnes, M.N., Matei, D.E., Koch, K.M., and Alvarez, R.D. (2008). A phase I study of lapatinib in combination with carboplatin in women with platinum sensitive recurrent ovarian carcinoma. Gynecol Oncol *111*, 95-101.
Kirisits, A., Pils, D., and Krainer, M. (2007). Epidermal growth factor receptor degradation: an alternative view of oncogenic pathways. Int J Biochem Cell Biol *39*, 2173-2182.
Konner, J., Schilder, R.J., DeRosa, F.A., Gerst, S.R., Tew, W.P., Sabbatini, P.J., Hensley, M.L., Spriggs, D.R., and Aghajanian, C.A. (2008). A phase II study of cetuximab/paclitaxel/carboplatin for the initial treatment of advanced-stage ovarian, primary peritoneal, or fallopian tube cancer. Gynecol Oncol *110*, 140-145.
Kostelansky, M.S., Schluter, C., Tam, Y.Y., Lee, S., Ghirlando, R., Beach, B., Conibear, E., and Hurley, J.H. (2007). Molecular architecture and functional model of the complete yeast ESCRT-I heterotetramer. Cell *129*, 485-498.
Lafky, J.M., Wilken, J.A., Baron, A.T., and Maihle, N.J. (2008). Clinical implications of the ErbB/epidermal growth factor (EGF) receptor family and its ligands in ovarian cancer. Biochim Biophys Acta *1785*, 232-265.
Landsberg, M.J., Vajjhala, P.R., Rothnagel, R., Munn, A.L., and Hankamer, B. (2009). Three-dimensional structure of AAA ATPase Vps4: advancing structural insights into the mechanisms of endosomal sorting and enveloped virus budding. Structure *17*, 427-437.
Li, L., and Cohen, S.N. (1996). Tsg101: a novel tumor susceptibility gene isolated by controlled homozygous functional knockout of allelic loci in mammalian cells. Cell *85*, 319-329.
Lin, C.K., Chao, T.K., Yu, C.P., Yu, M.H., and Jin, J.S. (2009). The expression of six biomarkers in the four most common ovarian cancers: correlation with clinicopathological parameters. APMIS *117*, 162-175.
Liu, L.Z., Hu, X.W., Xia, C., He, J., Zhou, Q., Shi, X., Fang, J., and Jiang, B.H. (2006). Reactive oxygen species regulate epidermal growth factor-induced vascular endothelial growth factor and hypoxia-inducible factor-1alpha expression through activation of AKT and P70S6K1 in human ovarian cancer cells. Free Radic Biol Med *41*, 1521-1533.
Lu, Q., Hope, L.W., Brasch, M., Reinhard, C., and Cohen, S.N. (2003). TSG101 interaction with HRS mediates endosomal trafficking and receptor down-regulation. Proc Natl Acad Sci U S A *100*, 7626-7631.
Maxfield, F.R., and McGraw, T.E. (2004). Endocytic recycling. Nat Rev Mol Cell Biol *5*, 121-132.
McNiven, M.A., Cao, H., Pitts, K.R., and Yoon, Y. (2000). The dynamin family of mechanoenzymes: pinching in new places. Trends Biochem Sci *25*, 115-120.
Nishijima, H., Yasunari, T., Nakayama, T., Adachi, N., and Shibahara, K. (2009). Improved applications of the tetracycline-regulated gene depletion system. Biosci Trends *3*, 161-167.

Obita, T., Saksena, S., Ghazi-Tabatabai, S., Gill, D.J., Perisic, O., Emr, S.D., and Williams, R.L. (2007). Structural basis for selective recognition of ESCRT-III by the AAA ATPase Vps4. Nature *449*, 735-739.
Oestreich, A.J., Davies, B.A., Payne, J.A., and Katzmann, D.J. (2007). Mvb12 is a novel member of ESCRT-I involved in cargo selection by the multivesicular body pathway. Mol Biol Cell *18*, 646-657.
Palayekar, M.J., and Herzog, T.J. (2008). The emerging role of epidermal growth factor receptor inhibitors in ovarian cancer. Int J Gynecol Cancer *18*, 879-890.
Peipp, M., Dechant, M., and Valerius, T. (2008). Effector mechanisms of therapeutic antibodies against ErbB receptors. Curr Opin Immunol *20*, 436-443.
Pennock, S., and Wang, Z. (2003). Stimulation of cell proliferation by endosomal epidermal growth factor receptor as revealed through two distinct phases of signaling. Mol Cell Biol *23*, 5803-5815.
Petit, A.M., Rak, J., Hung, M.C., Rockwell, P., Goldstein, N., Fendly, B., and Kerbel, R.S. (1997). Neutralizing antibodies against epidermal growth factor and ErbB-2/neu receptor tyrosine kinases down-regulate vascular endothelial growth factor production by tumor cells in vitro and in vivo: angiogenic implications for signal transduction therapy of solid tumors. Am J Pathol *151*, 1523-1530.
Pils, D., Horak, P., Gleiss, A., Sax, C., Fabjani, G., Moebus, V.J., Zielinski, C., Reinthaller, A., Zeillinger, R., and Krainer, M. (2005). Five genes from chromosomal band 8p22 are significantly down-regulated in ovarian carcinoma: N33 and EFA6R have a potential impact on overall survival. Cancer *104*, 2417-2429.
Pils, D., Pinter, A., Reibenwein, J., Alfanz, A., Horak, P., Schmid, B.C., Hefler, L., Horvat, R., Reinthaller, A., Zeillinger, R*., et al.* (2007). In ovarian cancer the prognostic influence of HER2/neu is not dependent on the CXCR4/SDF-1 signalling pathway. Br J Cancer *96*, 485-491.
Piper, R.C., and Katzmann, D.J. (2007). Biogenesis and function of multivesicular bodies. Annu Rev Cell Dev Biol *23*, 519-547.
Prewett, M., Rothman, M., Waksal, H., Feldman, M., Bander, N.H., and Hicklin, D.J. (1998). Mouse-human chimeric anti-epidermal growth factor receptor antibody C225 inhibits the growth of human renal cell carcinoma xenografts in nude mice. Clin Cancer Res *4*, 2957-2966.
Puertollano, R., and Bonifacino, J.S. (2004). Interactions of GGA3 with the ubiquitin sorting machinery. Nat Cell Biol *6*, 244-251.
Raiborg, C., Rusten, T.E., and Stenmark, H. (2003). Protein sorting into multivesicular endosomes. Curr Opin Cell Biol *15*, 446-455.
Raymond, C.K., Howald-Stevenson, I., Vater, C.A., and Stevens, T.H. (1992). Morphological classification of the yeast vacuolar protein sorting mutants: evidence for a prevacuolar compartment in class E vps mutants. Mol Biol Cell *3*, 1389-1402.
Russell, M.R., Nickerson, D.P., and Odorizzi, G. (2006). Molecular mechanisms of late endosome morphology, identity and sorting. Curr Opin Cell Biol *18*, 422-428.
Saksena, S., Wahlman, J., Teis, D., Johnson, A.E., and Emr, S.D. (2009). Functional reconstitution of ESCRT-III assembly and disassembly. Cell *136*, 97-109.
Salomon, D.S., Brandt, R., Ciardiello, F., and Normanno, N. (1995). Epidermal growth factor-related peptides and their receptors in human malignancies. Crit Rev Oncol Hematol *19*, 183-232.
Scaltriti, M., and Baselga, J. (2006). The epidermal growth factor receptor pathway: a model for targeted therapy. Clin Cancer Res *12*, 5268-5272.
Schilder, R.J., Pathak, H.B., Lokshin, A.E., Holloway, R.W., Alvarez, R.D., Aghajanian, C., Min, H., Devarajan, K., Ross, E., Drescher, C.W*., et al.* (2009). Phase II trial of single agent cetuximab in patients with persistent or recurrent epithelial ovarian or primary peritoneal carcinoma with the potential for dose escalation to rash. Gynecol Oncol *113*, 21-27.
Schlessinger, J. (2002). Ligand-induced, receptor-mediated dimerization and activation of EGF receptor. Cell *110*, 669-672.
Scott, A., Chung, H.Y., Gonciarz-Swiatek, M., Hill, G.C., Whitby, F.G., Gaspar, J., Holton, J.M., Viswanathan, R., Ghaffarian, S., Hill, C.P*., et al.* (2005). Structural and mechanistic studies of VPS4 proteins. EMBO J *24*, 3658-3669.

Sheng, Q., and Liu, J. The therapeutic potential of targeting the EGFR family in epithelial ovarian cancer. Br J Cancer *104*, 1241-1245.
Shields, S.B., Oestreich, A.J., Winistorfer, S., Nguyen, D., Payne, J.A., Katzmann, D.J., and Piper, R. (2009). ESCRT ubiquitin-binding domains function cooperatively during MVB cargo sorting. J Cell Biol *185*, 213-224.
Shim, S., Kimpler, L.A., and Hanson, P.I. (2007). Structure/function analysis of four core ESCRT-III proteins reveals common regulatory role for extreme C-terminal domain. Traffic *8*, 1068-1079.
Sibilia, M., Kroismayr, R., Lichtenberger, B.M., Natarajan, A., Hecking, M., and Holcmann, M. (2007). The epidermal growth factor receptor: from development to tumorigenesis. Differentiation *75*, 770-787.
Simon, M.A. (2000). Receptor tyrosine kinases: specific outcomes from general signals. Cell *103*, 13-15.
Siwak, D.R., Carey, M., Hennessy, B.T., Nguyen, C.T., McGahren Murray, M.J., Nolden, L., and Mills, G.B. Targeting the epidermal growth factor receptor in epithelial ovarian cancer: current knowledge and future challenges. J Oncol *2010*, 568938.
Slagsvold, T., Aasland, R., Hirano, S., Bache, K.G., Raiborg, C., Trambaiolo, D., Wakatsuki, S., and Stenmark, H. (2005). Eap45 in mammalian ESCRT-II binds ubiquitin via a phosphoinositide-interacting GLUE domain. J Biol Chem *280*, 19600-19606.
Sorkin, A., and von Zastrow, M. (2009). Endocytosis and signalling: intertwining molecular networks. Nat Rev Mol Cell Biol *10*, 609-622.
Stuchell-Brereton, M.D., Skalicky, J.J., Kieffer, C., Karren, M.A., Ghaffarian, S., and Sundquist, W.I. (2007). ESCRT-III recognition by VPS4 ATPases. Nature *449*, 740-744.
Sundquist, W.I., Schubert, H.L., Kelly, B.N., Hill, G.C., Holton, J.M., and Hill, C.P. (2004). Ubiquitin recognition by the human TSG101 protein. Mol Cell *13*, 783-789.
Sweeney, C., and Carraway, K.L., 3rd (2004). Negative regulation of ErbB family receptor tyrosine kinases. Br J Cancer *90*, 289-293.
Teis, D., Saksena, S., Judson, B.L., and Emr, S.D. ESCRT-II coordinates the assembly of ESCRT-III filaments for cargo sorting and multivesicular body vesicle formation. EMBO J *29*, 871-883.
Teo, H., Gill, D.J., Sun, J., Perisic, O., Veprintsev, D.B., Vallis, Y., Emr, S.D., and Williams, R.L. (2006). ESCRT-I core and ESCRT-II GLUE domain structures reveal role for GLUE in linking to ESCRT-I and membranes. Cell *125*, 99-111.
Teo, H., Perisic, O., Gonzalez, B., and Williams, R.L. (2004a). ESCRT-II, an endosome-associated complex required for protein sorting: crystal structure and interactions with ESCRT-III and membranes. Dev Cell *7*, 559-569.
Teo, H., Veprintsev, D.B., and Williams, R.L. (2004b). Structural insights into endosomal sorting complex required for transport (ESCRT-I) recognition of ubiquitinated proteins. J Biol Chem *279*, 28689-28696.
Thien, C.B., and Langdon, W.Y. (2001). Cbl: many adaptations to regulate protein tyrosine kinases. Nat Rev Mol Cell Biol *2*, 294-307.
Wheeler, D.L., Huang, S., Kruser, T.J., Nechrebecki, M.M., Armstrong, E.A., Benavente, S., Gondi, V., Hsu, K.T., and Harari, P.M. (2008). Mechanisms of acquired resistance to cetuximab: role of HER (ErbB) family members. Oncogene *27*, 3944-3956.
Wollert, T., and Hurley, J.H. Molecular mechanism of multivesicular body biogenesis by ESCRT complexes. Nature *464*, 864-869.
Xia, W., Mullin, R.J., Keith, B.R., Liu, L.H., Ma, H., Rusnak, D.W., Owens, G., Alligood, K.J., and Spector, N.L. (2002). Anti-tumor activity of GW572016: a dual tyrosine kinase inhibitor blocks EGF activation of EGFR/erbB2 and downstream Erk1/2 and AKT pathways. Oncogene *21*, 6255-6263.
Xu, Z., Liang, L., Wang, H., Li, T., and Zhao, M. (2003). HCRP1, a novel gene that is downregulated in hepatocellular carcinoma, encodes a growth-inhibitory protein. Biochem Biophys Res Commun *311*, 1057-1066.

Yarden, Y. (2001). The EGFR family and its ligands in human cancer. signalling mechanisms and therapeutic opportunities. Eur J Cancer *37 Suppl 4*, S3-8.
Yu, Z., Gonciarz, M.D., Sundquist, W.I., Hill, C.P., and Jensen, G.J. (2008). Cryo-EM structure of dodecameric Vps4p and its 2:1 complex with Vta1p. J Mol Biol *377*, 364-377.
Zamborlini, A., Usami, Y., Radoshitzky, S.R., Popova, E., Palu, G., and Gottlinger, H. (2006). Release of autoinhibition converts ESCRT-III components into potent inhibitors of HIV-1 budding. Proc Natl Acad Sci U S A *103*, 19140-19145.
Zerial, M., and McBride, H. (2001). Rab proteins as membrane organizers. Nat Rev Mol Cell Biol *2*, 107-117.

Curriculum Vitae

Persönliche Daten:

Name: Bettina Savarese Brenner

Geburtsdatum: 18.02.1987

Geburtsort: Wien

Staatsbürgerschaft: Österreich

Familienstand: verheiratet

Ausbildungsweg:

1993 – 1997 Volksschule Maria Enzersdorf

1997 – 2001 Sportrealgymnasium, Maria Enzersdorf

2001 – 2005 Bundesrealgymnasium Franz Keimgasse Mödling

mit Schwerpunkt Naturwissenschaften

Matura Juni 2005 mit gutem Erfolg

ab 2005 Beginn des Studiums Mikrobiologie

an der Hauptuniversität Wien

Fremdsprachen bzw. Fertigkeiten

Englisch Wort und Schrift (Sehr Gut)

Sprachaufenthalt in den Vereinigten Staaten

Französisch Wort und Schrift (Gut)

Praktika

31.07 – 28.08.2006 Praktikum im Labor für medizinische Diagnostik

Linz, Waltherstraße 5

Juni-September 2009 Praktikum am Structural Genomics Consortium (SGC) in Oxford, UK, bei Prof. Stefan Knapp PhD

Strukturen in der Protein Data Bank (http://www.pdb.org)

Structure of human Phosphorylase Kinase Gamma 2

Muniz, J.R.C., Shrestha, A., Savitsky, P., Wang, J., Rellos, P., Fedorov, O., Burgess-Brown, N., Brenner, B., Berridge, G., Elkins, J.M., Krojer, T., Vollmar, M., Che, K.H., Von Delft, F., Arrowsmith, C.H., Edwards, A.M., Weigelt, J., Bountra, C., Knapp, S.

Structure of human YSK1 (Yeast SPS1 – STE20 – Related Kinase 1)

Muniz, J.R.C., Rellos, P., Ugochukwu, E., Vollmar, M., Allerston, C., Chaikuad, A., Savitsky, P., Berridge, G., Brenner, B., Elkins, J.M., Daga, N., Gileadi, O., Mahajan, P., Shrestha, B., Vondelft, F., Arrowsmith, C.H., Edwards, A.M., Weigelt, J., Bountra, C., Knapp, S

Publikationen

hVps37A Status Affects Prognosis and Cetuximab Sensitivity in Ovarian Cancer.

Michael Wittinger[1#], Petr Vanhara[1#], Ahmed El-Gazzar[1], Bettina Savarese-Brenner[1], Dietmar Pils[1], Mariam Anees[1], Thomas W. Grunt[1], Maria Sibilia[2], Martin Holcmann[2], Reinhard Horvat[3], Michael Schemper[4], Robert Zeillinger[5], Christian Schöfer[6], Helmut Dolznig[7], Peter Horak[1*] and Michael Krainer[1]

accepted in Clinical Cancer Research

hVps37A Status Affects Prognosis and Cetuximab Sensitivity in Ovarian Cancer

Michael Wittinger[1#], Petr Vanhara[1#], Ahmed El-Gazzar[1], Bettina Savarese-Brenner[1], Dietmar Pils[1], Mariam Anees[1], Thomas W. Grunt[1], Maria Sibilia[2], Martin Holcmann[2], Reinhard Horvat[3], Michael Schemper[4], Robert Zeillinger[5] , Christian Schöfer[6], Helmut Dolznig[7], Peter Horak[1*] and Michael Krainer[1]

[1] Department of Internal Medicine I, Clinical Division of Oncology
[2] Department of Internal Medicine I, Institute for Cancer Research
[3] Clinical Institute of Pathology
[4] Center for Medical Statistics, Informatics, and Intelligent Systems
[5] Department of Obstetrics and Gynaecology, Division of Gynaecology
[6] Center for Anatomy and Cell Biology
[7] Department of Medical Genetics
Medical University of Vienna, Vienna, Austria

#These authors contributed equally to this work: Michael Wittinger and Petr Vanhara

Running title: hVps37A in Ovarian Cancer

Keywords: hVps37A, HCRP1, ovarian cancer, prognostic marker, cetuximab sensitivity

***Corresponding author:** Peter Horak, MD, Department of Internal Medicine I, Medical University of Vienna, Waehringer Guertel 18-20, A-1090 Vienna, Austria,
e-mail: peter.horak@meduniwien.ac.at

Supported by: the Austrian Science Fund (FWF); Project Number: P17891

Competing financial interests

The authors declare no competing financial interests.

Word count: 5123

Figures: 5

Tables: 2

Supplementary data: 5

Statement of Translational Relevance. Our study shows that hVps37A is downregulated in a large number of ovarian cancer tissues and influences prognostic relevance of EGFR and HER2 expression. Moreover, we find that loss of hVps37A leads to cetuximab resistance *in vitro*. We propose that hVps37A expression might be exploitable as a prognostic and predictive marker in ovarian cancer and possibly in other cancer entities as well.

Purpose: Although prognostic and predictive factors in ovarian cancer have been extensively studied for decades, only few have been identified and introduced to clinical practice. Here we evaluate hVps37A (HCRP1) as a possible novel predictive marker for ovarian cancer. hVps37A was originally described as a member of the membrane-trafficking ESCRT-I complex mediating the internalization and degradation of ubiquitinated membrane receptors.

Experimental Design: We analyzed a ovarian cancer tissue microarray for HCRP1, EGFR and HER2 expression. We used a tetracycline inducible ovarian cancer cell culture model to demonstrate the effects of hVps37A knockdown *in vitro* and *in vivo*. Additionally, we studied the effects of EGFR inhibitors cetuximab and lapatinib on ovarian cancer cells under conditions of hVps37A knockdown.

Results: We find that hVps37A is significantly downregulated in ovarian cancer and modifies the prognostic value of EGFR and HER2 expression. Additionally, hVps37A down-regulation in ovarian cancer cells leads to cytoplasmic pEGFR retention and hyperactivation of downstream pathways and is associated with enhanced xenograft growth in nude mice as well as invasion of the collagen matrix. Furthermore, due to subsequent sustained Akt- and MAPK-pathway activation, hVps37A-deficient cells become irresponsive to inhibition by the therapeutic antibody cetuximab.

Conclusions: We propose that hVps37A status could become a novel prognostic and therapeutic marker for EGFR or HER2 driven tumors.

Introduction

Reliable prediction of prognosis and therapeutic response based on molecular factors will undoubtedly lead to more personalized cancer medicine. Despite increasing biological knowledge though, only few biological markers for ovarian cancer have entered clinical practice so far. The ErbB family comprises four members (ERBB1-4), of which ERBB1 (EGFR) is the most prominent. EGFR is a 170 kDa transmembrane RTK that plays an essential role in governing multiple cellular processes, including cell proliferation, survival, and cell migration (1, 2). Targeting of epidermal growth factor receptor (EGFR) and other ErbB family members as well as their downstream pathways is a mainstay of treatment in many malignant diseases. Activation by EGF or EGF-like ligands leads to receptor dimerization and autophosphorylation of cytoplasmic residues (3). The phospho-tyrosine residue itself serves as a docking platform for several adaptor molecules, triggering the activation of various pathways including the RAS-RAF-MEK-ERK pathway, the PI3K-Akt pathway, and the PLC-gamma-PKC pathway (4). Hyperactivation of EGFR-dependent signal transduction often accompanies tumor development, and cancer patients with unbalanced EGFR activity generally present with a more aggressive disease leading to unfavorable clinical outcome (5). It is widely believed that hyperactivation of EGFR-mediated signal transduction can be triggered by a) increased ligand expression, b) elevated EGFR protein expression, c) activating EGFR mutations, d) defective EGFR down-regulation, and e) cross-talk with heterologous receptor systems (6). Introduction of the anti-EGFR antibody cetuximab (IMC-C225, Erbitux) to clinical practice represented a major breakthrough in cancer therapy. Cetuximab binding leads to inhibition of EGFR dependent signaling pathways, activation of antibody dependent cellular cytotoxicity (ADCC) and consequently to apopotosis and decreased cellular proliferation, survival and migration (1, 2). Cetuximab is a chimeric monoclonal antibody binding extracellular domain of EGFR, preventing receptor dimerization and activation as well as triggering its internalization and degradation (3).

EGFR down-regulation by the endosomal sorting process depends on receptor internalization via endocytosis, as well as subsequent vesicular shuttling towards one of three distinct cytoplasmic compartments (7). The internalized receptor can (1) be directed back to the cell surface, (2) enter the trans-Golgi network (TNG), or (3) be transported into the intraluminal vesicles (ILVs) forming multivesicular

bodies (MVBs), which are subsequently degraded upon fusion with the lysosome (8, 9). The endosomal sorting complex required for transport-I (ESCRT-I) is one of three protein complexes essential for sorting of ubiquitinated transmembrane proteins into internal vesicles of MVBs and subsequent degradation. Vps37A (vacuolar protein sorting 37 homolog A) was initially described in yeast as one of the three subunits of ESCRT-I (10).

The human homologue of Vps37A (hVps37A), is located on the short arm of chromosome 8. For this region, 8p22 loss of heterozygosity (LOH) occurs to a high frequency in several human cancers including ovarian cancer. The expression of hVps37A was found to be reduced or undetectable in hepatocellular carcinoma (HCC) (11) by a positional cloning approach and consequently the name HCRP1 (hepatocellular carcinoma related protein) was suggested. First functional data showed that overexpression in the HCC cell line SMMC-7721 significantly inhibited cell growth *in vitro*, whereas siRNA mediated knockdown of HCRP1 in the HCC cell line BEL-7404 resulted in increased cellular proliferation (11). In a more detailed study, hVps37A was shown to interact with Tsg101 and hVps28 via its mod(r) domain and depletion of hVps37A in HeLa cells diminished EGFR degradation (12). Nonetheless, hVps37A has been poorly characterized so far. Since hVps37A was reported to be involved in the EGFR degradation process and regulating cellular proliferation, we suspected that it might be also involved in ovarian cancer pathogenesis. We set out to characterize the function of hVps37A in an ovarian cancer model *in-vitro* and *in-vivo* as well as define its influence on prognosis of ovarian cancer patients.

Materials and Methods

Patient material

Samples of formaldehyde fixed-paraffin embedded (FFPE) ovarian tumors for establishing the tissue microarray (TMA) were obtained from archival material of 144 patients who underwent radical cytoreductive surgery or between the years 1987 and 2002 at the Medical University of Vienna, Vienna, Austria. Written and oral informed consent was obtained from all patients according to the Ethics Committee of the Medical University of Vienna for further processing and analysis of the clinical data. The clinical characteristics of patients from the cohort used for the tissue microarray are described in Table 1. Microarrays were composed by taking core needle

"biopsies" from specific locations in the pre-existing paraffin-embedded tissue blocks and re-embedding them in an array master block, using techniques and an apparatus developed by Beecher Instruments Inc., Micro-Array Technology (Sun Prairie, WI, USA). To achieve good representation of the tumor, three biopsies of tumor material were selected from each patient. None of the patients with borderline tumors died during the follow-up time and were excluded from the survival analysis. No data on chemotherapy treatment was available in this cohort, although most patients received platinum and taxane based adjuvant regimen according to the institutional standard operating procedures.

Samples of ovarian tumors for mRNA expression analysis were obtained from a second cohort of 115 patients who underwent radical surgery the Charité University Hospital, Berlin, Germany between years 2000 and 2004. Epithelial-enriched normal ovarian and benign cyst samples came from patients diagnosed without malignant disease at the Medical University of Vienna. In total, 20 benign ovarian samples and 115 primary tumor samples were assessed. Informed consent to sample and data collection by all patients was given according to the institutional review board of the Charité University Hospital Berlin and the Medical University of Vienna, as stated above. The clinical characteristics of these patients are described in Table 1. 85 (78.0%) of the patients with ovarian cancer in the second cohort underwent chemotherapy with a platinum and taxane based regimen.

RNA isolation, cDNA synthesis and quantitative RT-PCR

Total RNA from cell lines was prepared with the RNeasy Mini Kit (Qiagen, Hilden, Germany) and quality and quantity assessed on RNA Nano Chips (Lab-on-a-Chip, Agilent Technologies, Palo Alto, CA, USA). All steps were accomplished according to the manufacturers' protocols.

cDNA was synthesized from 1µg total RNA using the DuraScript RT-PCR Kit (Sigma-Aldrich, Saint Louis, MO, USA) in a volume of 20µl and subsequently diluted to a total volume of 100µl. The following Assay-on-Demand™ probes were selected for TaqMan real-time PCR: *FLJ32642*, Hs00329751_m1 and *beta 2-microglobulin (B2M)*, Hs99999907_m1, HPRT1 and GAPDH (Applied Biosystems, Foster City, CA, USA). The real-time PCR reaction mix was composed of 10µl TaqMan® Universal PCR Master Mix (Applied Biosystems) supplemented with 2µl of the obtained cDNA, 1µl of the probe and 8µl of ddH_2O to a total volume of 20µl. The reaction was

performed on the 5700 Sequence Detection System (Applied Biosystems, Foster City, CA, USA) with default cycle conditions. Expression was relatively quantified as described elsewhere (13) and its log-transformed values were used in the analysis. Briefly, PCR efficiencies were calculated from calibration curves for individual probes and expression rates were compared with control cells (calibrator). All PCR reactions were performed from three independent experiments, and reverse transcriptase-negative and template-negative controls were included.

Cell culture and shRNA silencing of hVps37A

The human ovarian carcinoma SK-OV-3 cell line was cultured in McCoy´s medium enriched with 10% fetal bovine serum (FBS) and cultured in humidified incubator (37°C / 5% CO_2). For applying the Tet-Off inducible system, founder cell lines were generated by transfecting SK-OV-3 cells with the pTet-Off vector (neo^r) encoding a tetracyclin repressible transactivator (tTA). Resistant colonies were selected with 200 µg/ml G418 and characterized by transient transfection with the luciferase reporter plasmid (pTRE-Luc) containing luciferase under the control of tTA. Cell lines with highest response were used to establish cells inducible for hVps37A-specific shRNA (Open Biosystems; #V2HS_21202, #V2HS_21203), which were subcloned into the SIN-TREmiR30-PIG vector (pur^r) downstream of the tetracycline inducible promoter. Presence of tetracycline (doxycycline, Dox) in the culture medium then suppresses shRNA expression, while its withdrawal would induce the knockdown of hVps37A. Puromycin-resistant colonies were isolated in the presence of doxycycline, and screened for silencing efficiency of hVps37A by qRT-PCR and Western blotting.

The human ovarian carcinoma cell line MDAH-2774 was cultured in RPMI medium with 10% FCS (fetal calf serum), 50 units/ml penicillin G, and 50 µg/ml streptomycin sulfate at 37 °C in a humidified atmosphere of 95% air with 5% CO_2. Three different shRNA constructs complementary exclusively to the *hVps37A* mRNA in addition to one nonsense construct serving as a control, were cloned into the vector pSilencer 4.1-CMV neo. Transfection was performed with Lipofectamine 2000 according to the manufacturers' protocol (Invitrogen, Carlsbad, CA, USA). Stable clones were selected with 700 µg/ml G418, picked, and sub-cultured with 350 µg/ml G418. Silencing efficiency was quantified by qRT-PCR and western blot.

Antibody production

Polyclonal and monoclonal peptide antibodies against hVps37A were used for immunohistochemistry experiments and western blotting. Tissue microarrays were analyzed using (at that time available) polyclonal antibody, whereas immunohistochemistry of mouse tumors and western blotting were performed using the monoclonal antibody. The following peptide sequence was selected: MSPYASQGFPFLPPY. Rabbit antiserum raised against this peptide sequence was prepared and affinity purified by Eurogentec (Seraing, Belgium). Rabbit monoclonal antibody was also prepared by Eurogentec.

Immunohistochemistry

After deparaffinization and rehydration, the samples were treated with 0.3% H_2O_2/PBS (pH 7.4) for 10 minutes to quench endogenous peroxidase activity and blocked with serum of the secondary antibody diluted 1:50 in PBS. Primary antibodies against EGFR (EGFR (1005) Santa Cruz Biotechnology, Inc., CA, USA) and hVps37A were diluted 1:100 in serum/PBS and applied on the samples for 1 hour. HER2 was stained using the Dako HercepTest™ (Dako, Glostrup, Denmark). The secondary anti-rabbit antibody was applied for 30 minutes. For Ki-67 stainings, epitope retrieval was done using Depp-9; endogenous peroxidase activity was quenched using 0.3% H_2O_2 in Methanol. The dilution for both the primary monoclonal mouse, anti-human Ki-67 (M7240, Dako, Glostrup, Denmark) and secondary anti-mouse antibody (Vector Laboratories) was 1:200. After visualization with DAB+ (Dako, CA, USA) and counterstaining with hematoxyline/eosin, the slides were mounted in Eukitt (O. Kindler GmbH, Freiburg, Germany) and analyzed on an Olympus BX50 upright light microscope (Olympus Europe, Hamburg, Germany) equipped with the Soft Imaging system CC12.

The tissue microarrays were treated in an identical manner and the entire cohort was analyzed in one batch containing three slides per staining. Reagent conditions, incubation times and temperatures, and antigen retrieval (if necessary) were performed as previously described.

Data analysis and statistics

In the tissue microarray analysis, staining intensities were evaluated by two independent investigators and classified as 0 (missing expression), 1 (low

expression), 2 (moderate expression), and 3 (high expression). The tissues were graded positive (high or moderate expression) only when more than 10% cells were positive for the respective staining. For EGFR and HER2, results of triplicates and both interpretations were averaged and re-scaled (0-3). Staining for HER2, according to standard procedures for breast cancer, was divided into two groups with low (0, 1) or high (2, 3) expression (Table 2). Patients were dichotomized into two groups at the median of hVps37A expression. Since 40% of the tumor samples stained negatively or very weakly positively for EGFR, we also dichotomized the samples into two groups of low and high EGFR expression (Table 2). Overall survival analysis was performed with a median follow-up of 40.0 months (range 0.4–168.7 months) and event rate of 30.4%. Kaplan-Meier estimates of overall survival were obtained and groups were compared using the log-rank test. Only patients with available staining for EGFR, HER2 and hVps37A were included in the survival analysis. Logistic regression (ROC curves) was used to calculate specificity and sensitivity for the 5-year survival prognosis of EGFR and HER2. Nonparametric correlations between expression levels and ordinal or binary clinical variables were calculated using Spearman's rho.

In-vivo xenograft experiments were analyzed using unpaired Student's t-test. The mRNA expression analysis used relative normalized expression values for hVps37A expression of the normal (N) and ovarian patient (PT) cohort as measured by qRT-PCR. Group means were compared using Student's t-test. All statistical analyses were performed using the SPSS statistical software (Chicago, IL, USA).

Protein isolation and western blotting

The following antibodies were used in the dilution indicated: hVps37A 1:200 (established as described above); primary antibodies (EGFR 1:300, pEGFR 1:100, HER2 1:200, pHER2 1:200, ERK1 1:5000, ERK2 1:5000 and beta-actin 1:300) and HRP-conjugated secondary antibodies (anti-goat 1:10000 and anti-rabbit 1:10000) were obtained from Santa Cruz Biotechnology, Inc. (Santa Cruz, CA, USA) Akt and pAkt were purchased from Cell Signaling Technology (Beverly, MA, USA). Upon treatment, cells were lysed and protein was prepared with RIPA+ buffer; protein concentration was determined by a standard Bradford absorbance assay (Sigmal Aldrich, Saint Louis, MO, USA). Equal amounts of proteins (30µg) were separated by SDS-PAGE, blotted on PVDF membranes (GE Healthcare, Buckinghamshire, UK),

incubated with the appropriate primary antibody, and visualized via HRP-conjugated secondary antibodies and treatment with the ECL chemiluminescent detection system (GE Healthcare, Buckinghamshire, UK).

Fluorescence microscopy and TUNEL assay

Cells were seeded on chamber slides, grown for 48 hours, fixed with 4% paraformaldehyde for 15 minutes, and permeabilized with 0.1% Triton X-100. The subsequent staining procedure was performed as described for immuno-histochemistry. The cells were incubated with the primary antibodies directed against pEGFR or EEA1 (1:100) for 1 hour. Alexa 610/350 secondary antibodies (1:100) were applied for 45 minutes. Afterwards the cells were analyzed on a confocal microscope.

The “In Situ Cell Death Detection Kit, Fluorescin” (TUNNEL Assay) was obtained from Roche (Mannheim, Germany) and conducted according to the manufacturers protocol. DNaseI-treated samples served as positive controls.

Proliferation assays

$2x10^5$ SK-OV-3 (with and without doxycycline, Dox) and MDAH (hVps37A silenced, nonsense control and wildtype) cells were seeded in 6-well plates in media complemented with 10% FCS and treated with 20 µg/ml cetuximab (Merck, Whitehouse Station, NJ, USA), 4 µM lapatinib (GlaxoSmithKline plc. London, UK), or were mock-treated. To maintain the logarithmic phase, cells were split at intervals of 48 hours, along with the determination of the cell number by a CASY cell counter (Innovatis AG, Bielefeld, Germany). This procedure was performed in triplicate over a time-span of 6 days and confirmed by a replication of the whole experiment. From the obtained data, doubling times (dt) were calculated and depicted as dt^{-1}.

3D cell culture experiments

SK-OV-3 ovarian cancer cells bearing a Dox inducible shRNA construct specific against hVps37A (described above) were induced to form multicellular spheroids in non-adhesive 96-well plates in the presence (control) or absence (knockdown) of Dox and grown for 72 hours. The spheroids were transferred to collagen gels (rat Collagen 1, Becton Dickinson, 1.75mg/ml Collagen) and incubated in FGM supplemented with 2.5% serum (+/- Dox) and grown for further 72 hours.

Spheroids were photographed and the areas of invasive structures were determined with the Axiovision software (Zeiss).

Mice xenograft experiments

Each treatment group consisted of 10 eight week old athymic *Foxn1*^{nu} mice, which were maintained under specific pathogen-free conditions at the Institute for Cancer Research of the Medical University of Vienna. All mice were subcutaneously inoculated with SK-OV-3 ovarian cancer cells bearing a doxycycline inducible shRNA construct specific against hVps37A (described above). Dox (125µg/day) was injected intraperitoneally in 50% of the mice in order to suppress hVps37A knockdown. The remaining mice were treated with PBS under the same conditions. Tumor size was measured every third day in two axes using a calliper. Tumor volume was calculated using the formula: volume = ½(length x width^2). Animal experiments were performed according to protocols approved by the Austrian Federal Ministry for Education, Science and Art.

Results

Prognostic Value of EGFR and HER2 is Dependent on hVps37A Status

Since hVps37A was suggested to be involved in endosomal RTK-degradation (12), we thought that it might potentially influence the impact of EGFR/HER2 expression on the survival of ovarian cancer patients. Thus, we undertook a tissue microarray (TMA) analysis to test this hypothesis. Median follow-up for patients with malignant ovarian tumors was 40.0 months (range 0.4–168.7 months), and 38 patients (30.4%) had already died. The TMAs were analyzed for protein expression of EGFR and HER2, as these receptors represent well studied markers for ovarian carcinogenesis and progression and are also targets of hVps37A-mediated receptor degradation. The representative staining intensities for hVps37A, EGFR and HER2 in the ovarian TMA are shown in Figure 1. Not surprisingly, high protein expression of the oncogenes EGFR ($p=0.005$) as well as HER2 ($p=0.002$) was associated with unfavorable overall survival rates, thus confirming our previous results and those of others (14) (Fig. 2A, D). Further, we looked at hVps37A expression in the same tumor samples. Consistent with the notion that hVps37A is involved in the endosomal sorting process of RTKs, it was primarily detected in the cytoplasm (Fig. 1). hVps37A expression was graded according to staining intensity (Fig. 1) and the patient cohort was divided at the median into two subgroups according to hVps37A expression. We observed a relatively high percentage (62%) of tumors with low or missing hVps37A expression in this patient population (Table 2), though hVps37A expression alone did not have an impact on overall survival of ovarian cancer patients (Fig. 2G). No significant differences regarding FIGO stage, grade or histological subtype were observed between high and low hVps37A expressing patients (Table 2). There was a weak, but significant positive correlation between EGFR and hVps37A expression (Spearman's $rho=0.348$, $p<0.001$).

To further identify and confirm the loss of hVps37A in ovarian cancer, we analyzed an independent cohort of ovarian cancer patients and measured hVps37A expression at the mRNA level. In this cohort, we also found hVps37A mRNA downregulation in ovarian cancer when compared to normal (epithelialy enriched) ovarian tissue (Fig. 3A), again indicating a deficiency of hVps37A expression in ovarian cancer. Further survival analysis of this cohort was not possible due to the short follow-up period.

To evaluate the impact of hVps37A expression on the prognostic impact EGFR and HER2, we stratified overall survival of our patients based on hVps37A expression. Interestingly, we can observe the strong impact of HER2 ($p<0.001$) as well as EGFR ($p=0.003$) expression on overall survival only in tumors with low or missing hVps37A protein expression (Fig. 2C, F). This well known prognostic influence of HER2 and EGFR is largely lost in cases with regular (high) hVps37A expression (Fig. 2B, E). Logistic regression (ROC curves) was used to calculate specificity and sensitivity for the 5-year survival prognosis of EGFR and HER2 (Supplementary Fig. 1A-D). In line with corresponding Kaplan-Meier curves, we observe that the prognostic specificity and sensitivity of EGFR and HER2 is dependent on hVps37A expression, as reflected by the area under the curve (AUC). This observation points towards a possible influence of the receptor degradation mechanism on clinical relevance of growth factor receptor expression. Consequently, EGFR or HER2 overexpression may have an impact on patients' prognosis only in tumors with decreased hVps37A expression.

Activated EGFR and HER2 Accumulate in hVps37A-Negative Cell Lines

We used ovarian cancer cell lines to gain closer insights into the causal biological mechanisms behind our findings. SK-OV-3 and MDAH-2774 ovarian cancer cell lines, which have detectable expression of EGFR and HER2, were established as model system for functional studies. hVps37A mRNA SK-OV-3 and MDAH-2774 was stably knocked down via a doxycycline inducible shRNA (SK-OV-3) or constitutive approach (MDAH-2774), respectively, and silencing efficiencies were determined on mRNA and protein levels (Fig. 3B, C, Supplementary Fig. 2A, B). We obtained clones with 60-70% reduction of hVps37A mRNA/protein, leading to elevated levels of activated EGFR and HER2 in the SK-OV-3 and MDAH-2774 cell lines. We juxtaposed hVps37A expression with activated EGFR receptor levels and found elevated phosphorylated EGFR while EGFR levels remained constant (Fig. 3B, Supplementary Fig. 2B). This resulted in a significant increase of the pEGFR/EGFR ratio. These observations suggest that activated EGFR accumulates within hVps37A–deficient cells as a result of defects in receptor degradation. We further aimed to define the cellular compartment harboring the aberrantly retained pEGFR protein using immunofluorescence. In control cells, pEGFR was hardly detectable (Fig. 3C). In contrast, pEGFR was detected at much higher levels in the cytoplasm of

hVps37A knockdown cells. Frequent co-localization with the early endosomal marker EEA1 (Fig. 3C) indicated that pEGFR may accumulate primarily in sorting endosomes. This observation further supports the notion of ineffective receptor sorting in hVps37A depleted cells. To see if this concept can be extended to other cell lines of ovarian and mammary origin, we quantified hVps37A, (p)EGFR and (p)HER2 by immunoblot analysis in 15 ovarian and breast cancer cell lines and plotted the ratios of activated to total receptor versus hVps37A (Fig. 4B). No significant association between hVps37A and EGFR ($r = 0.111$; $p=0.695$) was found, yet we observed a significant ($p<0.01$) reciprocal correlation between hVps37A and pEGFR protein expression ($r = -0.683$; $p=0.007$) as well as between hVps37A and pEGF/EGFR protein ratio ($r = -0.719$; $p=0.005$). A statistically weak correlation was also found between hVps37A and pHER2 protein expression, but did not reach the level of significance (data not shown). All these observations lead us to the conclusion that phosphorylated EGFR receptor accumulation in ovarian cancer may be caused by defects in endosomal protein degradation. To further validate this hypothesis, we studied the dynamics of pEGFR degradation in wild-type and hVps37A knockdown cells. After incubation in a serum-free medium, cells were stimulated with 100ng/ml EGF for 15 minutes to achieve receptor activation followed by re-incubation in serum-free medium. At defined time points, cells were harvested and pEGFR expression determined by Western blotting. pEGFR degradation was significantly impaired in hVps37A deficient cells while total receptor levels remained constant in SK-OV-3 and MDAH-2774 cell lines (Fig. 4A, Supplementary Fig. 2C), suggesting sustained EGFR signaling in these cells. This led us to investigate the effects of hVps37A upon treatment with EGFR inhibiting agents.

hVps37A Interferes with EGFR Signal Transduction and Anti-EGFR Antibody Treatment

Characterizing changes in EGFR-downstream signalling upon hVps37A knockdown might shed further light on the role of hVps37A in ovarian carcinogenesis. We therefore analyzed differences in ErbB-signalling pathways in hVps37A knockdown versus control cells. Consistent with extensive receptor phosphorylation and downstream pathway activation, knockdown of hVps37A was associated with increased phosphorylation of Erk1/2 (Fig. 4C, Supplementary Fig. 2D). Unlike Erk, Akt phosphorylation at serine 473 was not changed in the two cell lines studied,

arguing for baseline Akt phosphorylation not being affected by sustained growth factor signalling upon hVps37A knockdown in ovarian cancer cells. Next, we wondered if EGFR inhibition by anti-EGFR antibody cetuximab or EGFR/HER2 tyrosine kinase inhibitor lapatinib might have any consequences on EGFR phosphorylation in hVps37A knockdown cells. Lapatinib treatment did inhibit EGFR downstream signalling in both, hVps37A knockdown and wildtype cells, as evidenced by dephosphorylation of Erk1/2 and Akt in the SK-OV-3 and MDAH-2774 cell lines (Fig. 4C, Supplementary Fig. 2D). Interestingly, this was not the case for cetuximab. After cetuximab treatment, Erk1/2 and Akt remained phosphorylated in hVps37A knockdown cells. Cytoplasmic degradation of phosphorylated EGFR seems to be crucial for cetuximab-dependent inhibition of its downstream pathways. On the other hand, EGFR inhibition by lapatinib is rather mediated by its direct interaction with the tyrosine kinase domain, independent of endosomal processing and consequently unaffected by hVps37A status.

Dysfunctional activation of Erk-signal transduction leads to increased cellular proliferation, invasion and tumorigenesis. We studied the proliferation of control cells and hVps37A knockdown SK-OV-3 cells, which reveals comparable rates (25.5 versus 24.9 hours doubling time, respectively), thus indicating a limited impact of hVps37A on cellular proliferation under unstressed, untreated *in-vitro* conditions (data not shown). Incubation with cetuximab, however, significantly decreases the proliferation potential of the control cells expressing hVps37A ($p<0.01$), whereas the respective hVps37A knockdown cells remain unaffected. This fact indicates that the presence of hVps37A is essential for proper degradation of the receptor-antibody complex, which has been shown to be essential for efficient cetuximab mediated anti-tumor activity (15). EGFR/HER2 inhibition by lapatinib significantly reduced cell proliferation irrespective of hVps37A expression levels ($p<0.01$) in SK-OV-3 and MDAH-2774 cell lines (Fig. 4D, Supplementary Fig. 2E).

Loss of hVps37A Drives Invasive Potential of Cancer Cells

In order to simulate physiological tumor growth conditions, we allowed SK-OV-3 cells to grow in 3D collagen cultures. In detail, we seeded the cells into non-adhesive 96-well plates containing methylcellulose complemented media to generate tumor-like spheroids of several hundred cells. The spheroids were subsequently transferred to collagen gels and incubated for 72 hours. Overall growth rate of the

spheroids was not affected by hVps37A expression (data not shown). However, hVps37A-knockdown cells gained the ability to invade the collagen matrix more efficiently (Fig. 5A, B). The invasive potential was calculated as percentage area of outgrowing cells relative to the central area of the spheroid, resulting in a mean of 73.5% for the hVps37A knockdown cells compared to 30% for the controls (t-test $p < 0.001$). These data suggest that hVps37A affects *in-vitro* invasive characteristics of the cells rather than their proliferation.

Enhanced Growth of hVps37A Knockdown Cells in Mouse Xenografts

Next, we were curious about the *in-vivo* growth characteristics of the Vps37A-knockdown SK-OV-3 cells in a mouse xenograft model. $5x10^6$ cells were subcutaneously inoculated into hind flanks of nude mice, half of which were treated with doxycycline in order to obtain suppression of the shRNA construct. The mice were sacrificed according to the institutional ethics committee protocols. Tumor growth was increased in mice with hVps37A-knockdown xenografts, resulting in final mean tumor volumes of $1027mm^3$ compared to $683mm^3$ for the un-induced tumors ($p<0.001$, Fig. 5C). The tumors were paraffin-embedded for subsequent analysis and successful knockdown of hVps37A was confirmed via IHC staining (Fig. 5D). Interestingly, cellular proliferation was not significantly affected as determined by a Ki67 assay (Fig. 5F). However, we observed significantly decreased apoptosis rates for the Vps37A-knockdown tumors (Fig. 5E). These data indicate that the tumor growth effect can be traced back to sustained survival rather than elevated proliferation.

Discussion

Activation of ErbB RTK family isoforms is often associated with tumor development and progression. One of the mechanisms leading to hyperactivation of ErbB receptor signalling is defective receptor degradation. Recently, hVps37A has been recognized as a member of the ESCRT-I complex. While we could not detect mutations in the coding region of hVps37A (unpublished results), we observed hVps37A mRNA and protein expression to be significantly reduced in primary ovarian cancer, indicative for a negative selection pressure against hVps37A expression.

Due to the cytosolic orientation of the phosphorylated tail of RTKs, receptors targeted for endosomal degradation are still signaling competently, an effect which is probably increased by the observed cytoplasmic retention of pEGFR (16). In fact, we describe an increase in Erk1/2 phosphorylation upon knockdown of hVps37A, while basal phosphorylation of Akt remains unchanged. A possible explanation for this effect may be that endosomally located phosphorylated EGFR can not activate PI3K signaling (17), while other signaling pathways remain unaffected. MAPK activation leads to different responses dependent on the cellular background or intensity and duration of the signal (18-21).

Our findings resemble closely those established for Tsg101, another component of the ESCRT-I protein complex. It has been reported that the endosomal degradation of EGFR is impaired in Tsg101-deficient cells (22). In addition, non-functional Tsg101 causes EGFR accumulation within the cytoplasm (23). However, the function of Tsg101 as a tumor suppressor gene is controversial, since its knock-out did not result in cellular transformation and increased proliferation in mouse embryonic fibroblasts (24). Our results argue in favor of the occurrence of non-functional ESCRT-I complexes under conditions of hVps37A knockdown. We assume that in contrast to Tsg101, hVps37A might indeed constitute a novel tumor suppressor in ovarian cancer, as this function is assumed for the functional ESCRT-I complex (24).

EGFR is overexpressed in about 60% of ovarian epithelial cancers and its activation is correlated with increased tumor growth and invasion as well as poor patient outcome (25, 26). We found that hVps37A significantly affects the prognostic impact of EGFR and HER2 expression in ovarian cancer (14, 27). Under conditions of low hVps37A expression, both EGFR and HER2 expression levels were highly prognostic, a trait which was completely abrogated under conditions of high hVps37A

expression. Obviously, hVps37a deficiency tips the fine balance between RTK activation and subsequent degradation, furthermore influencing patients' survival. Multiple marker testing would thus be beneficial to obtain a more reliable and accurate picture of the disease. If our results can be confirmed in more comprehensive clinical studies, hVps37A-testing could define a novel path in EGFR - and HER2 testing of ovarian cancer.

The clinical use of several EGFR targeted therapies in ovarian cancer has been limited due to their low efficacy in phase I and II trials (26, 28). EGFR is at the same time a putative target for hVps37A mediated receptor degradation (12, 29). We propose that individual tumor cells can enhance their selective advantage in the course of disease progression via down-regulation of hVps37A. This subset of tumors could be more sensitive to a disruption of the EGFR pathway by EGFR targeted therapy using monoclonal antibodies or small molecule tyrosine kinase inhibitors (TKIs). So far, cetuximab has been studied and found ineffective in ovarian cancer in several phase II clinical trials (25, 30-32). Cetuximab is known to down-regulate EGFR signal transduction by various mechanisms, including induction of an immune response to the Fc-region *in-vivo* (33) also known as antibody dependent cellular cytotoxicity (ADCC). The role of ADCC in cetuximab mediated anti-tumor activity has been studied extensively (34), though the proportion to which ADCC and the immune system contribute to the clinical activity of cetuximab is controversial (35). In our study we focused on inhibition of EGFR downstream signaling by cetuximab, which is abrogated by hVps37A loss and could presumably be a determinant of its clinical activity.

While there are various mechanisms leading to resistance against anti-EGFR-therapies, including autocrine EGFR activation, mutation of downstream signaling effectors, and cross-activation of alternative RTKs, recently published studies add an additional twist: Cancer cell lines resistant to cetuximab by long term exposure developed increased EGFR levels as a result of defective receptor degradation (15). The genetic knockdown of hVps37A and the resulting resistance to cetuximab in our model confirm this molecular mechanism and propose a model of a pre-existing cetuximab resistance in advanced ovarian cancer. Further, in addition to the antagonistic effects, cetuximab also possesses the potential to trigger EGFR activation and dimerization prior to its down-regulation (36, 37). Following incubation with cetuximab, MAPK pathway and Akt-pathway remained active in hVps37A-

deficient cell lines, arguing for sustained functional signaling of the EGFR-cetuximab complex, resulting in resistance to cetuximab and unrestrained cell proliferation. In contrast to cetuximab, lapatinib directly blocks EGFR activation by targeting the ATP-binding domain. This leads to defective EGFR-dependent signal transduction independently of ESCRT mediated receptor down-regulation (38). This is in line with our observations, that PI3K/Akt and MAPK pathways, as well as cell proliferation, were inhibited by lapatinib irrespective of hVps37A expression levels.

Overall, we see hVps37A as a novel tumor suppressor gene with an essential role in receptor tyrosine kinase degradation pathway. We propose a clinical relevance for measuring hVps37A expression, in order to evaluate it further as a potential biomarker in ovarian cancer and beyond.

Supported by: the Austrian Science Fund (FWF); Project Number: P17891

Acknowledgements

Hartmut Beug, Bernd Mayer, Pavel Kovarik for helpful discussions and Thomas Pangerl and Andrea Schanzer for technical assistance.

Contributions

M.W., P.V., B.B., A.E., M.A. and M.H. performed the experiments. M.W., P.V., P.H. and M.K. designed the study and wrote the manuscript. M.S. supervised the *in-vivo* experiments. M.Sch. performed the statistical analysis. M.S., D.P., R.Z., T.G. and P.H. provided crucial ideas. R.H., C.S. and H.D. provided crucial reagents and protocols. All authors discussed and interpreted results.

Figure Legends

Figure 1: Expression of hVps37A, EGFR and HER2 in ovarian cancer.

(A)Tissue microarrays composed of 125 primary ovarian tumor samples and 19 borderline tumors spotted in triplicates with corresponding, surrounding normal tissue were stained for hVps37A, EGFR, HER2. The stainings were graded on a scale from 0-3 as 0-no expression, 1-weak expression, 2-moderate expression, 3-strong expression. Magnification 40x.

Figure 2: hVps37A status modifies the prognostic potential of EGFR and HER2 expression.

(A-G) Survival analysis was performed and depicted in plots of the corresponding Kaplan-Meier estimates. (A), (D) and (G) show unstratified Kaplan-Meier survival plots based on HER2, EGFR and hVps37A expression of TMA tissues. Samples were then stratified according to hVps37A expression and re-analyzed. Only tumors with low hVps37A expression retain the prognostic effect of EGFR (F) and HER2 (C) overexpression, while in patients with normal (high) hVps37A expression, neither EGFR (E) nor HER2 (B) expression influence overall survival.

Figure 3: hVps37A mRNA is decreased in ovarian cancer as compared to normal ovaries. hVps37A knockdown is associated with pEGF/pHER2 accumulation.

(A) hVps37A mRNA expression in tumor tissue of an independent cohort of 115 ovarian cancer patients (PT) and 20 age matched normal controls (N). Student's t-test was used to compare mean mRNA expression levels of hVps37A.

(B) hVps37A is silenced upon doxycycline treatment in SK-OV-$3_{tet\ off}$ cells, while hVps37A mRNA expression remains unaffected by doxycycline in SK-OV-3 wild type cells.

(C) Silencing of hVps37A leads to an increase in HER2 and EGFR phosphorylation. SK-OV-$3_{tet\ off}$ cells containing the hVps37A shRNA construct were cultivated in presence or absence of doxycycline and analyzed by SDS-PAGE and immunoblotting.

(D) pEGFR (red) accumulates in hVps37A silenced cells and is colocalized with early endosomal marker (EEA1, blue). SK-OV-$3_{tet\ off}$ cells were cultivated in presence or absence of doxycycline on chamber slides, probed against pEGFR and EEA1 and

analyzed by confocal microscopy. Colocalization of the pEGFR (red) and EEA1 (blue) signal is indicated by arrows. Green fluorescence of the nuclei arises from the presence of an EGFP cassette in the Tet-Off vector.

Figure 4: Loss of hVps37A impairs hVps37A degradation and cetuximab sensitivity in ovarian cancer cells.

(A) Time-pulsed activation of pEGFR is sustained in hVps37A silenced cells. SK-OV-$3_{tet\ off}$ cells cultivated in presence or absence of doxycycline were starved by serum withdrawal, then pulsed with 100ng/ml EGF and cultivated for indicated time in serum-free medium. pEGFR and EGFR levels were determined by SDS-PAGE and immunoblotting.

(B) hVps37A negatively correlates with pEGFR/EGFR ratio. hVps37A, EGFR and pEGFR protein amounts were determined in 15 ovarian and breast cancer cell lines by immunoblotting. Statistical significance was tested by Pearson Correlation (r=-0.719) with a p-value of 0.005

(C) hVps37A silencing leads to resistance against cetuximab mediated EGFR inhibition. SK-OV-$3_{tet\ off}$ cells cultivated in presence or absence of doxycycline were incubated for 24 hours with either 20µg/ml cetuximab, or 4µM lapatinib or remained untreated. Protein levels of pAkt, Akt, pErk1/2, Erk1/2 and actin were then determined by Western blotting.

(D) hVps37A silenced cells are resistant to cetuximab. $2x10^5$ SK-OV-$3_{tet\ off}$ cells were cultivated in presence or absence of doxycycline and exposed to 20µg/ml cetuximab, or 4µM lapatinib or remained untreated (U). Cell number was determined every 48 hours by a CASY cell counter over 8 days. Doubling time (dt) was calculated, normalized to untreated control and depicted as 1/dt. The columns indicate the mean of three independent experiments; error bars represent +/-SEM.

Figure 5: hVps37A silencing induces invasive phenotype *in-vitro* and tumor growth *in-vivo*.

(A) SK-OV-$3_{tet\ off}$ cells cultivated in presence or absence of doxycycline were cultured in a collagen matrix. Spheroids were analyzed by light microscopy.

(B) Area of outgrowing cells depicted in percentage relative to central spheroid. Error bars indicate mean +/- SEM.

(C) Tumors with silenced hVps37A exhibit enhanced growth *in-vivo*. Mice either treated or not-treated with doxycycline orally were inoculated with SK-OV-$3_{tet\ off}$ shRNA^{hVps37A} cells and examined for tumor formation. Mean tumor volume (mm^3) in treated and untreated mice is depicted against time (days). Error bars represent +/- SEM.

(D) In order to control for sustained hVps37A knockdown, formalin fixed-paraffin embedded tumor sections were immunostained with the hVps37A specific antibody. Magnification 40x.

(E) Average counts of apoptotic cells per field of view (Magnification 40x, triplicate counts) in tumors. Error bars indicate +/- SEM.

(F) Left panel shows representative Ki-67 stainings in mice xenografts (Magnification 10x and 40x). Right panel describes the quantitation (percentage) of Ki-67 positive cells. Error bars indicate +/- SEM.

Supplementary Figure Legends

Supplemetary Figure 1: hVps37A protein expression affects specificity and sensitivity of HER2 and EGFR testing.

(A-D) Area under the curve (AUC) shows that the prognostic value (sensitivity versus specificity) of EGFR and HER2 testing is dependent on hVps37A expression. Logistic regression (ROC curves) was used to calculate specificity and sensitivity for the 5-year survival prognosis of EGFR and HER2.

Supplemetary Figure 2: Loss of hVps37A impairs hVps37A degradation and cetuximab sensitivity in ovarian cancer cell line MDAH-2774.

(A) hVps37A mRNA is silenced by stable hVps37A specific shRNA expression in MDAH-2774 cells, as compared to vector controls

(B) Silencing of hVps37A leads to an increase in EGFR phosphorylation. MDAH-2774 cells containing the hVps37A shRNA construct were analyzed by SDS-PAGE and immunoblotting.

(C) Time-pulsed activation of pEGFR is sustained in hVps37A silenced cells. MDAH-2774 cells with and without stable hVps37A specific shRNA expression were starved by serum withdrawal, then pulsed with 100ng/ml EGF and cultivated for indicated time in serum-free medium. pEGFR and EGFR levels were determined by SDS-PAGE and immunoblotting.

(D) hVps37A silencing leads to resistance against cetuximab mediated EGFR inhibition. MDAH-2774 cells with and without stable hVps37A specific shRNA expression were incubated for 24 hours with either 20µg/ml cetuximab, or 4µM lapatinib or remained untreated. Protein levels of pAkt, Akt, pErk1/2, Erk1/2 and actin were then determined by Western blotting.

(D) hVps37A silenced cells are resistant to cetuximab. $2x10^5$ MDAH-2774 cells with and without stable hVps37A specific shRNA expression were exposed to 20µg/ml cetuximab, or 4µM lapatinib or remained untreated. Cell number was determined every 48 hours by a CASY cell counter over 8 days. Doubling time (dt) was calculated, normalized to untreated control and depicted as 1/dt. The columns indicate the mean of three independent experiments; error bars represent +/-SEM.

Supplemetary Figure 3: Specificity of the monoclonal hVps37A antibody.

SK-OV-$3_{tet\ off}$ shRNA^{hVps37A} cells were cultivated in presence or absence of doxycycline on chamber slides for 24 hours, fixed with 4% paraformaldehyde for 15 minutes, and permeabilized with 0.1% Triton X-100. The subsequent staining procedure was performed as described for immuno-histochemistry. Primary hVps37A antibody was omitted in the "no antibody" controls.

Supplemetary Figure 4: Confirmation of *in-vitro* and *in-vivo* effects of hVps37A loss.

(A) Wound healing assay. SK-OV-$3_{tet\ off}$ shRNA^{hVps37A} cells were plated in 6-well plated and cultivated in presence or absence of doxycycline for 12 hours, scratched using a sterile pipette tip and cultivated for another 24 hours with or without doxycycline. Wound closure was assessed by light microscopy. Accelerated migration can be observed in PBS treated SK-OV-$3_{tet\ off}$ shRNA^{hVps37A}.

(B) Tumors with silenced hVps37A exhibit enhanced growth rates *in-vivo*. Mice either treated or not-treated with doxycycline orally were inoculated with SK-OV-$3_{tet\ off}$ shRNA^{hVps37A} cells and examined for tumor formation. Relative tumor growth (x-fold volume of the tumor initially measured) is depicted against time (days). error bars represent +/-SD.

Supplemetary Figure 5: hVps37A expression in lung cancer.

FFPE tissues from two patients with lung cancer were analyzed for hVps37A expression by immunohistochemistry. We could observe strong staining in tumor tissue as well as stromal expression of hVps37A. Differential expression of hVps37A in lung and head and neck cancers is currently being studied by our group (unpublished data).

Tables

Table 1.	Tissue Microarray	RNA
Patients' characteristics	**N (percent)**	**N (percent)**
Type		
Normal ovaries		20
Primary tumors	125	115
Recurrent tumors		
Borderline tumors	19	
Grade	117 (8 missing)	114 (1 missing)
1	20 (17.1)	3 (2.6)
2	26 (22.2)	52 (45.6)
3	71 (60.7)	59 (51.8)
FIGO	125	113 (2 missing)
I	31 (24.8)	19 (16.8)
II	14 (11.2)	10 (8.9)
III	72 (57.6)	59 (52.2)
IV	8 (6.4)	25 (22.1)
Histology	125	115
Serous	70 (56.0)	70 (60.9)
Non-serous	55 (44.0)	45 (39.1)

Table 2. hVps37A expression and clinicopathological variables

	hVps37A	
	high	**low**
EGFR		
high	39	44
low	16	45
HER2		
high	14	25
low	41	64
Grade		
1	8	12
2	11	15
3	30	41
FIGO		
I	14	33
II	7	7
III	31	44
IV	3	5
Histology		
Serous	29	41
Non-serous	24	31

References

1. Hynes NE, Horsch K, Olayioye MA, Badache A. The ErbB receptor tyrosine family as signal integrators. *Endocr Relat Cancer* 2001;**8**: 151-9.
2. Hynes NE, Lane HA. ERBB receptors and cancer: the complexity of targeted inhibitors. *Nat Rev Cancer* 2005;**5**: 341-54.
3. Bogdan S, Klambt C. Epidermal growth factor receptor signaling. *Curr Biol* 2001;**11**: R292-5.
4. Scaltriti M, Baselga J. The epidermal growth factor receptor pathway: a model for targeted therapy. *Clin Cancer Res* 2006;**12**: 5268-72.
5. Holbro T, Civenni G, Hynes NE. The ErbB receptors and their role in cancer progression. *Exp Cell Res* 2003;**284**: 99-110.
6. Zandi R, Larsen AB, Andersen P, Stockhausen MT, Poulsen HS. Mechanisms for oncogenic activation of the epidermal growth factor receptor. *Cell Signal* 2007;**19**: 2013-23.
7. Maxfield FR, McGraw TE. Endocytic recycling. *Nat Rev Mol Cell Biol* 2004;**5**: 121-32.
8. Katzmann DJ, Odorizzi G, Emr SD. Receptor downregulation and multivesicular-body sorting. *Nat Rev Mol Cell Biol* 2002;**3**: 893-905.
9. Raiborg C, Rusten TE, Stenmark H. Protein sorting into multivesicular endosomes. *Curr Opin Cell Biol* 2003;**15**: 446-55.
10. Katzmann DJ, Babst M, Emr SD. Ubiquitin-dependent sorting into the multivesicular body pathway requires the function of a conserved endosomal protein sorting complex, ESCRT-I. *Cell* 2001;**106**: 145-55.
11. Xu Z, Liang L, Wang H, Li T, Zhao M. HCRP1, a novel gene that is downregulated in hepatocellular carcinoma, encodes a growth-inhibitory protein. *Biochem Biophys Res Commun* 2003;**311**: 1057-66.
12. Bache KG, Slagsvold T, Cabezas A, Rosendal KR, Raiborg C, Stenmark H. The growth-regulatory protein HCRP1/hVps37A is a subunit of mammalian ESCRT-I and mediates receptor down-regulation. *Mol Biol Cell* 2004;**15**: 4337-46.
13. Pfaffl MW. A new mathematical model for relative quantification in real-time RT-PCR. *Nucleic Acids Res* 2001;**29**: e45.
14. Pils D, Pinter A, Reibenwein J, Alfanz A, Horak P, Schmid BC, et al. In ovarian cancer the prognostic influence of HER2/neu is not dependent on the CXCR4/SDF-1 signalling pathway. *British journal of cancer* 2007;**96**: 485-91.
15. Wheeler DL, Huang S, Kruser TJ, Nechrebecki MM, Armstrong EA, Benavente S, et al. Mechanisms of acquired resistance to cetuximab: role of HER (ErbB) family members. *Oncogene* 2008;**27**: 3944-56.
16. Pennock S, Wang Z. Stimulation of cell proliferation by endosomal epidermal growth factor receptor as revealed through two distinct phases of signaling. *Mol Cell Biol* 2003;**23**: 5803-15.
17. Haugh JM, Meyer T. Active EGF receptors have limited access to PtdIns(4,5)P(2) in endosomes: implications for phospholipase C and PI 3-kinase signaling. *J Cell Sci* 2002;**115**: 303-10.
18. Lee SW, Fang L, Igarashi M, Ouchi T, Lu KP, Aaronson SA. Sustained activation of Ras/Raf/mitogen-activated protein kinase cascade by the tumor suppressor p53. *Proc Natl Acad Sci U S A* 2000;**97**: 8302-5.
19. Miaczynska M, Pelkmans L, Zerial M. Not just a sink: endosomes in control of signal transduction. *Curr Opin Cell Biol* 2004;**16**: 400-6.

20. Tang D, Wu D, Hirao A, Lahti JM, Liu L, Mazza B, et al. ERK activation mediates cell cycle arrest and apoptosis after DNA damage independently of p53. *J Biol Chem* 2002;**277**: 12710-7.
21. Zhang W, Liu HT. MAPK signal pathways in the regulation of cell proliferation in mammalian cells. *Cell Res* 2002;**12**: 9-18.
22. Raiborg C, Malerod L, Pedersen NM, Stenmark H. Differential functions of Hrs and ESCRT proteins in endocytic membrane trafficking. *Exp Cell Res* 2008;**314**: 801-13.
23. Lu Q, Hope LW, Brasch M, Reinhard C, Cohen SN. TSG101 interaction with HRS mediates endosomal trafficking and receptor down-regulation. *Proc Natl Acad Sci U S A* 2003;**100**: 7626-31.
24. Tanaka N, Kyuuma M, Sugamura K. Endosomal sorting complex required for transport proteins in cancer pathogenesis, vesicular transport, and non-endosomal functions. *Cancer Sci* 2008;**99**: 1293-303.
25. Siwak DR, Carey M, Hennessy BT, Nguyen CT, McGahren Murray MJ, Nolden L, et al. Targeting the epidermal growth factor receptor in epithelial ovarian cancer: current knowledge and future challenges. *Journal of oncology*;**2010**: 568938.
26. Sheng Q, Liu J. The therapeutic potential of targeting the EGFR family in epithelial ovarian cancer. *British journal of cancer*;**104**: 1241-5.
27. Crijns AP, Duiker EW, de Jong S, Willemse PH, van der Zee AG, de Vries EG. Molecular prognostic markers in ovarian cancer: toward patient-tailored therapy. *Int J Gynecol Cancer* 2006;**16 Suppl 1**: 152-65.
28. Kimball KJ, Numnum TM, Kirby TO, Zamboni WC, Estes JM, Barnes MN, et al. A phase I study of lapatinib in combination with carboplatin in women with platinum sensitive recurrent ovarian carcinoma. *Gynecologic oncology* 2008;**111**: 95-101.
29. Lafky JM, Wilken JA, Baron AT, Maihle NJ. Clinical implications of the ErbB/epidermal growth factor (EGF) receptor family and its ligands in ovarian cancer. *Biochim Biophys Acta* 2008;**1785**: 232-65.
30. Konner J, Schilder RJ, DeRosa FA, Gerst SR, Tew WP, Sabbatini PJ, et al. A phase II study of cetuximab/paclitaxel/carboplatin for the initial treatment of advanced-stage ovarian, primary peritoneal, or fallopian tube cancer. *Gynecologic oncology* 2008;**110**: 140-5.
31. Schilder RJ, Pathak HB, Lokshin AE, Holloway RW, Alvarez RD, Aghajanian C, et al. Phase II trial of single agent cetuximab in patients with persistent or recurrent epithelial ovarian or primary peritoneal carcinoma with the potential for dose escalation to rash. *Gynecologic oncology* 2009;**113**: 21-7.
32. Secord AA, Blessing JA, Armstrong DK, Rodgers WH, Miner Z, Barnes MN, et al. Phase II trial of cetuximab and carboplatin in relapsed platinum-sensitive ovarian cancer and evaluation of epidermal growth factor receptor expression: a Gynecologic Oncology Group study. *Gynecologic oncology* 2008;**108**: 493-9.
33. Peipp M, Dechant M, Valerius T. Effector mechanisms of therapeutic antibodies against ErbB receptors. *Curr Opin Immunol* 2008;**20**: 436-43.
34. Vincenzi B, Schiavon G, Silletta M, Santini D, Tonini G. The biological properties of cetuximab. *Critical reviews in oncology/hematology* 2008;**68**: 93-106.
35. de Souza AP, Bonorino C. Tumor immunosuppressive environment: effects on tumor-specific and nontumor antigen immune responses. *Expert review of anticancer therapy* 2009;**9**: 1317-32.
36. Mandic R, Rodgarkia-Dara CJ, Zhu L, Folz BJ, Bette M, Weihe E, et al. Treatment of HNSCC cell lines with the EGFR-specific inhibitor cetuximab (Erbitux)

results in paradox phosphorylation of tyrosine 1173 in the receptor. *FEBS Lett* 2006;**580**: 4793-800.
37. Yoshida T, Okamoto I, Okabe T, Iwasa T, Satoh T, Nishio K, et al. Matuzumab and cetuximab activate the epidermal growth factor receptor but fail to trigger downstream signaling by Akt or Erk. *Int J Cancer* 2008;**122**: 1530-8.
38. Xia W, Mullin RJ, Keith BR, Liu LH, Ma H, Rusnak DW, et al. Anti-tumor activity of GW572016: a dual tyrosine kinase inhibitor blocks EGF activation of EGFR/erbB2 and downstream Erk1/2 and AKT pathways. *Oncogene* 2002;**21**: 6255-63.

Figure 1

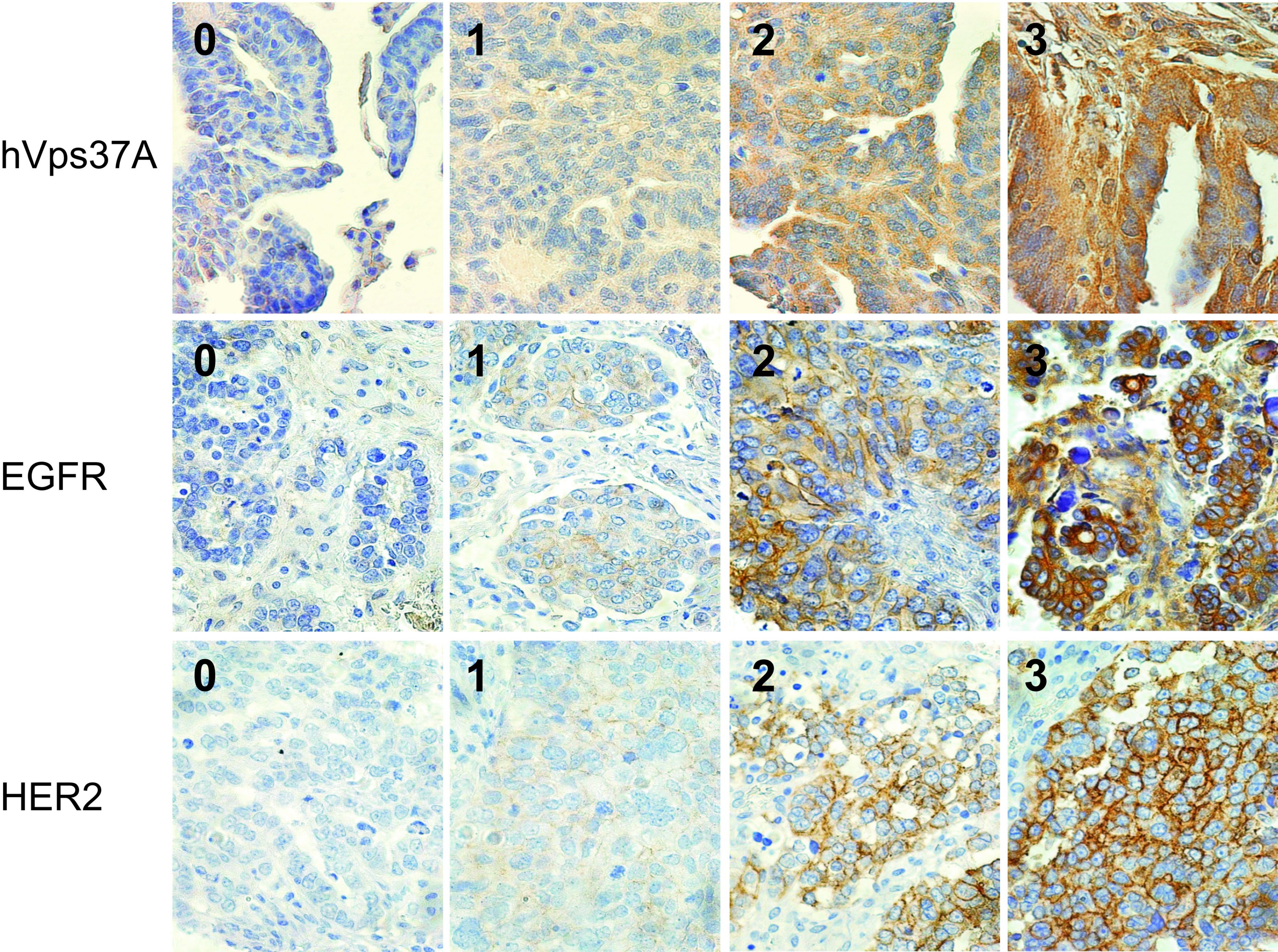

Figure 2

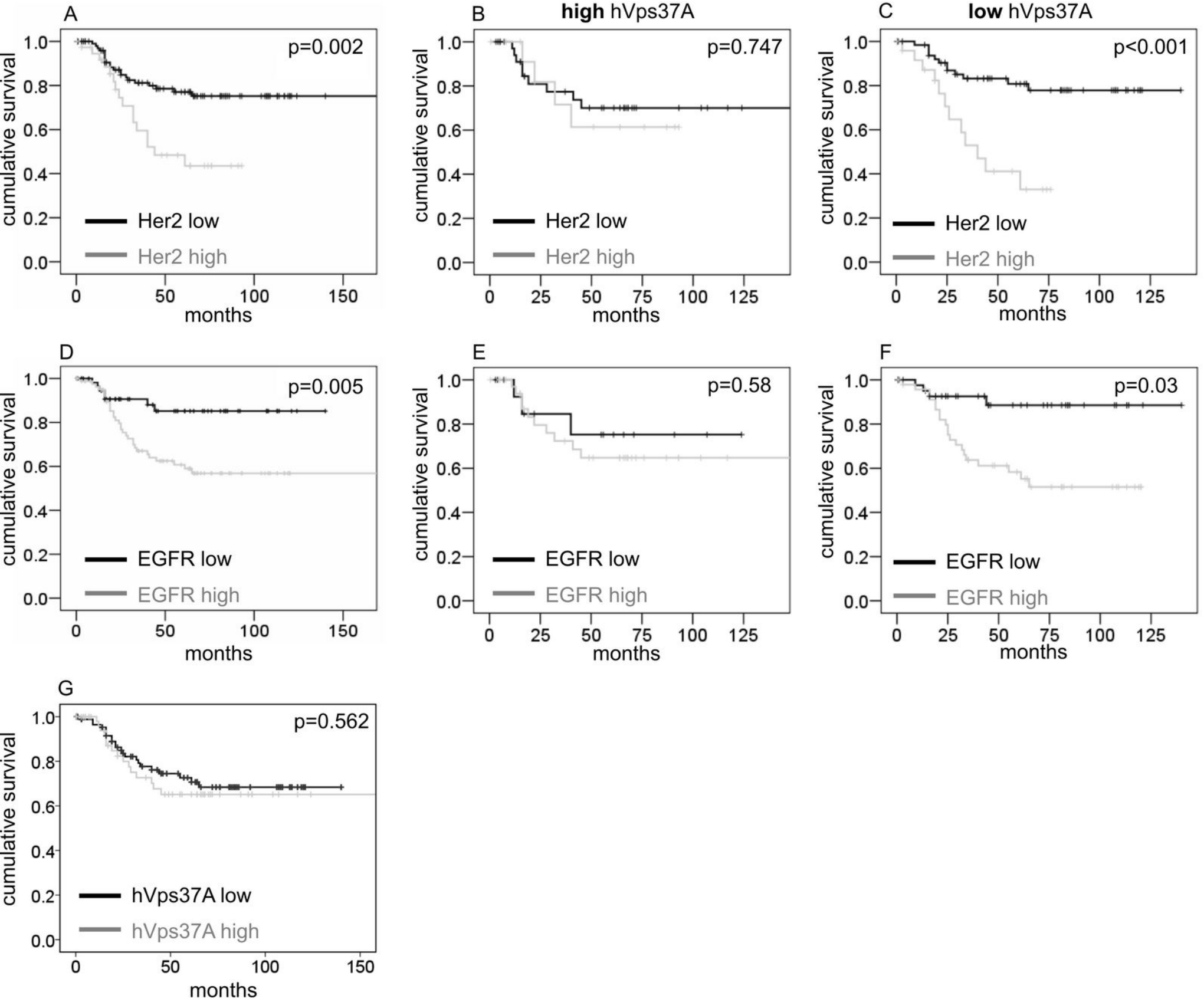
A
p=0.002
Her2 low
Her2 high
B
high hVps37A
p=0.747
Her2 low
Her2 high
C
low hVps37A
p<0.001
Her2 low
Her2 high
D
p=0.005
EGFR low
EGFR high
E
p=0.58
EGFR low
EGFR high
F
p=0.03
EGFR low
EGFR high
G
p=0.562
hVps37A low
hVps37A high
cumulative survival
months

Figure 3

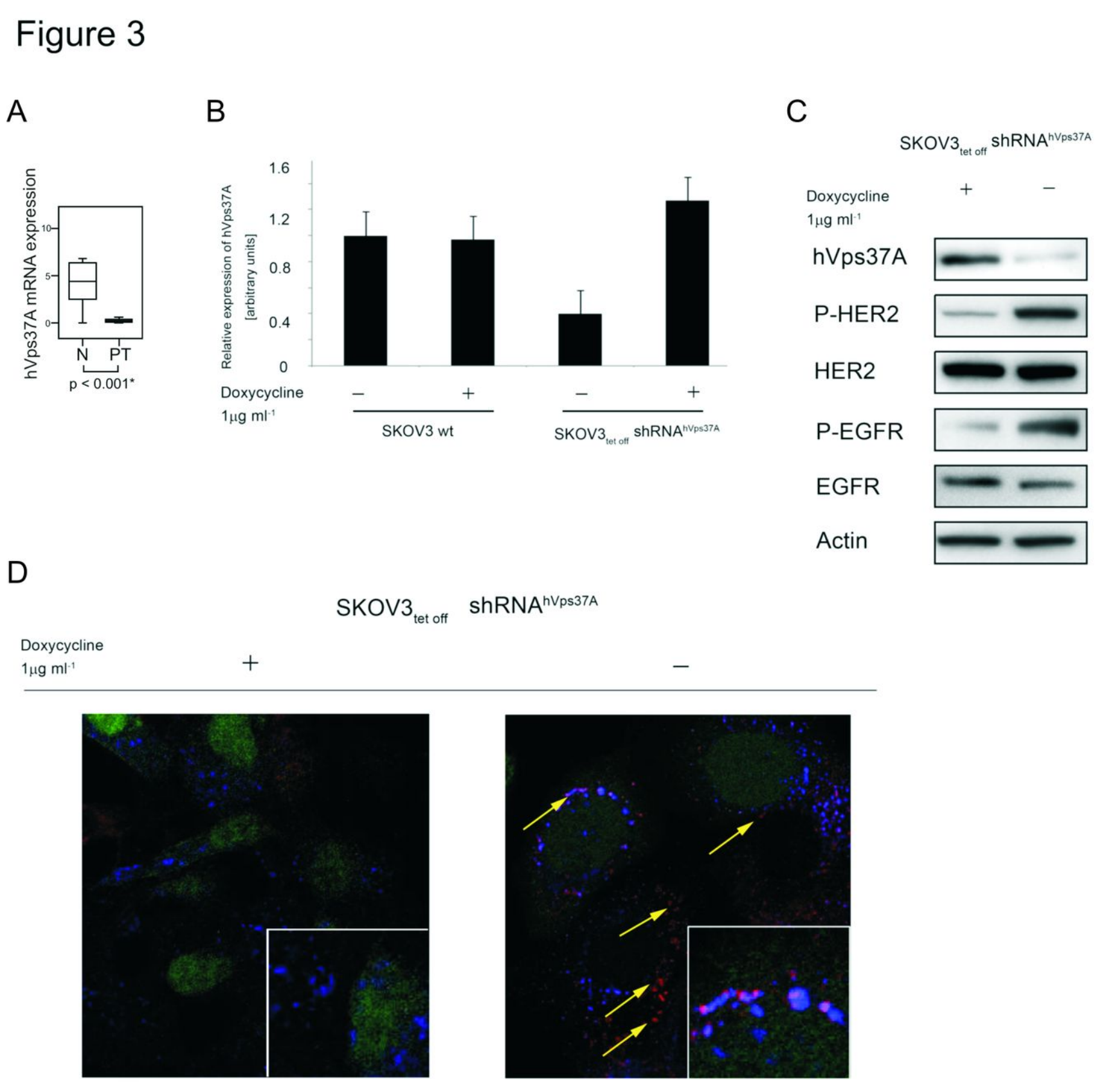
A
hVps37A mRNA expression
10
5
0
N
PT
p < 0.001*
B
Relative expression of hVps37A [arbitrary units]
1.6
1.2
0.8
0.4
0
Doxycycline
1μg ml-1
–
+
–
+
SKOV3 wt
SKOV3tet off shRNAhVps37A
C
SKOV3tet off shRNAhVps37A
Doxycycline
1μg ml-1
+
–
hVps37A
P-HER2
HER2
P-EGFR
EGFR
Actin
D
SKOV3tet off shRNAhVps37A
Doxycycline
1μg ml-1
+
–

Figure 4

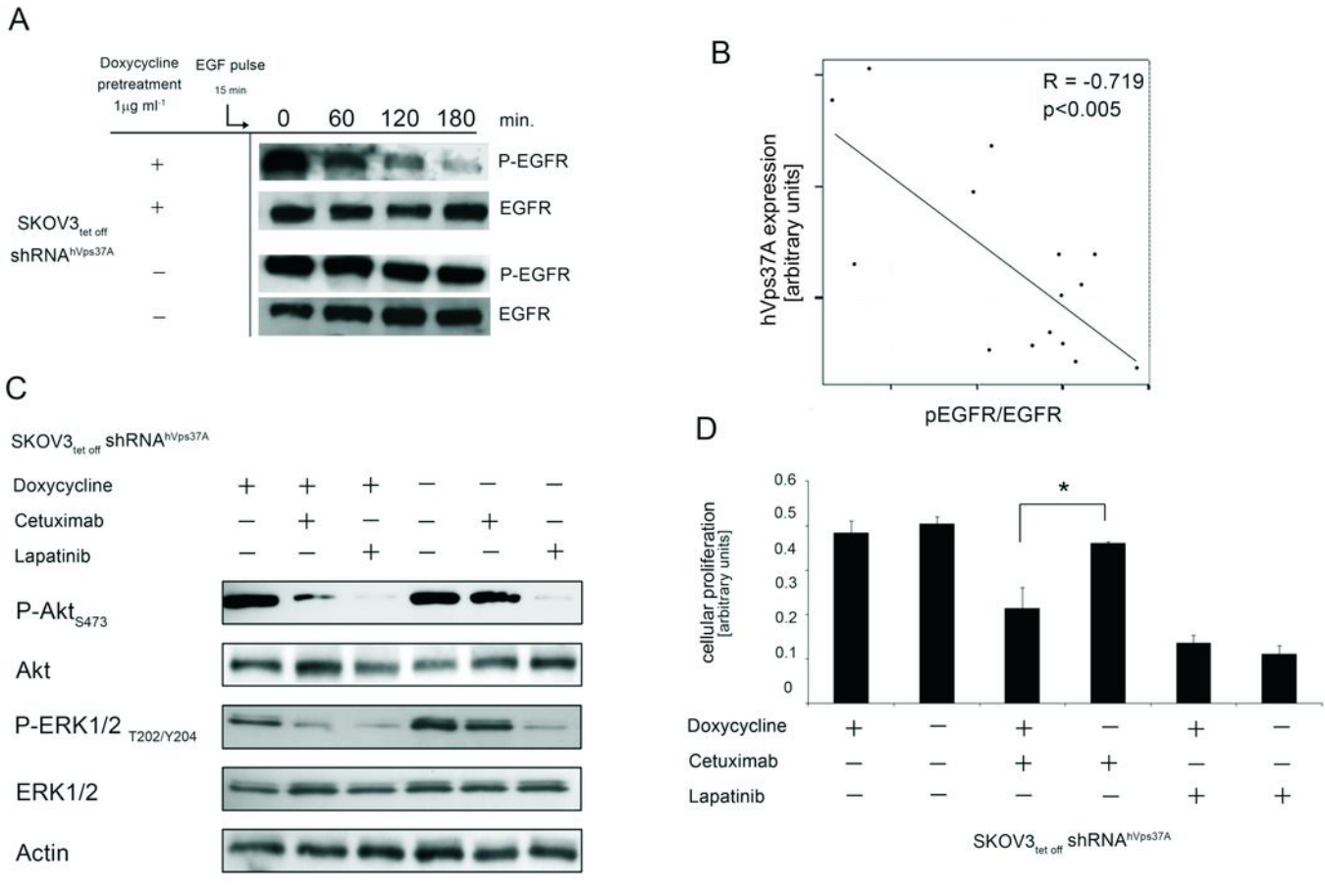
A
Doxycycline pretreatment 1µg ml-1
EGF pulse 15 min
0 60 120 180 min.
SKOV3tet off shRNAhVps37A
+
+
–
–
P-EGFR
EGFR
P-EGFR
EGFR
B
R = -0.719
p<0.005
hVps37A expression [arbitrary units]
pEGFR/EGFR
C
SKOV3tet off shRNAhVps37A
Doxycycline + + + – – –
Cetuximab – + – – + –
Lapatinib – – + – – +
P-AktS473
Akt
P-ERK1/2 T202/Y204
ERK1/2
Actin
D
cellular proliferation [arbitrary units]
0.6
0.5
0.4
0.3
0.2
0.1
0
*
Doxycycline + – + – + –
Cetuximab – – + + – –
Lapatinib – – – – + +
SKOV3tet off shRNAhVps37A

Figure 5

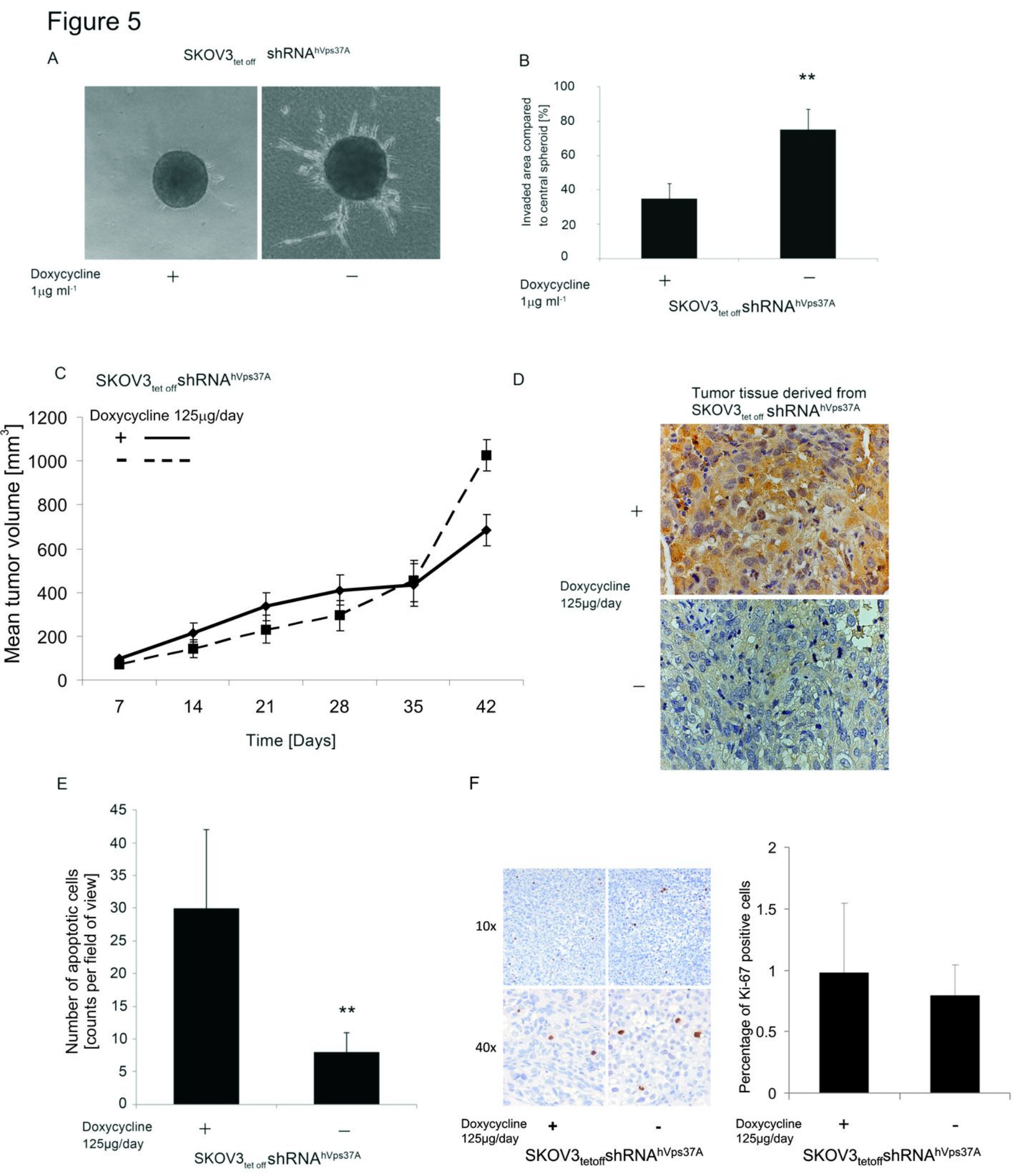
A
SKOV3tet off shRNAhVps37A
Doxycycline
1μg ml-1
+
–
B
Invaded area compared to central spheroid [%]
100
80
60
40
20
0
**
Doxycycline
1μg ml-1
+
–
SKOV3tet off shRNAhVps37A
C
SKOV3tet off shRNAhVps37A
Doxycycline 125μg/day
+
–
Mean tumor volume [mm3]
1200
1000
800
600
400
200
0
7
14
21
28
35
42
Time [Days]
D
Tumor tissue derived from
SKOV3tet off shRNAhVps37A
+
Doxycycline
125μg/day
–
E
Number of apoptotic cells
[counts per field of view]
45
40
35
30
25
20
15
10
5
0
**
Doxycycline
125μg/day
+
–
SKOV3tet off shRNAhVps37A
F
10x
40x
Doxycycline
125μg/day
+
-
SKOV3tetoff shRNAhVps37A
Percentage of Ki-67 positive cells
2
1.5
1
0.5
0
Doxycycline
125μg/day
+
-
SKOV3tetoff shRNAhVps37A